KANSAS GEOLOGICAL SURVEY
OPEN-FILE REPORT 81-18

Deposition and Diagenesis of the Five Finger Carbonate, Council Grove Group, Hugoton Field, Kansas

by

L. M. White

Disclaimer

Kansas Geological Survey
1930 Constant Avenue
University of Kansas
Lawrence, KS 66047-3726

KGS OF 81-18

DEPOSITION AND DIAGENESIS OF THE FIVE FINGER CARBONATE,

COUNCIL GROVE GROUP, HUGOTON FIELD, KANSAS

by

LARRY MICHAEL WHITE, B.A.

A THESIS

IN

GEOSCIENCES

Submitted to the Graduate Faculty
of Texas Tech University in
Partial Fulfillment of
the Requirements for
the Degree of

MASTER OF SCIENCE

Approved

Alonzo D. Jacka
Chairman of the Committee

Thomas DeKeyser

Accepted

Dean of the Graduate School

August, 1981

ACKNOWLEDGMENTS

Sincere appreciation is extended to Dr. Alonzo D. Jacka for his technical assistance, advice and encouragement.

I would like to express my gratitude to Walter Ralls and W. B. Osborn Oil and Gas for supplying this thesis problem, and providing financial support throughout the study.

Special thanks go to Walter Jenkins of Amoco Research in Tulsa, Oklahoma and Lynn Watney and staff of the Kansas Geological Survey in Lawrence, Kansas for the use of their facilities, and for allowing access to cores used in this study.

TABLE OF CONTENTS

LIST OF TABLES

LIST OF ILLUSTRATIONS

CHAPTER I

INTRODUCTION

The Hugoton Gas Field in southwestern Kansas represents part of the Panhandle-Hugoton Field of Kansas, Oklahoma and Texas (Fig. 1). Comprising almost 5.5 million acres, the Panhandle-Hugoton is the largest gas field in the United States, and constitutes one of the world's largest gas reserves.

Major gas production comes from dolostone and limestone reservoirs belonging to the Chase and Council Grove Groups of Early Permian (Wolfcampian) age (Fig. 3). Gas is largely produced from stratigraphic-diagenetic traps which result from abrupt lateral changes in the porosity and permeability of the reservoir rock. It is the intent of this investigation to describe the nature of these changes in relation to the depositional and diagenetic history of producing carbonates in a portion of the Hugoton Gas Field in southwestern Kansas. The interval of interest, herein assigned the descriptive term Five Finger Carbonate, represents the uppermost carbonate interval of the Council Grove Group (Figs. 5 to 14). The Five Finger carbonate interval varies in thickness from 10 to 40 feet over the study area. The term "Five Finger" is derived from the distinctive interfingering signature apparent on different types of log curves.

Area and Scope of Investigation

The study area is centered in Kearny, Grant and Stevens Counties, Kansas, although adjoining parts of several adjacent counties are also included (Fig. 2). The area of interest represents part of the Panoma Gas Area of the larger Kansas Hugoton Gas Field.

Although selection of the general area of study was governed by data availability, determination of study area boundaries was complicated by the disproportionate share of core and sample data from Kearny and Stevens Counties, and the paucity of such data from Grant County. Despite the lack of core and sample data from Grant County, the general availability of well logs throughout the county permitted its inclusion as part of the area of investigation.

Objectives

The major purpose of this study was to describe the depositional and diagenetic history of Five Finger carbonates, with particular attention given to the nature, distribution and predicatability of porosity trends within the Five Finger interval. This study had as its objectives interpretation of the following:

1. Structural and lithostratigraphic relationships
2. Environments of deposition, lithofacies, and biofacies
3. Diagenetic processes
4. Porosity and permeability relationships

Methods of Study

A total of twelve conventional cores were made available for study at Amoco Research's Core Laboratory in Tulsa, Oklahoma, and at the Kansas Geological Survey in Lawrence, Kansas. Sample cuttings were made available from four additional wells. Macroscopic examination of the chosen cores defined large-scale sedimentary structures and gross lithologic relationships. Chip samples, taken from the cores, were examined with a binocular microscope for sedimentary structures, mineralogic changes, colors and textures. 300 thin sections were prepared from these core chips at selected intervals, and each was stained, according to the technique of Lindholm and Finkelman (1972), with a combination of alizarin red-S and potassium ferricyanide solution to discriminate calcite from dolomite, and to highlight the presence of ferroan carbonates. Petrographic analysis of thin sections enabled recognition of smaller-scale sedimentary features, specific mineralogies, bioclastic constituents, textures and postdepositional diagenetic effects.

Electric and nuclear geophysical logs were available from most wells in the study area. The distinctive interfingering signature so characteristic of the Five Finger interval was in most cases readily distinguishable on the resistivity, sonic, and neutron logs (Fig. 15). These logs also provided a reasonably reliable marker for the base of the Five Finger interval. The accompanying gamma-ray response was used for gross lithologic correlation.

Various types of porosity logs were available, most notably from the sonic tool, with limited amounts from density and neutron surveys. Effective use of log porosity values was hampered by the generally ubiquitous distribution of fine terriginous clastics throughout the carbonate, which complicated porosity interpretations.

Local Structure

Five Finger carbonates within the study area were originally deposited on a broad homoclinal to monoclinal structure striking generally north-south; carbonates dip to the east and southeast at approximately 16 feet per mile. In the northern portion of the field beds dip to the northeast.

A structure contour map was prepared of the top of the Council Grove Group (Fig. 4). This map reveals a series of roughly linear structurally closed highs striking approximately northwest-southeast within the eastern portions of Grant and Kearny Counties. These positive features are elongate, and achieve maximum development in the east-central portion of Kearny County, where as much as 50 feet of closure exists. They appear to have developed from a series of southeastward plunging anticlinal folds. Other gentle flexures are superimposed on regional structure throughout the study area.

The two types of structures described represent the only deviations from an otherwise consistent monoclinal dip within the study area.

Previous Studies

Structural History

Numerous studies have been made concerning the structural history of the Hugoton Embayment (Fig. 1.1). The embayment is generally regarded as a shallow shelflike northwestward extension of the larger Anadarko Basin to the southeast (Merriam, 1956; Thomas, 1956; Worden, 1959). Merriam (1956) traced the structural evolution of the embayment, and the following discussion is largely paraphrased from this paper.

The Hugoton Embayment is a synclinal extension of the Anadarko Basin, and extends into southwest Kansas, southeastern Colorado, and the Oklahoma and Texas panhandles. It is bordered on three sides by uplifts which limited the extent of transgressing seas, and served as source areas for clastic sediment.

Initial downwarping of the embayment occurred during the Precambrian. Transgression of the seas during the Cambrian initiated the depositional history of the embayment. The Paleozoic history of the embayment is one of alternating marine and continental sedimentation in response to periodic, cyclic fluctuations in sea level. Tectonism is manifested as mild epeirogenic movements consisting of differential subsidence of the basin accompanied by possible uplift of marginal areas. These movements continued throughout the Paleozoic, and ceased towards the close of the Permian. Major structures developed at the close of Arbuckle, Viola, Chester, Morrow, and Permian time. Regional uplift in Atokan time in northwest portions of the Anadarko Basin caused a reversal of dip in southwestern Kansas from west to southeast (Pippin, 1968).

Depositional and structural conditions changed markedly toward the close of the Permian. Marine sedimentation was gradually replaced by continental deposition of clastics and evaporites as seas retreated and shelf areas became subaerially exposed.

Petroleum Geology

Most workers agree that updip wedgeout of porous carbonates and their interfingering with continental clastics to the west form a stratigraphic trap for gas in the Hugoton Embayment (Garlough and Taylor, 1941; Thomas, 1956; Jewett, 1960; Mason, 1965; Pippin, 1968). In addition, a hydrodynamic component contributes to the trapping mechanism (Hubbert, 1953; Mason, 1965; Pippin, 1968). Southeastward, downdip flow of groundwater through regions of low permeability provides a partial updip barrier to gas migration, and causes gas-water interfaces to become tilted in the direction of water movement, producing the trap (Hubbert, 1953; Mason, 1965).

The origin of gas in Wolfcamp reservoirs is not clearly understood. The most likely source for gas seems to be marine shales and carbonates of the Anadarko Basin (Page, 1940; Pippin, 1968). Additional sources may have been equivalent shales and carbonates of shelf areas in deeper portions of the Hugoton Embayment.

CHAPTER II

DEPOSITIONAL ENVIRONMENTS

Lower Permian Five Finger carbonates and associated clastics record deposition within subtidal, intertidal, supratidal, and continental sabkha-deflation flat environments. Environments are characterized as they relate to both modern and ancient analogs to the depositional model proposed for the Kansas Wolfcamp.

Subtidal

Subtidal Five Finger carbonates accumulated below mean low tide in high energy to low energy open marine environments. In high energy areas with vigorous circulation, lime sands (grainstones) may record deposition in subtidal channels, beaches or offshore shoals. Packstones and wackestones accumulated under progressively lower energy regimes in areas where wave and current energy was dampened. These textures may record deposition in lagoons or other topographically low areas of the shelf. Clastic muds concentrated in low energy areas were admixed to varying degrees with carbonate sediment to yield lithologies ranging from shaly wackestone to calcareous shale (Fig. 17). Higher energy grainstones and packstones contain diverse fossil assemblages of echinoderms, foraminifera, bryozoans, phylloid algae, brachiopods, and mollusks. Lower energy wackestones and shales contain restricted assemblages consisting mainly of brachiopods and mollusks.

Intertidal

Intertidal sedimentation occurred along shorelines in the zone between mean high and low tide. It is probable that both high and low energy tidal flat deposits are represented. Blue-green algal mats and flat algal laminated sediments formed on low energy intertidal flats in protected places. Algal mats contain shell debris derived from subtidal areas offshore, as well as terrigenous clastics deflated from eolian flats landward. Most algal mats developed along protected coastlines, and possibly along landward margins of low relief islands which may have existed offshore (Fig. 16). Similar islands exist offshore from present day coastlines of the Permian Gulf, and afford protection for algal mats developed along their landward margins (Kinsman, 1969). Some grainstone and packstone may represent tidal channel deposits. However, with only subsurface data, the distinctive channel morphology could not be recognized.

Supratidal (Coastal and Continental Sabkhas)

Coastal sabkhas are supratidal areas which exist landward of intertidal zones. They record deposition of carbonates, clastics and evaporites on arid to semiarid flats occurring above the mean high tide mark. Carbonate sediments are derived from intertidal and subtidal environments and transported onto the sabkha surface by storms and abnormally high tides. Clastics are incorporated in sabkha sediments by deflation and fluvial transport from distant upland source areas.

Gypsum commonly precipitates interstitially within coastal sabkha sediments. As coastal areas prograde seaward, increases in temperature and salinity of pore fluids convert gypsum to anhydrite (Butler, 1969; Kinsman, 1969). Anhydrite may pseudomorph gypsum crystals, or may form dense nodular mosaics or isolated nodules (Jacka and Franco, 1974). As gypsum precipitates, Ca ions are removed, and the Mg/Ca ratio is elevated. This leads to penecontemporaneous dolomitization of unstable aragonitic sediment (Butler, 1969; Kinsman, 1969). Some Five Finger dolostones represent penecontemporaneous dolomitization of unstable aragonitic sabkha muds. These dolostones also contain nodular anhydrite (Fig. 18).

Extension of algal flats into supratidal areas is not uncommon. Within seaward edges of supratidal zones, algal mats are subjected to periodic wetting and drying. The resulting desiccation produces features such as birdseye vugs, flat pebble conglomerate and irregularly crenulated algal stromatolites (Ginsburg, 1957; Kendall and Skipwith, 1969; Schmidt and others, 1969). Many examples of birdseye vugs (Fig. 19), flat pebble conglomerate (Fig. 20), and flat laminated to crinkled stromatolites (Fig. 19) were noted in supratidal carbonates of the Five Finger interval.

Continental sabkhas are defined by Kinsman (1969) as representing inland, evaporite-bearing clastics deposited in areas where the continental groundwater table lies within one meter of the surface, or intersects the surface to form a brine pan. The following characteristics are described by Kinsman (1969) as being indicative of continental sabkha environments. Laminated deposits of sulfate and clastic host sediment commonly occur in continental sabkhas. Gypsum is precipitated interstitially within clastic host sediment. During progradation of coastal areas, gypsum becomes replaced by anhydrite, which may pseudomorph gypsum crystals or precipitate directly as nodules. Continental sabkhas may contain brine pan deposits consisting of magnesite, gypsum needle crusts, and halite with intercalated clastics (Jacka and Franco, 1974). Jacka and Franco (1974) interpreted halite-cemented red-brown sandstones and siltstones as continental sabkha deposits. No halite was observed in any of the cores studied for the present report.

Continental sabkhas are distinguishable from coastal sabkhas by a lack of carbonate. Marine water underlies coastal sabkhas, while continental sabkhas are underlain by meteoric groundwater (Kinsman, 1969). Regressive clastics above and below the Five Finger interval contain continental sabkha deposits consisting of evaporite-bearing red-brown clastics (Fig. 21), and laminated deposits of sulfate and red-brown siltstone and shale (Fig. 22).

Deflation Flat

Deflation flat deposits are abundantly recorded in regressive clastics which overlie and underlie Five Finger carbonates. Deflation flats occur inland from coastal sabkhas, and they surround or engulf continental sabkhas (Jacka and Franco, 1974). Deposits consist of red-brown sands and silts cemented by dolomite and anhydrite. Nodular anhydrite is present in areas where the water table was close enough to the surface to permit interstitial precipitation of evaporites

(Jacka and Franco, 1974).

Jacka and Franco (1974) identified a variety of sedimentary structures common to deflation flats. These include mud polygon clasts, adhesion ripples, formed when wind blown sands adhere to moist surfaces, crust clasts, which record differential cementation of surficial crusts, and lag deposits, produced by entrapment of coarse sand in deflation hollows.

Deflation flat clastics above and below Five Finger carbonates consist of red-brown very fine sandstone cemented by dolomite and anhydrite. Sands contain nodular anhydrite (Fig. 23), adhesion ripples, burrow structures, and some minor cross-lamination (Fig. 24).

CHAPTER III

LITHOFACIES

The Five Finger interval consists, in ascending order, of a lower carbonate unit, a middle clastic-carbonate unit, and an upper carbonate unit (Table 1). A description of each lithofacies follows, along with inferred environments of deposition.

Lower Carbonate Unit

Lower unit carbonates are 4-24 feet in thickness. Wackestones and packstones are common in lower portions of the unit, and are light gray to dark gray-green in color. Darker colors are imparted by high shale and organic content. The base of the unit contains quartz sand and silt derived from subjacent clastics. Lithologies in basal portions of the unit range from calcareous siltstone to wackestones and packstones containing thin clastic lenses. Fossils common in lower portions of the unit include echinoderms, brachiopods, bryozoans, mollusks and forams.

Sedimentary sturctures in lower portions include undulatory laminations, which may have been produced by sluggish bottom currents, and varying degrees of mottling, indicative of bioturbation.

Upward from its base, lower unit carbonates contain less shale, and become lighter colored and more fossiliferous. Packstones and grainstones are dominant in upper portions of the unit. Shallow clear water conditions permitted green algae to flourish within a diverse fossil assemblage. Most shell fragments are enveloped by thick algal

TABLE 1

Description of Carbonate Lithofacies and Associated Clastics

Lithofacies	Thickness (Ft.)	Lithology	Genetic Facies	Depositional Environment
Regressive Clastics		Red-brown sandstone and shale	Regressive	Continental sabkha, deflation flat
Upper Carbonate Unit	4-15	Mudstone to grainstone	Transgressive	Sabkha, tidal flat, open marine
Middle Clastic-Carbonate Unit	1-5	Shaly wackestone, calcareous shale	Transgressive	Subtidal, low energy
Lower Carbonate Unit	4-24	Wackestone to grainstone	Transgressive	Subtidal, open marine
Regressive Clastics		Red-brown sandstone and shale	Regressive	Continental sabkha, deflation flat

coatings (Fig. 26). In a landward direction, higher energy limestones undergo a facies change to supratidal stromatolitic dolostones which are represented in the #1 Dreese core (Fig. 25).

Lower unit carbonates were deposited in subtidal environments under transgressive conditions as seas began to inundate the shallow shelf. Limy siltstone and clastic-rich subtidal limestones represent initial basal transgressive deposits. Locally this clastic-rich basal zone is overlain by foram-rich grapestone grainstone and packstone. Higher energy conditions prevailed in such areas to winnow out lime mud and fine clastics. Higher energy shallow water carbonates at the top of the unit reflect deposition during periods of high sea level stillstand and decreased turbidity. These carbonates probably represent broad areas of offshore bars or shoals which developed over the shallow shelf.

Middle Clastic-Carbonate Unit

This unit could be included within either the upper or lower carbonate unit. However, its usefulness as a marker bed for the Five Finger interval and its regional correlation in the subsurface merit a separate lithofacies designation.

Middle clastic-carbonates are 1-5 feet in thickness. The unit is characterized by a consistently high clastic content; lithologies vary from dark gray to black calcareous shale to dark gray shaly, dolomitic wackestone (Fig. 17). In a landward direction, marine shales undergo a facies change to red-brown continental shales, which are represented in the #1 Dreese core (Fig. 25).

Middle clastic-carbonates represent deposition within subtidal open marine environments. Lower energy conditions in these areas was probably the controlling factor in the deposition of shales and lime mud-rich carbonates (Bathurst, 1971). Entrapment of clastics may have been facilitated by topographically lower areas of the shelf which acted as settling basins for fine clastics. Shales were probably deposited in broad low energy swales where wave and current energy was dampened by offshore bars or low relief islands (Fig. 16). Shaly lime mud-rich carbonates probably reflect deposition on topographically higher areas of the shelf where circulation was more vigorous.

Turbid water, muddy substrates and sluggish to moderate circulation limited the biota to an assemblage of brachiopods, mollusks and some echinoderms. Extensive fragmentation and lack of rounding of bioclasts suggests breakage by burrowing organisms.

Upper Carbonate Unit

Upper unit carbonates are 4-15 feet thick. Textures in lower portions of the unit range from wackestone to packstone. Colors range from dark gray-green to light gray, depending on the clastic and organic content, which decreases upward in the unit. The fossil assemblage is diverse, with echinoderms, bryozoans, brachiopods and mollusks being dominant.

Upward from the base, carbonates become lighter-colored, less shaly, and more fossiliferous. Textures consist of packstone, grainstone and packstone-grainstone. Cores 1, 7 and 8 contain thin supratidal stromatolites which cap the entire upper carbonate unit.

Stromatolites, which are irregular and flat to crinkly, contain scattered bioclastic debris and silt-size clastics. Finely crystalline supratidal dolostones and subtidal dolostones are intercalated with stromatolites in some areas.

Sedimentary structures within upper unit carbonates include some mottling due to burrowing and undulatory laminations in lower portions. Toward the top crude irregular stromatolitic laminations and small styolitic seams occur.

In higher energy areas fossil assemblages are diverse, and bioclasts commonly develop thick algal coatings (Fig. 27). Green algae (Dasyclads) become more numerous toward the top of the unit, suggesting shallower, less turbid conditions through time.

Upper unit carbonates were deposited during times of maximum submergence of the shallow shelf and coastline. Carbonates in lower portions of the unit reflect deposition within subtidal open marine environments. Those higher in the unit accumulated in open marine, intertidal and supratidal environments.

Regressive Clastics

Regressive clastics are subjacent and superjacent to Five Finger carbonates throughout the area of study (Figs. 28 and 29). Although detailed analysis of these clastics was beyond the scope of this study, samples were taken in some cores to aid in accurately determining overall facies patterns and relationships.

Supratidal Clastics

Supratidal clastics directly overlie and underlie Five Finger carbonates, and consist of calcareous red-brown siltstones and shales. Shales contain some gray-green mottling. Thicknesses range from 1-5 feet. Gray to tan carbonate clasts are present in some cores. Clastics are highly fractured and crumbly, and resemble mudstone "rubble" (Fig. 21). The "rubble" condition is inferred to result from massive dissolution of sulfates, and possibly halite, from clastics. Dissolution probably occurred relatively soon after deposition.

These clastics represent continental deposition on subaerially exposed arid to semiarid continental sabkhas and brine pans during depositional regressions.

Deflation Flat Clastics

Deflation flat clastics underlie and overlie supratidal clastics. Deposits consist of light red-brown shaly, fine-grained sandstones which are cemented to varying degrees by dolomite and anhydrite. Some anhydrite occurs as nodules (Fig. 23). Gamma ray curves reflect decreased shaliness in these sands as compared with supratidal clastics.

These sands represent continental deposition on low relief deflation flats which existed inland from supratidal areas.

Facies Relationships and Depositional Cycles

Within the stratigraphic interval that includes Five Finger carbonates and regressive clastics, lithofacies may be grouped into the following four categories, which reflect deposition within a spectrum of four laterally contiguous environments: 1) carbonate, shale, and admixtures of shale, sand, and carbonate were deposited in subtidal and intertidal environments; 2) supratidal carbonates contain nodular anhydrite and were penecontemporaneously dolomitized; 3) red-brown clastic mudstones contain some sulfate and were deposited in continental sabkhas and brine pans; 4) red-brown fine-grained sandstones were deposited by eolian and fluvial processes on broad deflation flats. Categories 1 and 2 represent the lower carbonate unit, middle clastic-carbonate unit and upper carbonate unit of the Five Finger interval. Categories 3 and 4 correspond to regressive clastics above and below Five Finger carbonates. These four categories, along with related information, are shown in Table 2.

Five Finger carbonates and associated clastics are vertically intercalated in the following manner: 4,3,1,2,3,4 from the base upward. Categories 4 and 3 represent clastic deposition on exposed coastal plains and shelf areas, and form part of a regressive sequence within an earlier depositional cycle. The sequence of 1,2,3 and 4 which follows represents carbonate deposition during a transgression and a subsequent depositional regression (progradation) during high stillstands of sea level.

Lithostratigraphic and Facies Relationships from Log Cross-Sections

A total of five log cross-sections were constructed at selected intervals across the study area to determine lithostratigraphic and facies relationships within the Five Finger interval. Cross-sections at each interval are drawn relative to both a stratigraphic and structural datum.

TABLE 2

Description of Environmental Categories

Environmental Categories		Depositional Environments	Relative Sea Level Position	Lithofacies Equivalents
4	Regressive clastics	Deflation flats	Progradation - stable or slowly falling sea level	Regressive clastics
3		Inland sabkhas and brine pans		
2	Supratidal carbonates	Supratidal	Progradation - stable or slowly falling sea level	Upper carbonate unit
1	Carbonates and admixed carbonates and clastics	Subtidal and intertidal	Transgressive	Lower carbonate unit, middle clastic-carbonates, and portions of upper carbonate unit
3	Regressive clastics	Inland sabkhas and brine pans	Progradation - stable or slowly falling sea level	Regressive clastics
4		Deflation flats		

Figures 5, 9, 11 and 13 reveal that upper carbonates generally thicken to the west (landward), while lower carbonates thicken to the east (seaward). These relationships are consistent with the interpretation that upper carbonates are regressive, and lower carbonates are transgressive.

Figures 7, 11 and 13 reveal that carbonates and shales of the middle unit thicken slightly to the east. This suggests that clastics were transported into the region possibly from eastern margins of the Hugoton Embayment, or perhaps during periods of active delta outbuilding over shelf areas to the north and south of the study area.

Regressive clastics above and below Five Finger carbonates generally thicken to the west, as shown in figures 5, 7, 9 and 13. This relationship is consistent with the interpretation that clastics were continentally derived, and represent seaward progradation over Five Finger carbonates during depositional regressions.

Upper carbonates are much thicker and cleaner in northern portions of the study area, as illustrated in figure 13, suggesting that depositional regressions were more extensive in these areas. These carbonates are relatively clastic-free because clastic source areas probably existed farther south. Southward from the region encompassed by cross-section E-E' (Fig. 13), upper carbonates become thinner, and unit thicknesses become relatively uniform across the study area. Apparently, depositional regressions were not as extensive over areas generally south of central Kearny County. In these areas, upper carbonates are locally thinner over topographic highs (Fig. 10).

Facies changes in upper portions of lower carbonates are illustrated in figures 5, 9 and 13. Supratidal stromatolitic dolostones represented in the #1 Dreese core constitute updip (westward) facies equivalents to subtidal shelf limestones to the east. Dolostone facies of lower carbonates thin markedly in the vicinity of the #1 Dreese well.

Transgressive lower carbonates are thickest in southern portions of the study area (Figs. 7 and 9), where water was probably slightly deeper and the coastline was probably farther to the west. In northern portions, lower carbonates are relatively thin (Fig. 13), and represent deposition in more proximal positions of the shelf where shallower conditions existed.

CHAPTER IV

DIAGENESIS

Early Diagenesis in the Marine Evnironment

Blue-green algae affect the most significant diagenetic changes in subtidally deposited Five Finger carbonates. Their action leads to micritization of carbonate allochems, and the encrustation of allochem surfaces by algal coatings.

Bathurst (1966) first identified the process of micritization whereby carbonate allochems are converted to microcrystalline calcite. This conversion results from extensive centripetal boring of allochem surfaces by algae, and subsequent infilling of vacated bores by micritic aragonite or magnesium calcite. Incomplete micritization produces micrite envelopes, and if the process goes to completion, whole allochems may be converted to structureless peloids. These peloids, by virtue of their micritization, are more susceptible to abrasion and rounding (Bathurst, 1971).

In Five Finger carbonates, micritization of both aragonite and calcite shells, followed by transportation and rounding, produced peloids (Fig. 27). Thin walled shells of foraminifers and some bryozoans were thoroughly micritized, while thicker shells of echinoderms, brachiopods and mollusks developed only thin micritic rinds.

Micritized carbonate allochems were highly resistant to later diagenetic alteration. This effect was recognized by Jacka (1978), who observed that replacement of, and cementation within micritized shells were significantly inhibited (Figs. 30 and 51).

Higher energy Five Finger carbonates contain abundant algal coated grains. Grains are invariably of the Osagid type (Fig. 31), first described by Twenhofel (1919) from the Lower Permian of Kansas and Oklahoma, and also reported by Toomey (1974) from the Upper Pennsylvanian of the midcontinent region. Osagid grain coatings are composed largely of the blue-green alga Girvanella (Johnson, 1946). Algal thalli commonly form crude concentric laminations around shell nuclei. In some cases, coatings lack any trace of concentricity, and appear as dark brown, fine-grained micrite in thin section. The obliteration of algal structure is probably due to recrystallization of algal thalli (Toomey, 1974).

Epizoic organisms associated with Girvanella include the encrusting calcareous foraminifer Tuberitina, and the encrusting alga (?) Tubiphytes (Fig. 32).

Algal coated grain nuclei may be derived from almost any available bioclast, although phylloid algal fragments form the nuclei for most grains. Fragments of calcite shells form nuclei for some grains. Internal structures of aragonitic shells are commonly obliterated by extensive boring by Girvanella, dissolution, or recrystallization to calcite (Toomey, 1974). Thick-shelled calcitic bioclasts, which normally do not recrystallize, undergo limited perforation by boring algae, and usually retain their internal structure.

Algal coatings usually envelope shell nuclei evenly on all sides. This implies formation in an environment which provided enough turbulence to regularly roll the grains over. Where optimal conditions for growth existed, algal encrustations accreted outward to incorporate other grains into its structure to produce complex algal coated grains, or grapestone (Fig. 27). Within certain intervals, coalescence of these grains produced textures approaching that of a boundstone.

Some Five Finger grainstones contain isolated thin submarine cement crusts in primary voids. Cements are fibrous to bladed, and line intrabiotic cavities and interparticle pores. Acicular crusts are oriented perpendicular to grain surfaces (Fig. 30). Cements probably represent original thin acicular aragonite and bladed high magnesium calcite crusts which precipitated from shallow seawater.

Early Fresh Water Diagenesis and Calcitization

Most Five Finger carbonates stabilized and lithified in a fresh water environment. Originally unstable aragonite and magnesium calcite mineralogies were converted to stable low magnesium calcite by exposure to fresh meteoric groundwater.

Original aragonitic lime mud inverted to low magnesium calcite according to the process outlined by Matthews (1968). Inversion results from solution-precipitation reactions that initiate on calcite nuclei, such as bioclastic material, in the sediment. Initially high lime mud matrix porosities of 40-70% are occluded by inversion to calcite micrite (Bathurst, 1971). Recrystallization of lime mud to microspar, and less commonly to pseudospar, occurred in response to prolonged exposure to fresh water (Jacka and Brand, 1977).

Aragonitic bioclasts (phylloid algae and various mollusks) dissolved to form biomolds (Figs. 33 and 34). In some instances, dissolution occurred prior to complete lithification of sediments to produce vertical, crumbly nontectonic fractures (Fig. 35) similar to those described by Jacka and Brand (1977). Aragonite shells rimmed by micrite envelopes dissolved, leaving hollow micrite envelopes which were later filled to different degrees with calcite cement (Fig. 36). Cement may have been derived from the 8% surplus of $CaCO_3$ resulting from calcite replacement of aragonitic lime mud (Pingatore, 1970). Precipitation of cement in and around micrite-filled algal bores closely mimicked recrystallization fabrics. Some aragonite shells stabilized by inversion to coarse anhedral calcite mosaics which destroyed original shell textures (Bathurst, 1964; Friedman, 1964). Textures of calcitic shells were unaffected by fresh water diagenesis. Magnesium calcite echinoderms and bryozoans stabilized to calcite by incongruent dissolution with preservation of original shell textures (Friedman, 1964; Land, 1967). According to Gavish and Friedman (1969), Mg calcite stabilizes to calcite at greater rates than calcitization of aragonite.

Early lithification of Five Finger carbonate sediments involved not only mineralogic stabilization but also cementation in pore spaces to yield stable, lithified limestone.

Substrate fabrics placed definite constraints on calcite cement precipitation. Within intrabiotic cavities of calcitic bioclasts most cement was precipitated as epitaxial extensions of prismatic, foliated, and crossed-lamellar shell layers (Figs. 37 and 38). Highest rates of calcite cement precipitation occurred as large epitaxial aureoles on monocrystalline echinoderm components (Jacka, 1974a) (Fig. 36). In some intervals, the absence of calcite cement within micritized shells and hollow micrite envelopes indicates that cement precipitation on micritic foundations was significantly inhibited.

Criteria associated with the meteoric vadose environment as described by Jacka and Brand (1977) are poorly represented in Five Finger carbonates. Mineralogic stabilization proceeded rapidly within the fresh water phreatic environment, where criteria for phreatic diagenesis as outlined by Jacka and Brand (1977) are abundantly recorded. Solution of aragonite and precipitation of calcite occurred at greater rates in the phreatic zone than in the vadose zone due to continuous movement of fresh water through sediments (Steinen, 1974). Recrystallization of micrite to microspar and pseudospar is a by-product of phreatic diagenesis (Jacka and Brand, 1977). Some primary and secondary voids were filled with ferroan calcite cement (Fig. 34) which, according to Bathurst (1971), commonly precipitates within reducing environments of the phreatic zone. Drusy cement fabrics (Fig. 38) and partial collapse of dissolution molds to produce crumbly nontectonic fractures provides further evidence of extensive fresh water phreatic diagenesis.

Dolomitization and Dolomite Cementation

According to Jacka (1975), dolomitization may occur neomorphically to produce rhombic crystalline dolomite. Paramorphic dolomitization occurs when calcite and magnesium calcite crystal fabrics are preserved after dolomitization.

Some dolomitization occurred within supratidal and subtidal Five Finger carbonates. Dolomitization of supratidal lime mud produced neomorphic rhombic crystal textures (Fig. 18). Dolomitization probably was induced by elevated Mg/Ca ratios of seawater-derived pore fluid brines. Increased ratios resulted from Ca ion depletion by early precipitation of gypsum and aragonite. Within Persian Gulf sabkhas ratios of 5.3 in the lagoons increase to as much as 35 in interstitial brines of the coastal sabkha (Butler, 1969). Reaction of supratidal sediment with Mg-enriched brines leads to penecontemporaneous dolomitization of unstable aragonitic mud to produce dolomite muds with 1-2 micron crystals (Kinsman, 1969).

Neomorphic dolomitization of aragonitic peloids and bioclasts produced finer textures than replacement of lime mud. Peloids and shells possess greater packing densities of aragonite crystals; thus, later replacement by dolomite yielded dense crystalline textures. The presence of organic "sludge" in peloids may have also influenced replacement textures by restricting the size of rhombic replacement crystals in peloids (Shearman, in Bathurst, 1971). Aragonite needles of original lime mud are less densely packed to yield later dolomitization textures of loosely arranged rhombic crystals. Illing and others (1965) demonstrated that in supratidal environments, aragonitic lime mud is preferentially dolomitized before aragonitic peloids and shells. Greater susceptibility of lime mud to replacement is probably related to large surface areas of needle crystals and high initial porosities.

Neomorphic dolomitization of subtidal carbonate occurred in the westernmost core studied (Dreese #1). Original lime mud matrix was replaced by loose fabrics of rhombic dolomite crystals. Aragonitic shells rimmed by micrite envelopes were partially dissolved and partially replaced by coarse inclusion-rich dolomite (Fig. 39). Dissolution molds were later filled with clear rhombic dolomite and anhydrite cement (Figs. 39 and 40).

Many wackestones intercalated with packstones and grainstones were subjected to partial to intensive neomorphic matrix dolomitization. Calcitic shells in wackestones were largely unaltered by dolomitization (Fig. 41).

Occurrences of paramorphic dolomitization are limited to subtidal dolostones, where magnesium calcite shell textures of echinoderm components were preserved after dolomitization (Fig. 42). Elsewhere, echinoderms stabilized to calcite.

Diagenetic fabrics of dolostones may be classified using terminology developed by Friedman (1965). He prescribed the terms idiotopic, hypidiotopic and xenotopic to refer to euhedral, subhedral and anhedral crystals, respectively. Neomorphic replacement of lime mud initially produces idiotopic fabrics of loosely packed euhedral crystals with high intercrystalline porosities (Fig. 43). Continued flux of Mg-rich brines forms hypidiotopic fabrics of subhedral crystals produced by epitaxial cementation on earlier formed rhombs (Figs. 44 and 45). Epitaxial overgrowths restrict intercrystal pores and therefore significantly reduce porosity and permeability.

On a small scale, the introduction of clays and oxides into intercrystal pores inhibited overgrowth cementation in some supratidal dolostones (Fig. 46). Intercrystalline porosity of idiotopic fabrics may be preserved, or largely occluded by continued illuviation of clays.

A progression exists from limestones with scattered dolomite rhombic porphyroblasts to slightly dolomitic limestones to highly dolomitic limestones to dolostones. Most Five Finger limestones are slightly to very dolomitic. Dolomite is emplaced as cement in some primary voids (Figs. 30 and 37) and as porphyroblastic replacement of lime mud. In some instances, porphyroblastic replacement rhombs are scattered throughout the micritic matrix. Rhombs are euhedral, and crystal boundaries generally appear sharp and uncorroded (Fig. 47).

In some instances, epitaxial calcite cement crystals which line intrabiotic voids of calcitic shells are overlain and partially replaced by dolomite cement (Fig. 37). Dolomite cement crystals are then overlain by sparry calcite cement which fills the remainder of the void, and in some instances replaces earlier dolomite. This void-filling sequence represents an interruption in the normal vadose-phreatic cementation progression. Apparently, geochemical changes in pore fluids occurred to precipitate dolomite cement subsequent to epitaxial calcite, but prior to the introduction of phreatic calcite cement. In grainstones, coarse rhombic dolomite cement in interparticle voids is overlain by calcite spar. In some instances, dolomite cement rhombs were dedolomitized (Fig. 30).

Petrographic evidence suggests that three separate variables influenced dolomitization reactions: proximity to coastal areas where dolomitizing fluids probably evolved; ratios of original lime mud to grains; and volumes of magnesium calcite in sediments.

Dolomitizing fluids probably evolved beneath coastal plains along the western edge of the study area. In these areas, supratidal lime mud was penecontemporaneously dolomitized. Brines discharged laterally and seaward to replace subtidal carbonates at shallow depths. Continued discharge of magnesium-rich brines through previously dolomitized sediments up flow lines resulted in epitaxial overgrowth precipitation around earlier formed replacement rhombs. Five Finger dolostones in the #1 Dreese possess well-developed hypidiotopic fabrics where inter-crystal voids are largely filled by dolomite cement. Along the path of discharge, progressive magnesium depletion inhibited overgrowth cementation, and idiotopic fabrics were preserved farther seaward. Cuttings from the #1 Bowlus east of the Dreese well contain porous dolostone with preserved idiotopic fabrics. Evidence thus indicates that hypidiotopic fabrics in proximal areas grade into idiotopic fabrics down flow lines in an eastward direction primarily as a function of decreasing magnesium concentrations. Dolomitization effects thus diminished with increasing distance from coastal areas to the west.

The ratio of grains to original lime mud matrix in Five Finger sediments had a pronounced effect on subsequent dolomitization reactions. Wackestone textures of all carbonate lithofacies display partial to complete matrix dolomitization. Dolomitized wackestone intervals range in thickness from less than a foot to as much as five feet, and are overlain and underlain by limestone. Transitions from grainstones and packstones to wackestones are often gradual, and the degree of matrix replacement increases in proportion to increases in the lime mud matrix/grain ratio. The observed relationship may be explained by the fact that dolomite preferentially replaces aragonite before calcite and magnesium calcite. Studies by Matthews (1968) on Barbados indicate that an originally homogeneous distribution of calcitic nuclei will result in rapid calcitization of aragonitic sediment. Five Finger limestones consisting predominantly of calcitic shells (packstones and grainstones) were therefore calcitized, while wackestones with larger volumes of lime mud were preferentially dolomitized.

Limestones from the Garden C-10 core, located in more distal portions of the shelf, contain abundant porphyroblastic dolomite. Dolomite was emplaced as cement in body cavities of bioclasts, and as replacement of carbonate material. In rare instances, replacement dolomite is concentrated around magnesium calcite shells. The presence of porphyroblastic dolomite suggests that local sources of magnesium were available for dolomitization. Friedman (1964) and Land (1967) have shown that magnesium calcites lose their magnesium to an aqueous solution during stabilization to calcite. Jacka (1974b) documented a similar loss of magnesium from magnesium calcite shells. In such instances, magnesium released by silicification resulted in partial dolomitization of shells. Magnesium calcite in the matrix may have represented an additional minor local source of magnesium for dolomitization (Jacka, personal communication). Magnesium was thus apparently derived from the stabilization of high magnesium shells of bryozoans, foraminifers and echinoderms.

Anhydrite Emplacement

Anhydrite morphologies and diagenesis from supratidal areas of the present study resemble those described from modern environments of the Persian Gulf by Kinsman (1969) and Butler (1969), and ancient sabkhas of the Permian Basin by Jacka and Franco (1974).

Interstitially precipitated gypsum in sabkha sediments becomes replaced by anhydrite during seaward progradation of supratidal areas

(Kinsman, 1969). Replacement results from increased temperature and salinity of interstitial brines. Anhydrite replacement of gypsum forms isolated nodules, nodular mosaics and gypsum pseudomorphs of felted lath crystals (Jacka and Franco, 1974). As supratidal areas become increasingly isolated during progradation, anhydrite may precipitate directly as isolated nodules of felted lath crystals with no gypsum precursor (Kinsman, 1969).

Isolated anhydrite nodules occur in Five Finger supratidal deposits. Nodules formed as replacement of supratidal algal laminated and sabkha sediments (Fig. 18). In some instances, anhydrite nodules were recrystallized to large crystals of anhydrite spar. Boundaries of individual spar crystals are sharp, and transect numerous corroded lath crystals (Fig. 48). Coalescence of nodules in some intervals resulted in massive replacement of carbonates (Fig. 68). Anhydrite cement fills birdseye vugs (Fig. 19), dissolution molds (Fig. 40) and randomly oriented fractures (Fig. 44) in supratidal and subtidal Five Finger dolostones.

The most commonly observed anhydrite morphology is the sparry replacement porphyroblast (Figs. 49 and 58). These crystals possess distinctive rectangular stairstep outlines, as noted by Jacka and Stevenson (1977), and are abundant within subtidal limestones. Porphyroblasts nucleated in organic-rich material such as peloids, algal coated grains and shell fragments (Figs. 50 and 51). Although it preferred to maintain its rectangular morphology, sparry replacement porphyroblasts sometimes conformed to the shape of the material being replaced. In some instances, the internal, concentric morphology of algal coated grains was preserved after replacement (Fig. 31). Replacement fronts expanded outward from nucleation sites to replace adjacent matrix and grains. Coalescence of individual porphyroblasts produced patchwork replacement fabrics.

Discharge of fresh water fluids resulted in retrograde diagenesis of anhydrite to gypsum in some intervals. Some anhydrite was dissolved, or replaced by calcite and silica (Fig. 52). Leaching of anhydrite by fresh water has produced much of the open porosity observed in Five Finger limestones.

Anhydrite occurs within all carbonate lithofacies, but is most abundant within upper unit carbonates. Anhydrite probably was emplaced by calcium sulfate-enriched brines which discharged laterally and seaward through sediments. Dissolution and/or replacement occurred during subsequent subaerial exposure and fresh water diagenesis.

Silicification

Two separate episodes of silicification are recorded in Five Finger carbonates. The first involves early partial silicification of organic-rich allochems by length slow chalcedony and microquartz. Jacka (1974b and 1978) has shown that silica nucleates in organic-rich material such as shells, peloids and algal coated grains. Partial replacement of bioclasts is restricted to fragments of brachiopods, pelecypods and echinoderms (Figs. 38 and 53). Micritic material of peloids and algal coated grains was replaced by microquartz. Fibrous and prismatic shell layers of bioclasts were pseudomorphed by replacement silica. Partially silicified echinoderms contain rhombic dolomite inclusions in areas of silica replacement. The dolomite, some of which is ferroan, is optically continuous with unreplaced monocrystals (Fig. 54). Similar occurrences of dolomite associated with silicification have been described by Jacka (1974b) from Middle Permian carbonates of the Delaware Basin. According to Jacka (1974b), dolomite exsolves from centers of magnesium enrichment in magnesium calcite shells as a result of ionic mobilization associated with silicification. Magnesium for dolomite nucleation thus was derived locally from high magnesium echinoderm components.

The timing of silicification relative to other diagenetic reactions is difficult to predict, because replacement silica rarely extended beyond shell margins. There are some instances where silica extended beyond boundaries of echinoderms to partially replace surrounding epitaxial overgrowths. This indicates that partial silicification of shells occurred before or during initial fresh water stabilization and cementation. Partial silicification of shells suggests that organic decomposition products provided a microenvironment conducive to silicification (Jacka, 1974b). Silica was probably derived from fresh meteoric groundwater, which is normally saturated with SiO_2.

Late diagenetic reactions involve migration of silica replacement fronts to produce nodular chert in some intervals (Fig. 26). Micritic material (micrite matrix, peloids and algal coated grains) was replaced by microquartz (Figs. 55 and 56), and shells were replaced by length-slow chalcedony (Fig. 57). Calcite shells and cement were least susceptible to replacement, and in many instances resisted complete silicification. Voids not cemented with carbonate were filled with void-filling varieties of silica such as length-fast chalcedony and megaquartz (Figs. 56 and 57).

Large ferroan dolomite rhombs were observed within silicified areas, and probably represent additional exsolution phenomena.

Euhedral quartz overgrowths are present on some detrital quartz grains scattered within limestones. Their development occurred by replacement of surrounding carbonate material, which may be preserved within individual overgrowths (Fig. 59). Silica also was emplaced as replacement porphyroblasts in organic rich material.

Replacement of porphyroblastic and nodular anhydrite by length-slow chalcedony is observed in all carbonate facies (Fig. 52). In some instances, individual lath crystals of replacement nodules were pseudomorphed by silica.

Occurrences of Pyrite

Pyrite occurs as thin stringers of disseminated cubes, and as replacement of small shell fragments (Fig. 60). Pyrite was emplaced in organic rich material of micro-reducing environments. Emplacement probably occurred prior to precipitation of anhydrite, because pyrite and other material contained within solution residue stringers are displaced and engulfed by anhydrite porphyroblasts.

CHAPTER V

POROSITY AND PERMEABILITY RELATIONSHIPS

Porosity in Five Finger carbonates is a result of diagenetic processes superimposed on original depositional processes. Original primary porosity is depositionally controlled, while secondary and tertiary porosity developed by later diagenesis. In this chapter, observed porosity types are described, and diagenetic processes which controlled occlusion and preservation of porosity are discussed.

Primary Porosity

Primary porosity occurs as internal cavities of bioclasts, and as interparticle void space between allochems. Grainstones in upper unit carbonates, and upper portions of lower unit carbonates contained very high porosities and permeabilities following deposition. Although some primary pores were filled partially by submarine cement (Fig. 30), most primary porosity was occluded by meteoric cementation in a fresh water environment (Fig. 36). Some primary voids also were cemented partially by dolomite (Fig. 30). Although very little intergranular porosity was preserved, body cavities of some micritized shells are partially open (Fig. 61). In most cases this can be attributed to the inhibiting effect of micritization on cementation. Jacka (1978) discovered that cementation rates are lowest on micritic foundations. Moreover, cementation rates are faster in the meteoric phreatic zone than in the vadose environment. Prolonged exposure to low salinity fluids therefore resulted in a high degree of primary porosity occlusion by meteoric cementation. Limited residence time in the fresh water phreatic environment yielded only partially cemented voids.

Secondary Porosity

Secondary porosity in Five Finger carbonates consists of dissolution molds, nontectonic fractures, fenestral cavities (birdseye vugs), and intercrystal voids in neomorphic dolostones.

Dissolution molds record leaching of aragonitic shells by fresh water, and are represented by biomolds and hollow micrite envelopes. Molds are cemented largely by calcite (Figs. 33 and 36), although some also are cemented by sparry anhydrite and dolomite (Figs. 39 and 40). Hollow micrite envelopes are abundant in Five Finger packstones and grainstones, while biomolds occur largely in mud-rich wackestones. Very little biomoldic porosity is preserved due to extensive cementation. However, in some areas hollow micrite envelopes contribute significantly to porosity in upper unit carbonates.

Some minor fractures occur in upper unit carbonates, and upper portions of lower unit carbonates (Fig. 35). Fractures are generally vertically oriented, and probably result from early dissolution of aragonitic shells and partial collapse of carbonate sediment prior to lithification. Some minor fractures occur in dolostones, and are filled with coarse, blocky dolomite cement (Fig. 67). Five Finger carbonates do not exhibit extensive fracture development, except in the Smalley "C" 1-A, where vertical fractures are well developed in the upper carbonate unit. At least a portion of the fractures, however, are artifacts of the coring operation, because no cement or internal sediment were observed in fractures.

Fenestral cavities, or birdseye vugs, are postdepositional features produced by shrinkage and decay of algal mats in supratidal areas. Birdseye vugs are common in Five Finger stromatolitic supratidal dolostones, and are partially to completely cemented by dolomite and anhydrite (Fig. 19).

Neomorphic dolomitization of subtidal upper unit carbonates in the #1 Dreese produced loose, idiotopic fabrics possessing significant intercrystal pore space. Later epitaxial dolomite cementation formed compromise boundaries in voids, and occluded much of the porosity to form hypidiotopic fabrics (Fig. 44). Intercrystalline porosity in supratidal stromatolitic dolostones is occluded to varying degrees by dolomite cement, and in minor isolated instances by clays and oxides. Other Five Finger neomorphic dolostones contain minor amounts of intercrystalline porosity, where pores are poorly formed and lack interconnection. Apparently, the dolomitization process was terminated before significant intercrystal pore space could develop.

Tertiary Porosity

In many instances, anhydrite, emplaced in carbonates, was dissolved by fresh water to produce tertiary moldic porosity. Anhydrite molds display blocky, stairstep outlines which directly reflect the original crystal morphology of sparry replacement porphyroblasts. Molds are partially to completely cemented by dolomite, calcite and second generation anhydrite (Figs. 62 and 63). Anhydrite moldic porosity is best developed in upper unit carbonates, where emplacement of anhydrite porphyroblasts and later dissolution by fresh water occurred on a large scale (Fig. 64).

Distribution of Porous Carbonates

Within the Five Finger interval, upper unit carbonates contain the best porosity and permeability. Porosity development is largely due to postdepositional diagenesis which resulted in incomplete cementation of primary voids, and the development of secondary and tertiary porosity.

The most porous Five Finger limestones occur in upper unit carbonates of the #1 Rose (Fig. 29), where some residual primary porosity has been preserved. Deposition of regressive clastics over porous upper unit carbonates may have formed a partial seal which retarded downward percolation of fresh water into subjacent limestones. Positioning of clastic material over porous carbonates may have prevented the establishment of donor-receptor relationships, as described by Jacka and Brand (1977). In such instances, some original primary porosity may have been preserved due to limited fresh water diagenesis and cementation.

Early leaching of aragonitic shells, and later dissolution of anhydrite by fresh water, produced second and third order voids which enhanced original primary porosities.

Anhydrite molds are abundant in upper unit carbonates of the #1 Rose, and may indicate that generation and seaward discharge of Ca-rich hypersaline brines occurred on a large scale in northern portions of the study area. The structurally higher position of the #1 Rose well relative to surrounding areas probably resulted in numerous and extended periods of subaerial exposure. Fresh water diagenesis associated with periods of emergence leached large amounts of anhydrite that was emplaced in carbonates during more arid progradational cycles. The #1 Rose well appears to have been located along seaward flanks of low relief structures in an area of high energy subtidal carbonate deposition (Fig. 16). It is likely that depositional patterns, diagenesis and porosity development are similar in carbonates deposited along seaward margins of these structures both north and south of the #1 Rose well.

Significant porosity in Five Finger dolostones occurs primarily in supratidal deposits which cap upper and lower unit carbonates. Relatively tight dolostones of the #1 Dreese probably represent more proximal portions of progradational cycles. Intercrystalline porosity of these dolostones is largely occluded by epitaxial dolomite cementation (Fig. 45). Progressive Mg depletion of dolomitizing fluids that discharged seaward may have precluded epitaxial cementation in neomorphic dolostones east of the #1 Dreese well. Significantly, thin sections of cuttings from the #1 Bowlus contain neomorphic dolostone with preserved intercrystalline voids (Fig. 43). The lateral extent of dolostone facies north or south of the #1 Dreese well cannot be accurately determined without additional core or sample control. Because no comparable dolostone facies are present in the four southernmost cores examined (wells 9-12), it may be possible that supratidal "lobes" extended farther seaward in northern as compared to southern portions of the study area. Moreover, shallower water in northern portions of the study area probably facilitated progradation of supratidal facies seaward. Dolomitizing environments and porous dolostone facies were thus extended farther to the east in these areas. Slightly deeper water in shelf areas of southern portions may have inhibited seaward progradation of coastal plain facies. Porous dolostone facies, if present, must exist farther to the west (landward) because they do not occur in cores examined from southern parts of the study area. Carbonates of these cores may represent more distal portions of progradational cycles, where seaward discharge of Mg-rich fluids and associated dolomitization did not occur on a sufficient scale to produce porous dolostone.

Landward (westward) of the #1 Dreese well, the Five Finger zone consists of dolostones which represent proximal portions of progradational cycles. Intercrystal voids in these dolostones probably are tightly cemented by epitaxial dolomite overgrowths and anhydrite. These dolostones are thus nonporous, and do not constitute reservoir quality rock. They may actually serve as vertical and in part horizontal permeability barriers for porous carbonates to the east.

Porous supratidal dolostones which cap the Five Finger zone in the Tate-Hutton #2 may have developed in the lee of low relief islands which possibly existed offshore. These dolostones contain significant open porosity in the form of intercrystal voids, birdseye vugs and anhydrite molds. Supratidal algal mat facies may have developed along landward margins of these structures in a general north-south direction (Fig. 16).

Analysis of the four cores in Stevens County (wells 9-12) reveals a general decline in reservoir quality in southern portions of the study area. Three of these cores possess carbonate units containing higher percentages of admixed clastics compared with cores to the north. Lower unit transgressive carbonates consist of relatively thick sequences of clastic-rich wackestone and packstone, while regressive carbonates of the upper unit are thin and poorly developed. However, upper and lower unit carbonates in the Kimzey 1-A core contain relatively clastic-free grainstone and packstone. The large volumes of primary porosity in these carbonates were occluded largely by meteoric cementation (Fig. 27), but some open pore space does exist as minor residual primary pores and small anhydrite molds.

Upper unit carbonates of the Neer "A" #1 contain a porous zone consisting mainly of tertiary anhydrite molds (Fig. 64). This zone, however, is very thin (1-2 feet) compared to porous upper carbonates of the #1 Rose to the north.

CHAPTER VI

PARAGENESIS

Deposition of Five Finger carbonates occurred in supratidal, intertidal and subtidal environments of arid coastal plains and adjacent shallow shelf areas. Their depositional and diagenetic history initiated in the subtidal environment, where original mineralogies consisted of aragonite and high magnesium calcite. Bioclasts were micritized and bound together by the action of blue-green algae. Grainstones deposited in higher energy peritidal marine environments developed thin fibrous to bladed submarine crusts which lined primary voids in a few intervals.

Interstitial precipitation of gypsum in seaward portions of supratidal areas elevated Mg/Ca ratios, leading to penecontemporaneous dolomitization of aragonitic lime mud. Inland from and approximately parallel to zones of gypsum precipitation, anhydrite replaced gypsum in response to increasing temperature and salinity of interstitial brines.

Early subaerial exposure led to mineralogical stabilization of subtidally deposited carbonates. Aragonitic lime mud inverted to calcite micrite, and aragonitic shells either recrystallized to calcite, or dissolved to form biomolds and hollow micrite envelopes. Magnesium calcite shells stabilized to calcite with preservation of original shell textures.

Subtidal carbonates were exposed to early Mg-rich fluids which discharged seaward to emplace dolomite as cement in primary voids and as replacement of lime mud. Initial cementation sequences involved epitaxial calcite, dolomite and ferroan and nonferroan calcite. Magnesium for porphyroblastic dolomite emplacement in dolomitic limestones was derived locally from the stabilization of magnesium calcite shells, and possibly from magnesium calcite in lime mud. Extensive neomorphic matrix dolomitization in wackestones resulted from exposure to dolomitizing fluids which discharged seaward from beneath coastal plains.

Cyclic fluid invasion sequences can be recognized from Five Finger carbonates. Paragenetic sequences closely resemble those from Middle Permian (Guadalupian) carbonates of the Permian Basin as reported by Jacka and others (1980), and from Horquilla carbonates (Pennsylvanian-Permian) of the Big Hatchet Peak section in New Mexico described by Thompson and Jacka (1981). Discharge of fluids usually occurs in the following sequence:

1) Dolomitizing fluid;
2) Anhydritizing fluid;
3) Low salinity (fresh water) fluid.

Fluid invasion sequences involve cyclic episodes of fresh and salt water diagenesis. Magnesium rich fluids discharged seaward to neomorphically replace unstable carbonate material. Dolomitization of aragonitic lime mud produced rhombic crystal textures with initially high intercrystalline porosities. Many shells were partially dissolved and partially replaced by dolomite. Continued flux of the dolomitizing fluid precipitated epitaxial dolomite cement on initial rhombs. Epitaxial cements formed compromise boundaries and largely restricted secondary intercrystal pores. Dolomitizing fluids were followed by calcium sulfate-rich fluids which emplaced anhydrite as cement in fractures and dissolution molds, and as porphyroblasts in subtidal sediments. Anhydritizing brines were replaced by low salinity fluids which dissolved anhydrite to produce third-order voids (tertiary porosity). In many instances, a second dolomitizing fluid emplaced dolomite cement in tertiary voids, and a second anhydritizing fluid emplaced second generation anhydrite in first generation anhydrite molds (Figs. 65 and 66).

In some intervals, calcitization occurred as the initial step. Subsequent dolomitizing fluids emplaced dolomite as cement and partial replacement of lime mud. Calcium-sulfate-rich hypersaline brines next emplaced anhydrite as replacement porphyroblasts. Anhydrite was dissolved out by subsequent low salinity fluids to leave tertiary, third-order voids. Leaching of anhydrite may have enriched groundwaters with calcium for dedolomitization. A second dolomitizing fluid precipitated dolomite cement in some intervals, although this is not commonly observed. The last diagenetic fluids to discharge through many carbonate sediments were low salinity fluids which dissolved some anhydrite, or replaced it with silica, calcite or gypsum.

Although both diagenetic histories are composed of similar fluid invasion sequences, the major difference lies in the chemistry of the initial fluid. In some instances, it is a Mg-rich dolomitizing fluid, while in others it is a low salinity fluid. Chemistry of the initial fluid appears to be controlled by proximity to coastal areas beneath which dolomitizing fluids probably are generated, and from which they migrate in a general seaward direction. Increasing distance from coastal areas may result in a lack of dolomitization, and subsequent calcitization of carbonate sediments. It is important to emphasize that the chemistry of discharging fluids (whether fresh or saline) and their flux within sediments largely control diagenesis and resultant porosity preservation and occlusion. In addition, fresh water fluids may affect numerous diagenetic changes, such as the dissolution of anhydrite, the replacement of anhydrite by silica, calcite and gypsum, or the replacement of dolomite by calcite (dedolomitization). The point at which the fluid invasion sequence is terminated largely determines whether porosity is occluded or preserved. Termination of the sequence at any one point appears to be controlled by eustatic sea level fluctuations and associated climatic changes, although other factors also may be involved.

Generation of anhydritizing brines is generally believed to occur during progradational episodes when sea levels are at a high stillstand and climates are arid. While this may be true in many cases, it is also possible that anhydritizing brines evolve during times of increased rainfall associated with subaerial exposure (Jacka, personal communication). In such instances, brines may become enriched in calcium sulfate by dissolution of anhydrite up flow lines in more proximal portions of diagenetic cycles. If this is true, parts 2 and 3 of the fluid invasion sequence (i.e. anhydritizing fluids and low salinity fluids) may be triggered by the same causal process of increased rainfall associated with subaerial exposure.

CHAPTER VII

CONCLUSIONS

1. Five Finger carbonates were originally deposited on a broad homoclinal to monoclinal structure striking approximately north-south across the study area. Shelf carbonates dip to the east and southeast at approximately 16 feet per mile. Major structure consists of small anticlines which develop as much as 50 feet of closure in eastern portions of Grant and Kearny Counties. Other small flexures are superimposed on regional structure throughout the study area.

2. From the base upward, the following vertical sequence of lithofacies is recorded in Five Finger carbonates: 1) lower carbonate unit, 2) middle clastic-carbonate unit and 3) upper carbonate unit. Lower unit carbonates are transgressive, and record deposition within low energy and high energy subtidal environments. Subtidal lower unit shelf carbonates change facies updip (westward) to supratidal stromatolitic dolostones, which cap lower carbonates in the westernmost core studied. The middle clastic-carbonate unit consists of dark calcareous shales and shaly wackestones deposited in low energy subtidal environments. Continental red-brown clastics constitute updip equivalents to marine shales farther shelfward. Upper carbonates are regressive, and record deposition in subtidal, intertidal and supratidal environments. The upper carbonate unit is capped by supratidal stromatolitic dolostones in some areas.

3. Five Finger carbonates are overlain and underlain by regressive continental clastics, which represent deposition in inland sabkhas, brine pans and deflation flats.

4. Five Finger carbonates were deposited predominantly in the subtidal marine environment, where original mineralogies consisted of aragonite and high magnesium calcite. Carbonate allochems were micritized intensively by blue-green algae. Algal coated grains are abundantly represented. Some grainstones developed isolated thin fibrous to bladed submarine cement crusts in primary voids.

5. Stabilization of most carbonates occurred during periods of subaerial exposure and fresh water diagenesis. Aragonitic lime mud inverted to calcite micrite, and aragonite shells either dissolved, or recrystallized to calcite with preservation of original shell textures. Primary and secondary porosity was largely occluded by meteoric cementation in the fresh water phreatic environment.

6. Some dolomitization occurred within subtidal and supratidal environments of Five Finger carbonates. Petrographic evidence suggests that three separate variables controlled dolomitization reactions: 1) proximity to coastal areas where dolomitizing fluids probably evolved, 2) ratios of original lime mud to grains, and 3) volumes of magnesium calcite in sediments.

7. Anhydrite was emplaced in Five Finger carbonates as cement, and as replacement nodules and porphyroblasts.

8. Five Finger carbonates record complex diagenetic histories, involving numerous cyclic fluid invasion sequences consisting of 1) Mg-rich dolomitizing fluids, 2) Ca-rich anhydritizing fluids and

3) low salinity meteoric groundwaters.

9. Upper unit carbonates contain the best porosity and permeability recorded in the Five Finger interval. Porous dolostones contain intercrystal voids, birdseye vugs and anhydrite molds. Porous limestones contain some residual primary porosity, small amounts of secondary moldic porosity, and large amounts of tertiary anhydrite moldic porosity. Porous carbonates are largely confined to northern portions of the study area, where dolomitization and associated emplacement and leaching of anhydrite accompanied more laterally extensive progradational cycles.

LIST OF REFERENCES

Bathurst, R.G.C., 1964, The replacement of aragonite by calcite in the molluscan shell wall, In: Imbrie, J. and Newell, N.D. (ed.), Approaches to Paleoecology. Wiley, New York, N.Y., pp. 357-376.

_____, 1966, Boring algae, micrite envelopes and lithification of molluscan biosparites: Liverpool Manchester Geol. Journal, 5:15-32.

_____, 1975, Carbonate Sediments and their Diagenesis: Developments in Sedimentology, v. 12, 2nd Enlarged Edition, Elsevier, Amsterdam, 658 pp.

Butler, G.P., 1969, Modern evaporite deposition and geochemistry of coexisting brines, the sabkha, Trucial Coast, Arabian Gulf: Jour. Sed. Petrology, 39:70-89.

Evans, G., Schmidt, V., Bush, P., and Nelson, H., 1969, Stratigraphy and geologic history of the sabkha, Abu Dhabi, Persian Gulf: Sedimentology, 12:145-159.

Friedman, G.M., 1964, Early diagenesis and lithification in carbonate sediments: Jour. Sed. Petrology, 34:777-813.

_____, 1965, Terminology of crystallization textures and fabrics in sedimentary rocks: Jour. Sed. Petrology, 35:643-655.

Garlough, J.L. and Taylor, G.L., 1941, Hugoton Gas Field, Grant, Haskell, Morton, Stevens, and Seward Counties, Kansas, and Texas County, Oklahoma, In: Levorsen, A.I. (ed.), Stratigraphic Type Oil Fields - a Symposium, Am. Assoc. Petroleum Geologists, pp. 78-104.

Gavish, E. and Friedman, G.M., 1969, Progressive diagenesis in Quaternary to Late Tertiary carbonate sediments: sequence and time scale: Jour. Sed. Petrology, 39:980-1006.

Hemsell, C.C., 1939, Geology of Hugoton Gas Field of southwestern Kansas: Am. Assoc. Petroleum Geologists Bull., 23:1054-1067.

Hubbert, M.K., 1953, Entrapment of petroleum under hydrodynamic conditions: Am. Assoc. Petroleum Geologists Bull., 37:1954-2026.

Illing, L.V., Wells, A.J., and Taylor, J.C.M., 1965, Penecontemporary dolomite in the Persian Gulf, In: Pray, L.C. and Murray, R.C. (ed.), Dolomitization and Limestone Diagenesis, a Symposium: Soc. Econ. Paleontologists and Mineralogists, Spec. Publ. no. 13, pp. 89-111.

Jacka, A.D., 1974a, Differential cementation of a Pleistocene carbonate fanglomerate, Guadalupe Mountains: Jour. Sed. Petrology: 44:85-92.

_____, 1974b, Replacement of fossils by length-slow chalcedony and associated dolomitization: Jour. Sed. Petrology: 44:421-427.

_____, 1975, Observations on paramorphic and neomorphic dolostones and associated porosity relationships (abs.): Am. Assoc. Petroleum Geologists Annual Convention Book of Abstracts, pp. 38-39.

_____, 1978a, Deposition and diagenesis of the Fort Terett Formation (Edwards Group) in the vicinity of Junction, Texas, In: Bebout, D.G. and Loucks, R.G. (ed.), Cretaceous Carbonates of Texas and Mexico, applications to subsurface exploration: Bur. Econ. Geology, Univ. of Texas (Austin), Inv. Rept. No. 89, pp. 182-200.

Jacka, A.D., Barone, W.E., Muir, N.J., Foley, D.C., Tully, T., and Worthen, J.A., 1980, Cyclic hydrologic and diagenetic events in the San Andres Formation - geologic implications (abs.): Am. Assoc. Petroleum Geologists, Southwest Section, Annual Convention Book of Abstracts, p. 37, 27.

Jacka, A.D. and Brand, J.P., 1977, Biofacies and development and differential occlusion of porosity in a Lower Cretaceous (Edwards) reef: Jour. Sed. Petrology: 47:366-381.

Jacka, A.D. and Franco, L.A., 1974, Deposition and diagenesis of evaporites and associated carbonates and clastics on shelf areas of the Permian Basin: Fourth International Symposium on Salt, Northern Ohio Geol. Society, pp. 67-89.

Jacka, A.D. and Stevenson, J.C., 1977, The JFS Field, Dimmit County, Texas - some unique aspects of Edwards-McKnight diagenesis: Gulf Coast Assoc. Geol. Soc. Trans., 27:45-60.

Jewett, J.M., 1960, How major geologic features developed in Kansas: World Oil, Jan.:119-124.

Johnson, J.H., 1946, Lime-secreting algae from the Pennsylvanian and Permian of Kansas: Geol. Soc. America Bull., 57:1087-1120.

Kendall, C.G.St.C. and Skipwith, P.A.d'E., 1969, Holocene shallow-water carbonate and evaporite sediments of Khor al Bazam, Abu Dhabi, southwest Persian Gulf: Am. Assoc. Petroleum Geologists Bull., 53:841-869.

Kinsman, D.J.J., 1969, Modes of formation, sedimentary associations, and diagnostic features of shallow water and supratidal evaporites: Am. Assoc. Petroleum Geologists Bull., 53:830-840.

Land, L.S., 1967, Diagenesis of skeletal carbonates: Jour. Sed. Petrology, 37:914-930.

Lindholm, R.C. and Finkelman, R.B., 1972, Calcite staining: semi-quantitative determination of ferrous iron: Jour. Sed. Petrology, 42:239-242.

Mason, J.W., 1968, Hugoton Panhandle Field, Kansas, Oklahoma and Texas, In: Beebe, B.W. (ed.), Natural Gases of North America - a Symposium, Mem. 9, 2:1539-1547.

Matthews, R.K., 1968, Carbonate diagenesis: equilibrium of sedimentary mineralogy to the subaerial environment: coral cap of Barbados, West Indies: Jour. Sed. Petrology, 38:1110-1119.

Merriam, D.F., 1956, Hugoton Embayment commands fresh look: Oil and Gas Jour., 54:82-86.

Page, J.H., 1940, Larger gas fields in Kansas: Am. Assoc. Petroleum Geologists Bull., 24:1779-1797.

Pingatore, N.E., 1970, Diagenesis and porosity modification in Acropora Palmata, Pleistocene of Barbados, West Indies: Jour. Sed. Petrology, 40:712-721.

Pippin, L., 1969, Panhandle-Hugoton Field, Texas-Oklahoma-Kansas-the first fifty years, In: Halbouty, M.T. (ed.), Geology of Giant Petroleum Fields - a Symposium: Am. Assoc. Petroleum Geologists Mem. 14, pp. 204-222.

Steinen, R.P., 1974, Phreatic and vadose diagenetic modification of Pleistocene limestone: Petrographic observations from subsurface of Barbados, West Indies: Am. Assoc. Petroleum Geologists Bull., 58:1008-1024.

Thomas, G.F., 1956, What the Hugoton activity means: World Oil, v. 142, no. 2, pp. 75-82.

Thompson, S. and Jacka, A.D., 1981, Pennsylvanian stratigraphy, petrography, and petroleum geology of Big Hatchet Peak section, Hidalgo County, New Mexico: New Mexico Bur. of Mines and Mineral Resources, Circular 176, 125 pp.

Toomey, D.F., 1974, Algally coated grains from the Leavenworth Limestone (U. Pennsyl., Midcontinent Region, USA.), In: Neues Jahrbuch f. Geologic and Paleontologic Monatshefte, #3, pp. 175-191.

Twenhofel, W.H., 1919, Precambrian and Carboniferous algal deposits: Am. Jour. Sci., 4th Ser., 48:339-352.

Watney, W.L., 1980, Cyclic sedimentation of the Lansing-Kansas Groups in northwestern Kansas and southwestern Nebraska: Kansas Geol. Survey, Bull. 220, pp. 1-72.

Worden, J.A., 1959, Amarillo-Hugoton: fast-growing giant: Oil and Gas Jour., 57:128-130.

APPENDIX A

NAMES AND LOCATIONS OF CONTROL WELLS USED IN THIS STUDY

Well No.	Operator/Well Name	County	Sample Type	Location
1.	Computer Pet. Expl. Dreese #1	Hamilton	core	11-21S-40W
2.	Wagner and Brown Rose #1	Kearny	core	34-21S-37W
3.	Champlin Garden C-10	Finney	core	16-23S-34W
4.	Amoco Miles Gas Unit "B" #2	Kearny	core	29-23S-37W
5.	Amoco Dotson Gas Unit #3	Kearny	core	15-24S-37W
6.	W. B. Osborn Smalley "C" 1-A	Kearny	core	2-25S-38W
7.	Amoco Tate-Hutton Gas Unit #2	Kearny	core	28-25S-37W
8.	Amoco Eveleigh Gas Unit "A" #2	Kearny	core	23-26S-38W
9.	Anadarko Rhinehart Estate "C" #1	Stevens	core	22-32S-38W
10.	Anadarko Neer "A" #1	Stevens	core	7-33S-38W
11.	Anadarko Light "D" #1	Stevens	core	34-33S-39W
12.	Anadarko Kimzey "A" #1	Stevens	core	1-34S-38W
13.	M. L. Brown M. Maune #1	Kearny	cuttings	22-21S-38W
14.	W. B. Osborn Miller #3	Kearny	cuttings	6-22S-37W
15.	W. B. Osborn Bowlus #1	Kearny	cuttings	21-22S-37W
16.	W. B. Osborn Davis #2-A	Kearny	cuttings	35-22S-37W

APPENDIX B

DRAFTED ILLUSTRATIONS, PHOTOGRAPHS AND PHOTOMICROGRAPHS

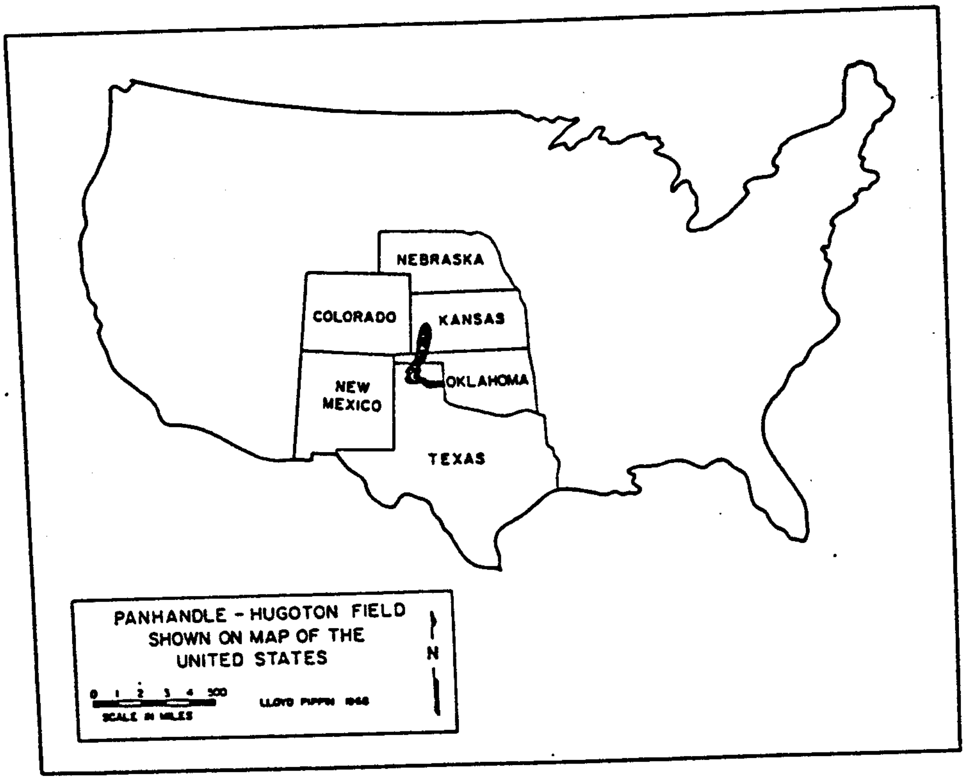

Fig. 1.--Index map showing the location of the Panhandle-Hugoton Field.

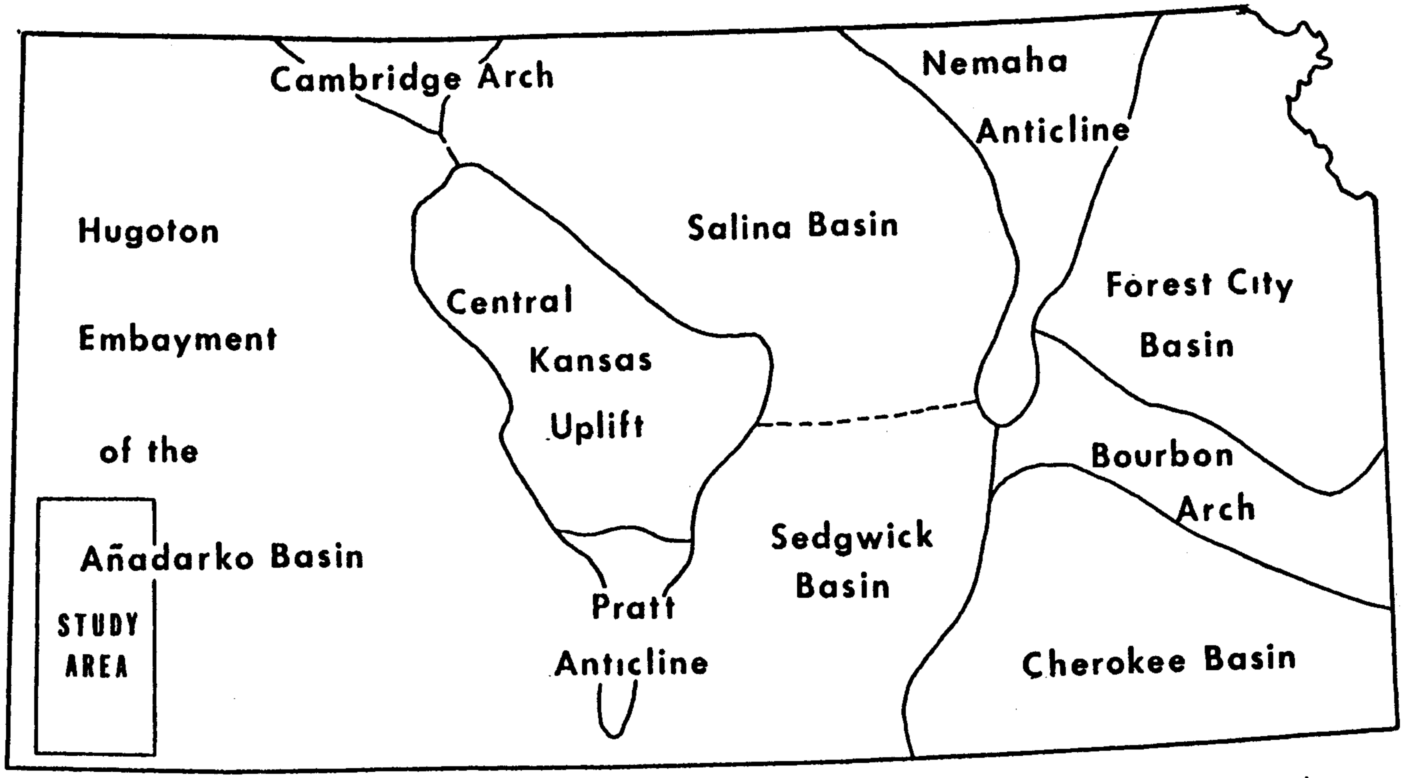

Fig. 1.1.--Paleogeographical province map showing the location of the study area (adapted from Jewett, 1960).

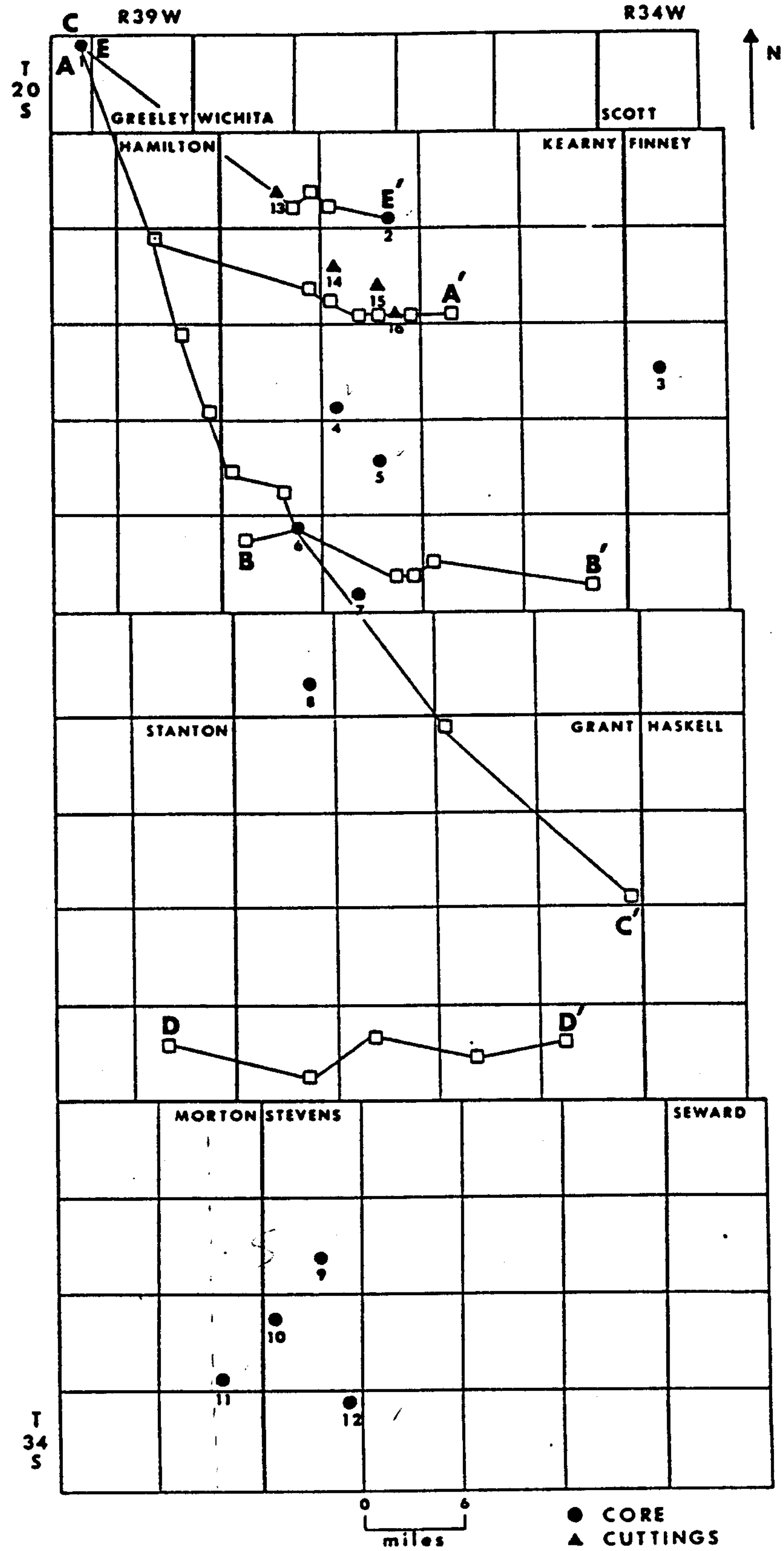

FIGURE 2 - LOCATION OF CONTROL WELLS
LINES OF CROSS SECTION SHOWN

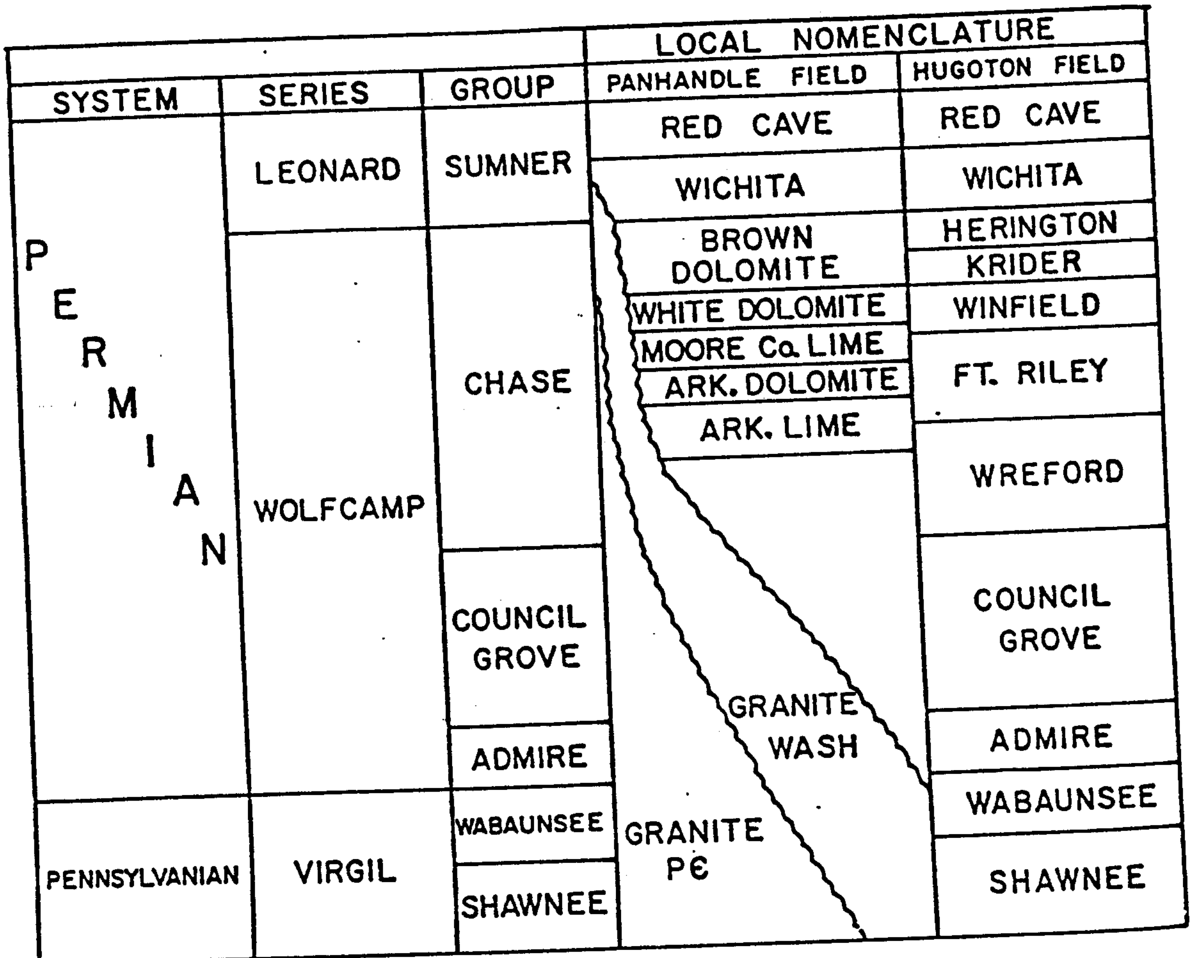

Fig. 3.--Stratigraphic column of the Panhandle-Hugoton Field.

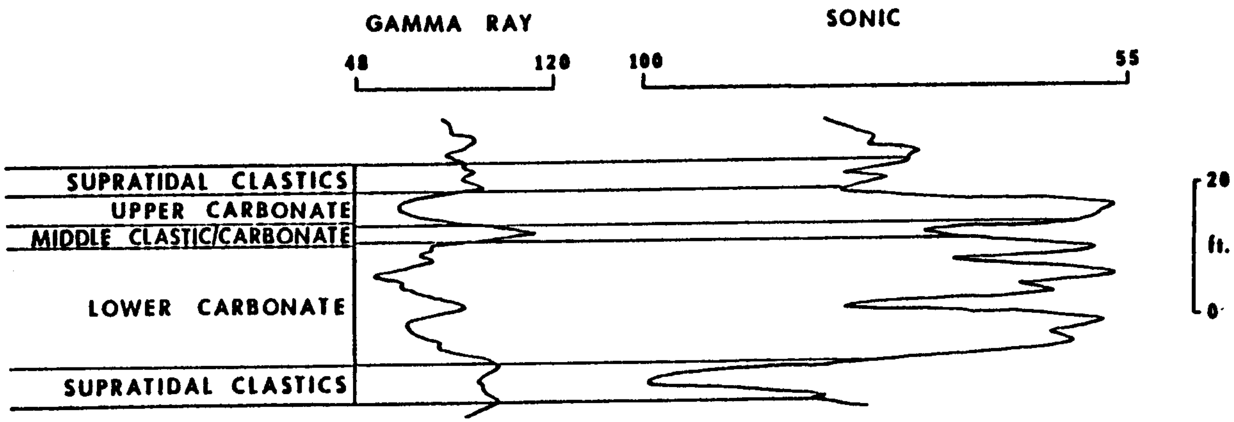

Fig. 15.--Delineation of lithofacies and associated clastics on a gamma ray log of the Smalley "C" 1-A.

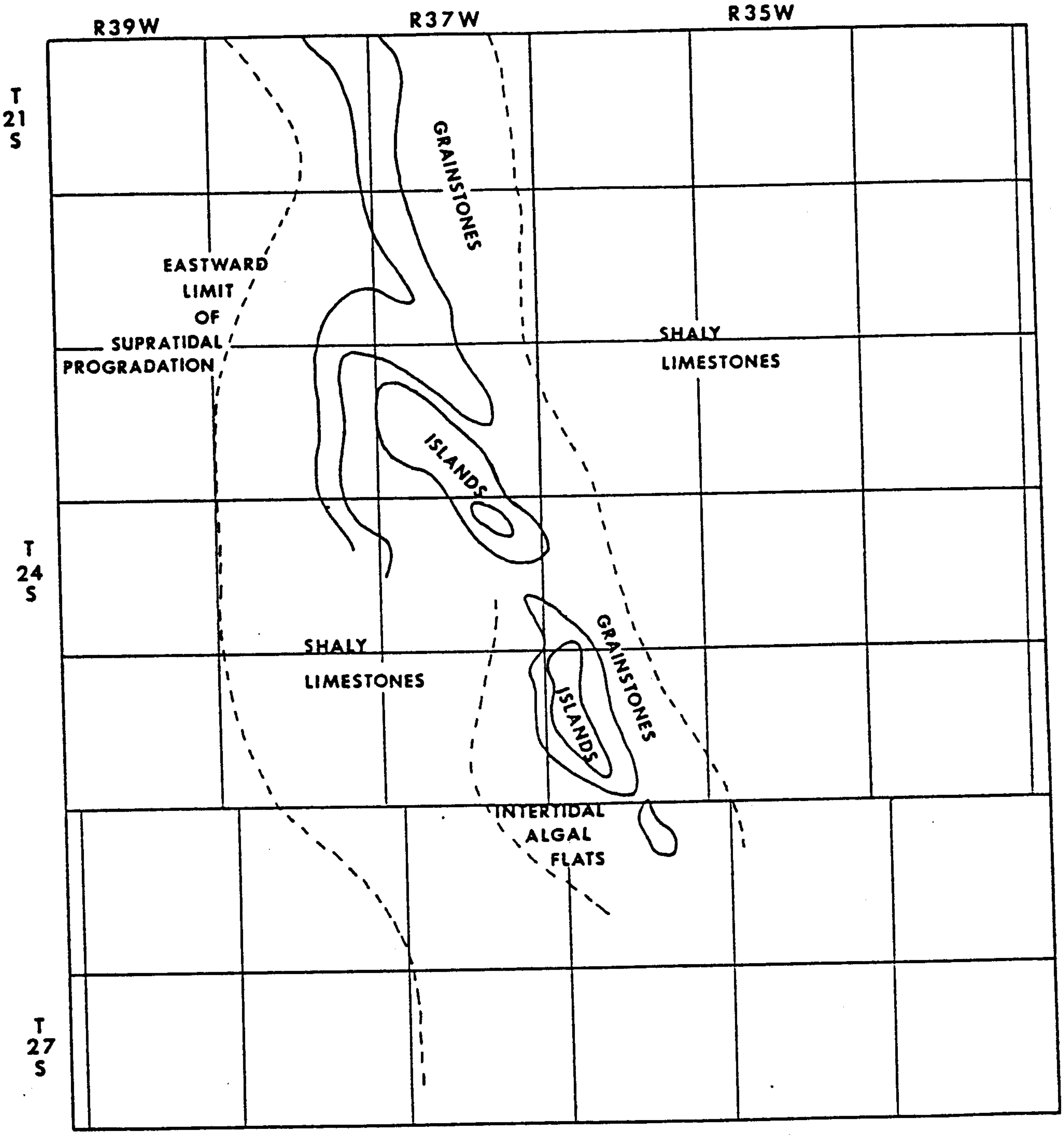

Fig. 16.--Distribution of depositional environments.

Some micrographs were taken with a reticle that superimposes a micrometer grid across the center of the field. The scale of each photo is indicated according to the smallest division of the grid, d, which ranges from 5.2 to 120 microns, which are herein designated by u; one micron equals 0.0001 mm.

Some micrographs contain a bar scale which is imprinted along the margins of the field. The appropriate scale is shown in microns (u) and millimeters (mm).

Micrographs taken under crossed polarizers are specified with an X. Those taken in plane polarized light are given no designation. All thin sections were stained with potassium ferricyanide and alizarin-red S which stains normal calcite red, ferroan calcite purple-red and ferroan dolomite blue. Normal dolomite is unstained.

In some micrographs key features are labelled with letter symbols, which are explained in captions.

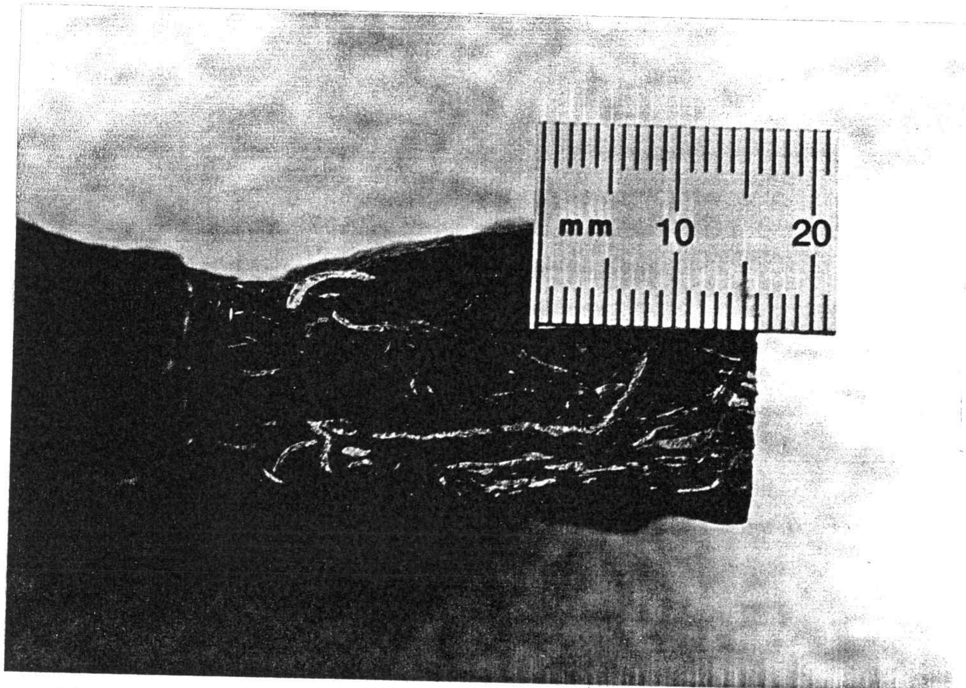

Fig. 17.--Core chip of dark fossiliferous shale from the middle clastic-carbonate unit of the Amoco Eveleigh "A" #2 (2771 ft.).

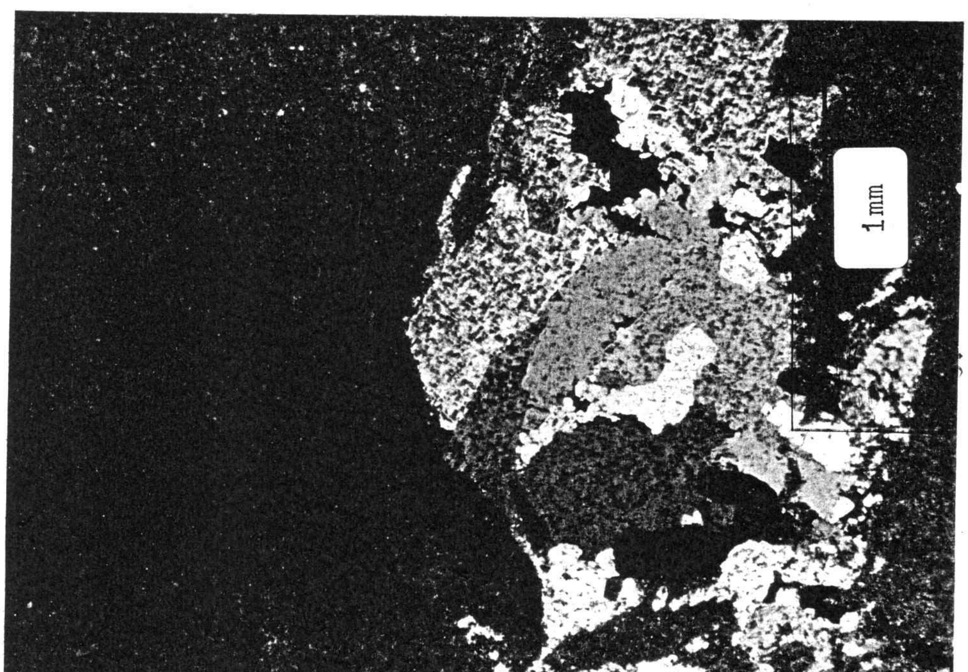

Fig. 18.--Tate-Hutton #2, 2673.5 ft., (X). Supratidal dolostone with nodular anhydrite. Aragonitic sabkha mud was penecontemporaneously dolomitized to microcrystalline dolomite.

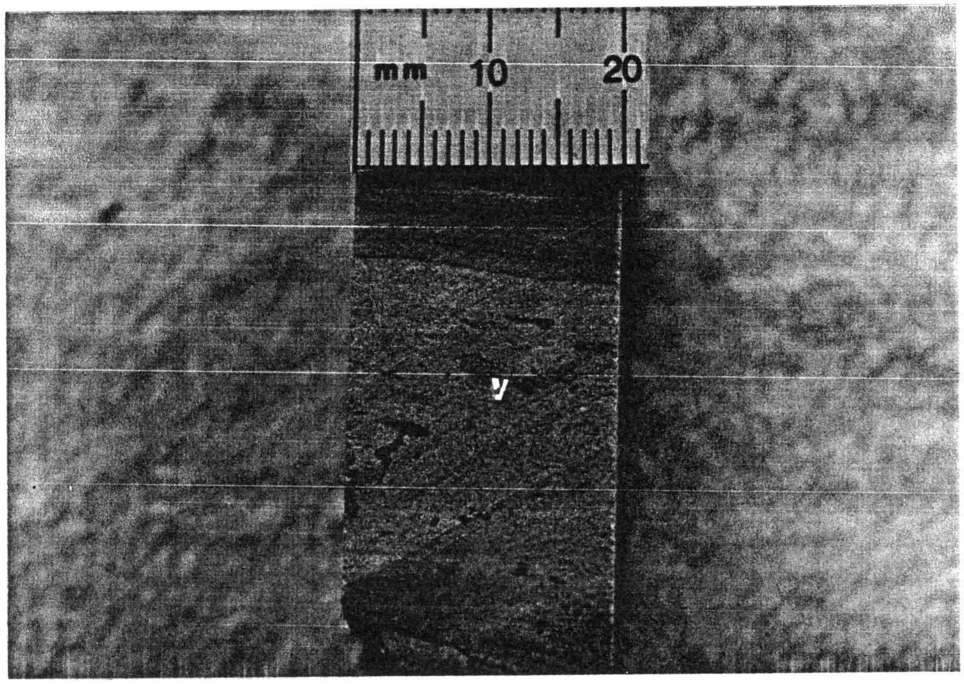

Fig. 19.--Core chip of supratidal stromatolites from the Amoco Eveleigh "A" #2 (2750 ft.), containing several birdseye vugs (V) cemented by anhydrite.

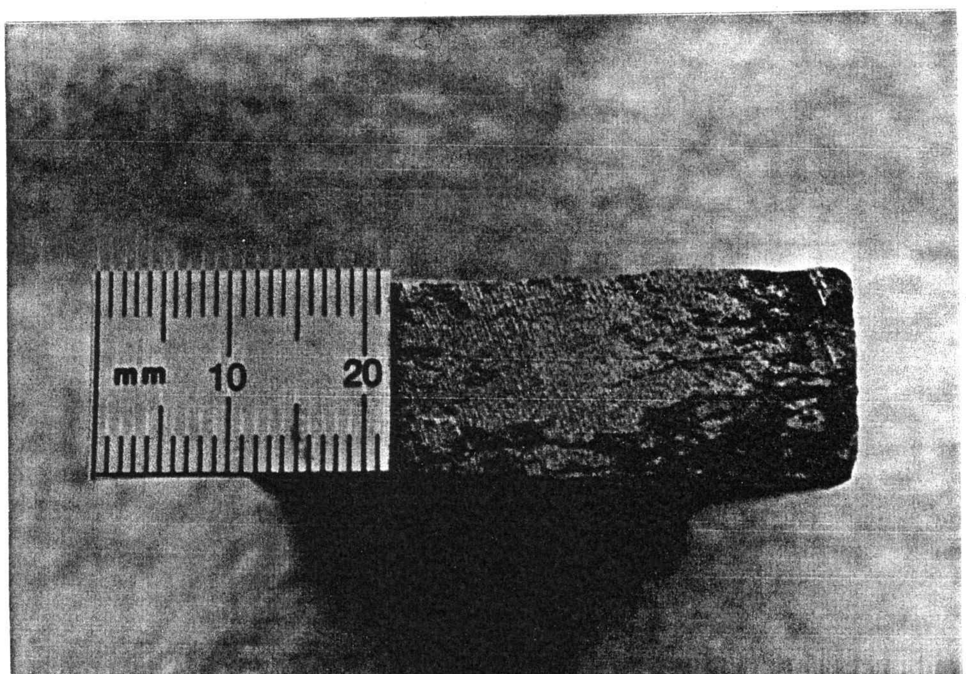

Fig. 20.--Core chip from the Computer Pet. Dreese #1 (2989 ft.), containing supratidal intraclasts (flat pebble conglomerate) in a red-brown regressive shale.

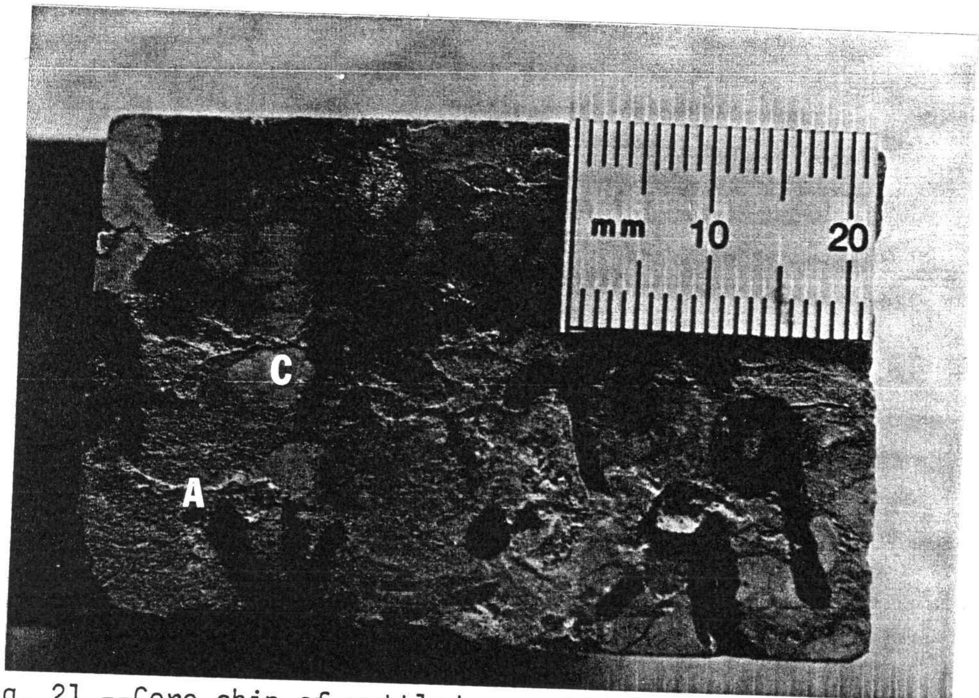

Fig. 21.--Core chip of mottled supratidal clastics ("rubble") from the Amoco Eveleigh "A" #2 (2788 ft.). Clastics contain gray to tan carbonate clasts (C) and thin stringers of nodular anhydrite (A).

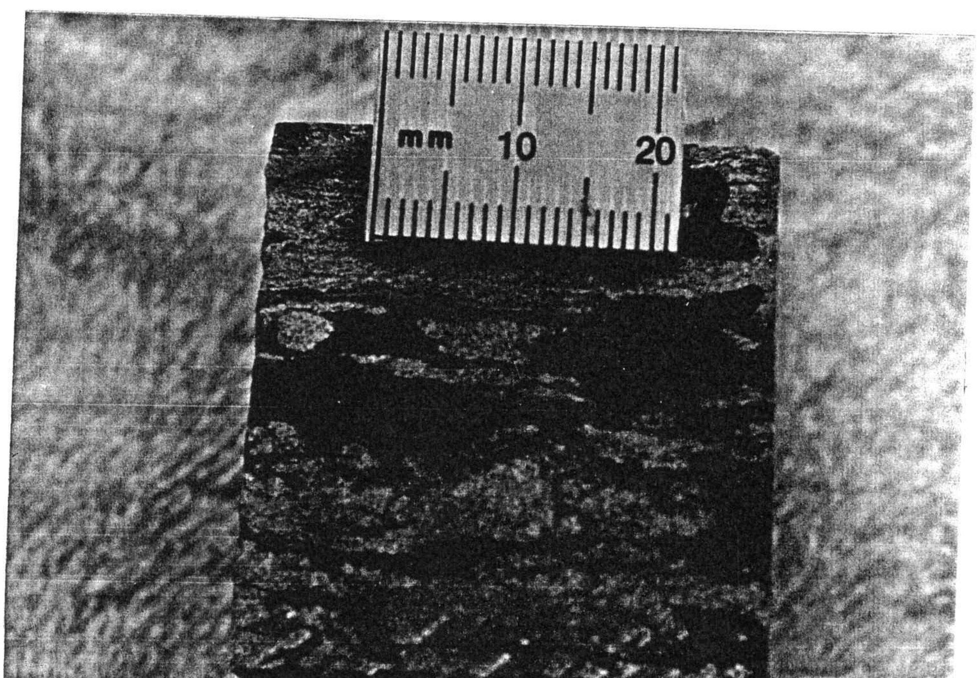

Fig. 22.--Core chip of laminated sulfates and red-brown clastics from the Anadarko Rhinehart Estate "C" #1 (2882 ft.).

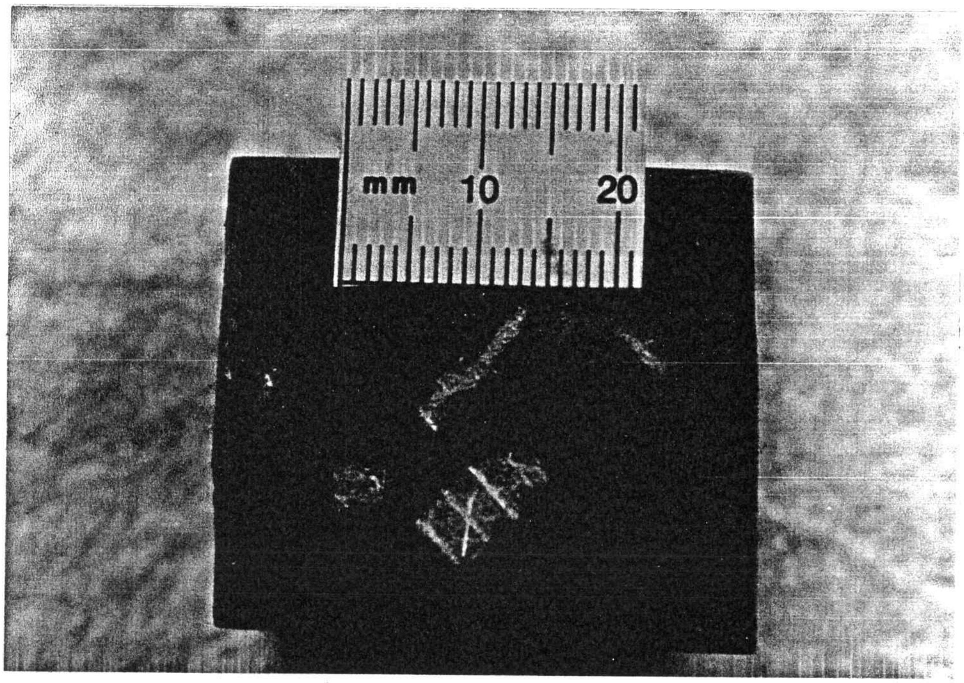

Fig. 23.--Core chip of a deflation flat sandstone with nodular anhydrite from the Anadarko Neer "A" #1 (2803 ft.).

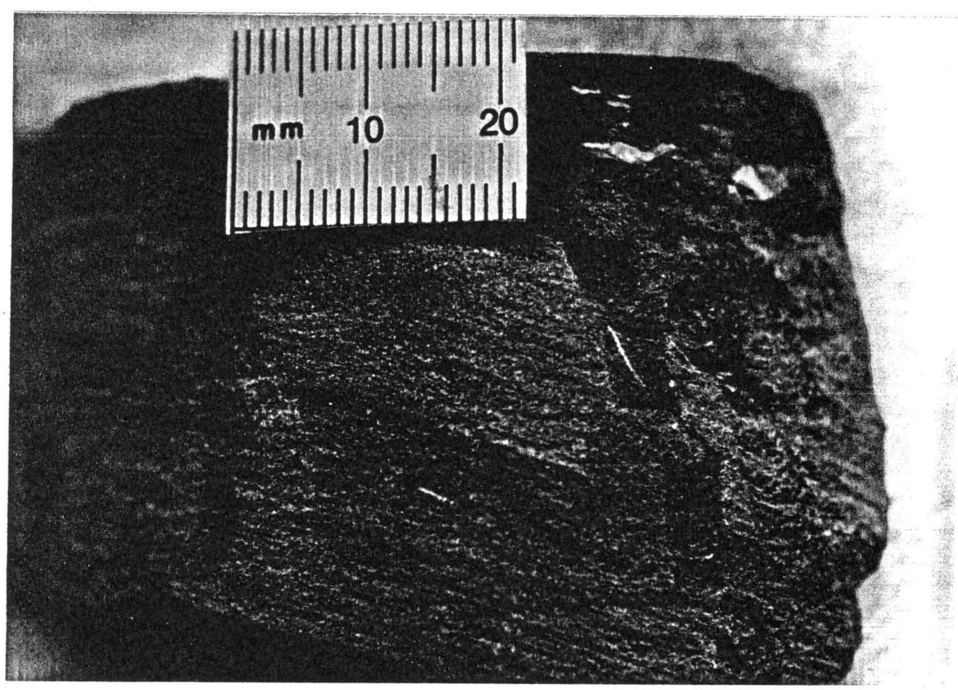

Fig. 24.--Core chip from the Anadarko Light "D" #1 (2860 ft.), showing backfilled vertical burrows and crosslaminations in a deflation flat sandstone.

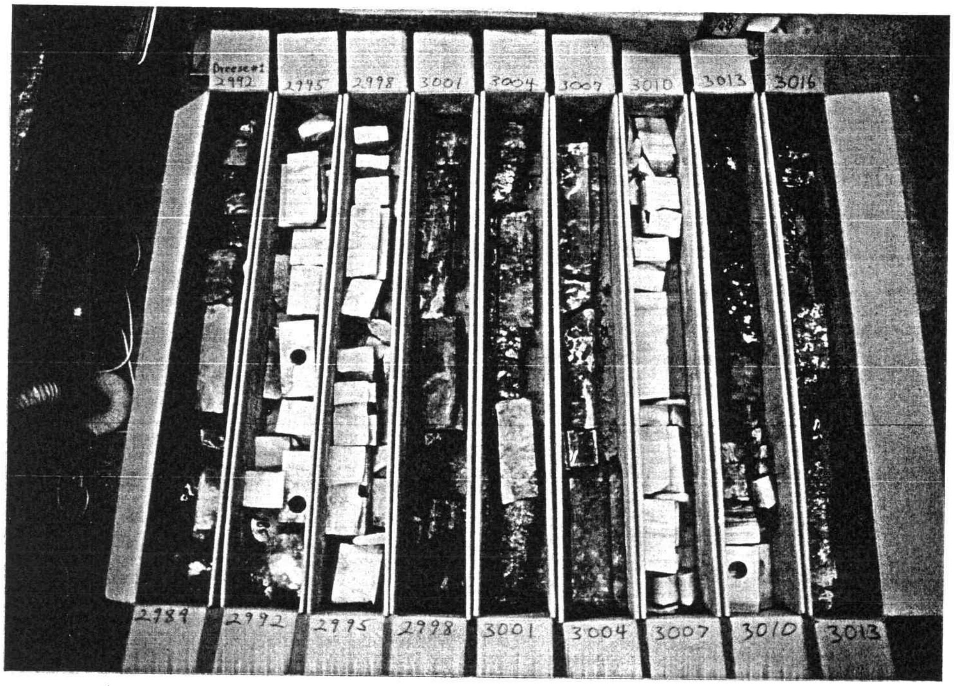

Fig. 25.--Core photograph of the Computer Pet. Dreese #1. Upper unit carbonates (2992-98 ft.) are separated from lower unit carbonates (3007-11 ft.) by red-brown regressive clastics (2998-3007 ft.) Regressive clastics also overlie and underlie the Five Finger carbonate interval.

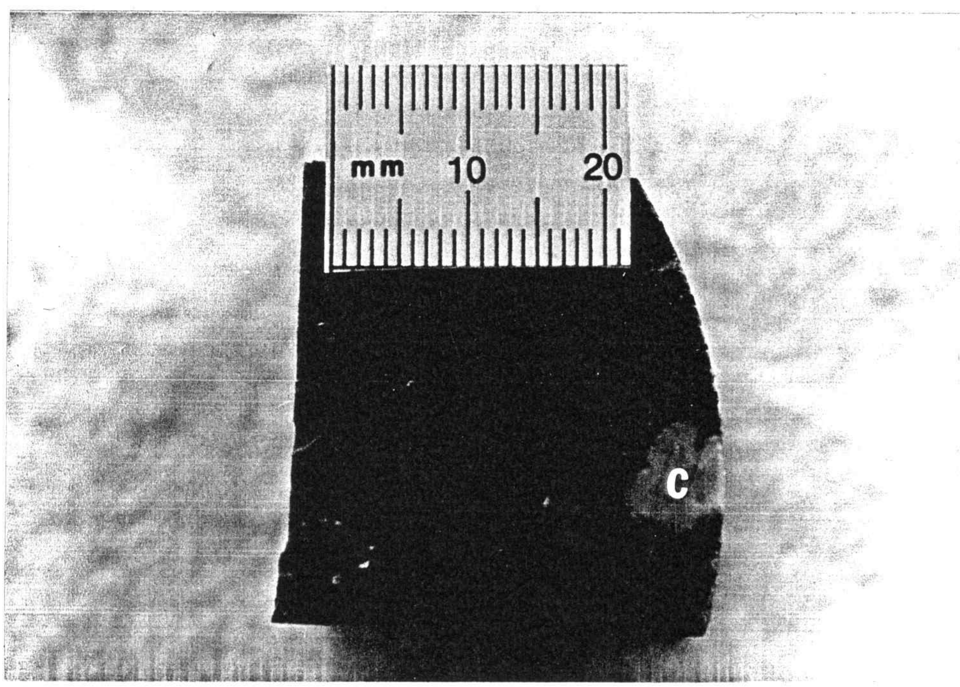

Fig. 26.--Core chip of a limestone from the Anadarko Neer "A" #1 (2830 ft.), containing dark algal coated grains and nodular chert (C).

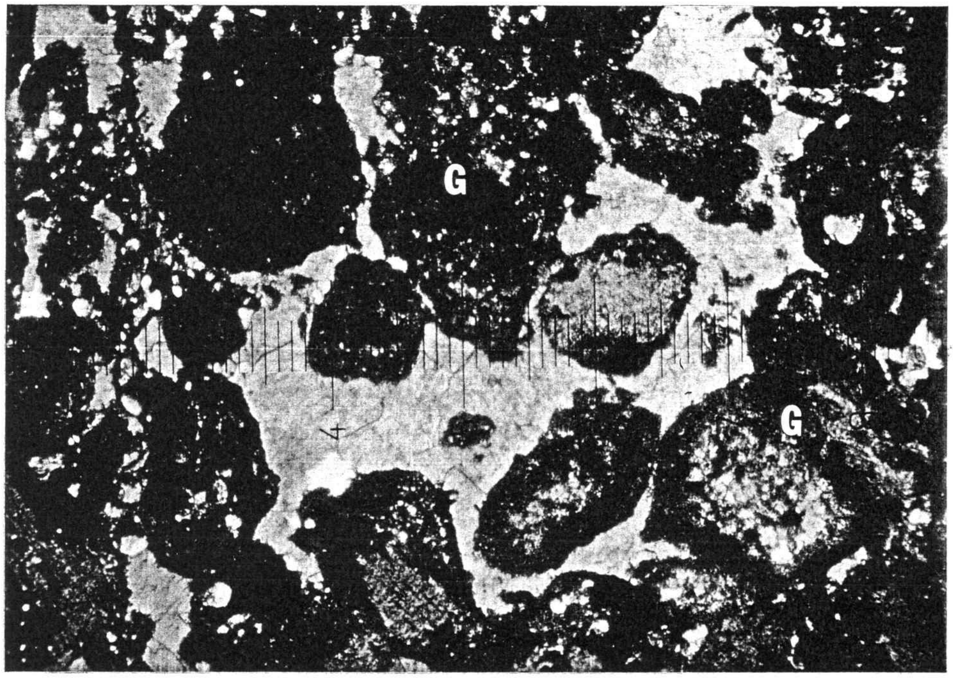

Fig. 27.--Kimzey "A" #1, 2944 ft., d=42u. Biopelgrapestone-grainstone. Thick algal coats envelope carbonate grains. Some algal coated grains and peloids have coalesced to form grapestone grains (G). Primary voids are filled with sparry calcite cement.

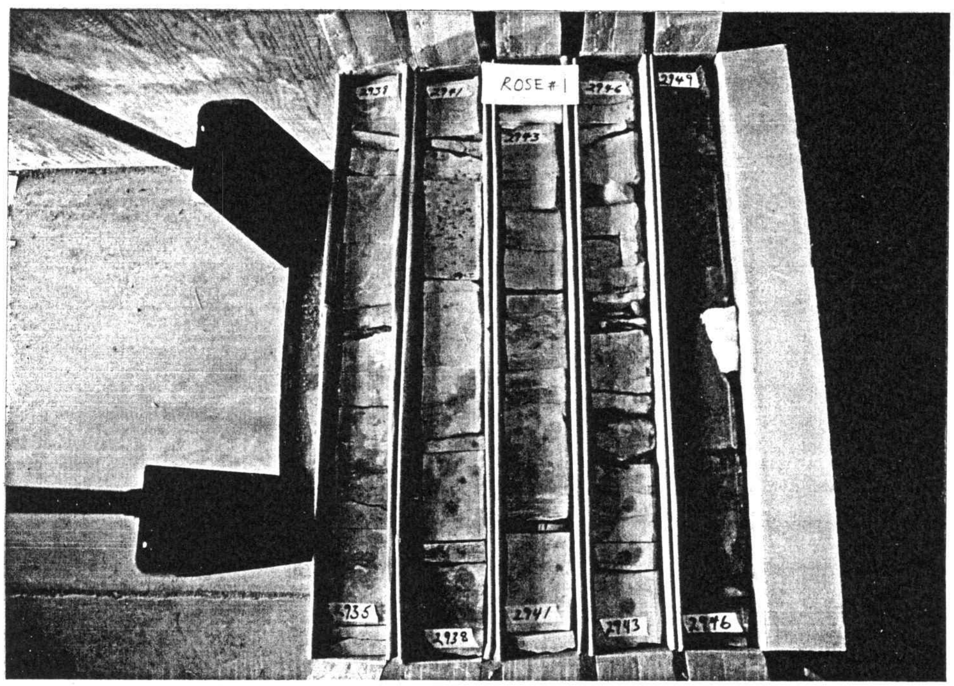

Fig. 28.--Core photograph of the Wagner and Brown Rose #1, showing lower unit carbonates (2935-46 ft.) and underlying regressive clastics (2946-49 ft.).

Fig. 29.--Core photograph of the Wagner and Brown Rose #1, showing upper unit carbonates (2923-35 ft.) and overlying regressive clastics (2917-23 ft.).

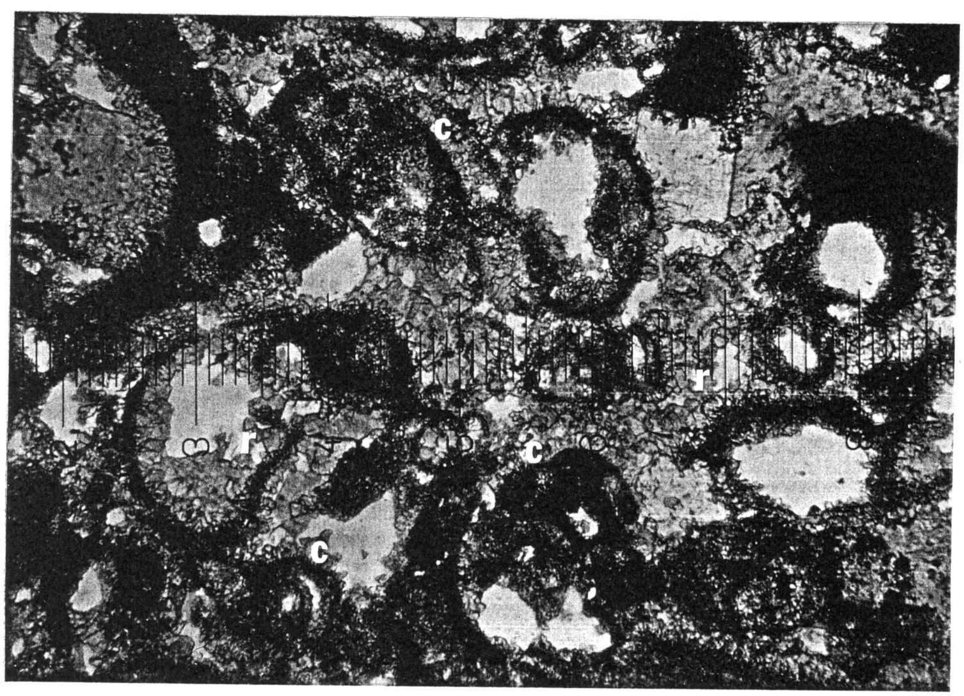

Fig. 30.--Rose #1, 2923 ft., d=11u. Biopelgrainstone. Some primary pores are lined with thin, fibrous to bladed submarine cement crusts (c). Coarse rhombic dolomite and sparry calcite fill some interparticle voids. Small red rhombs (r) record dedolomitization of early dolomite cement by fresh water. Intrabiotic cavities of micritized shells are largely open.

Fig. 31. Eveleigh "A" #2, 2741 ft., d=42u. Replacement of an Osagid-type algal coated grain by anhydrite. Crudely concentric morphology of the algal coat has been preserved following replacement.

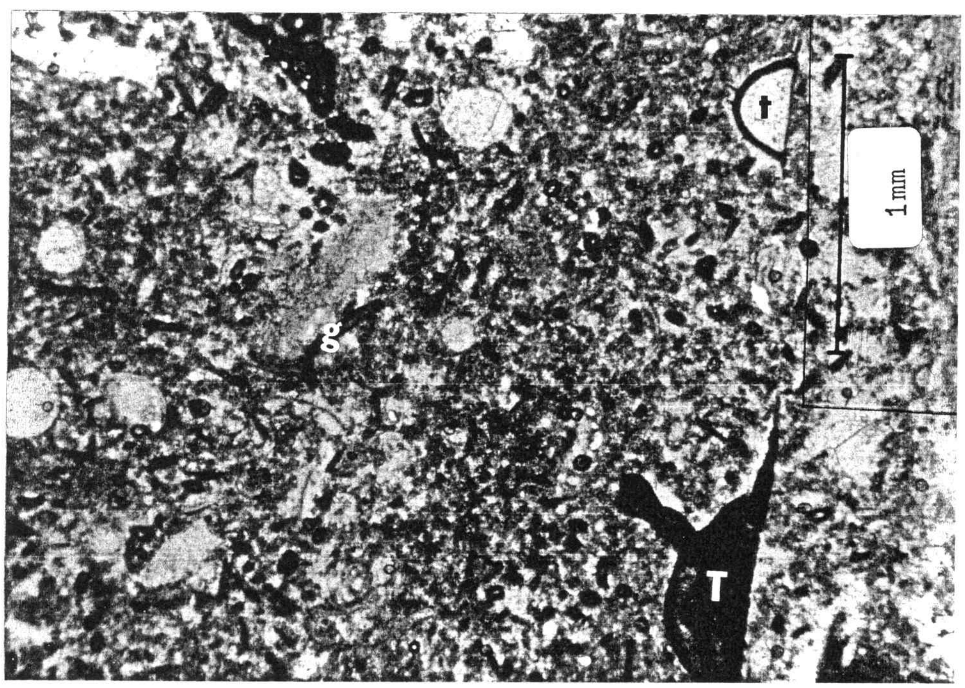

Fig. 32.--Smalley "C" 1-A, 2680 ft. Biowackestone contains loose fragments of the blue-green encrusting alga Girvanella (g), the encrusting foraminifer Tuberitina (t) and the encrusting alga (?) Tubiphytes (T).

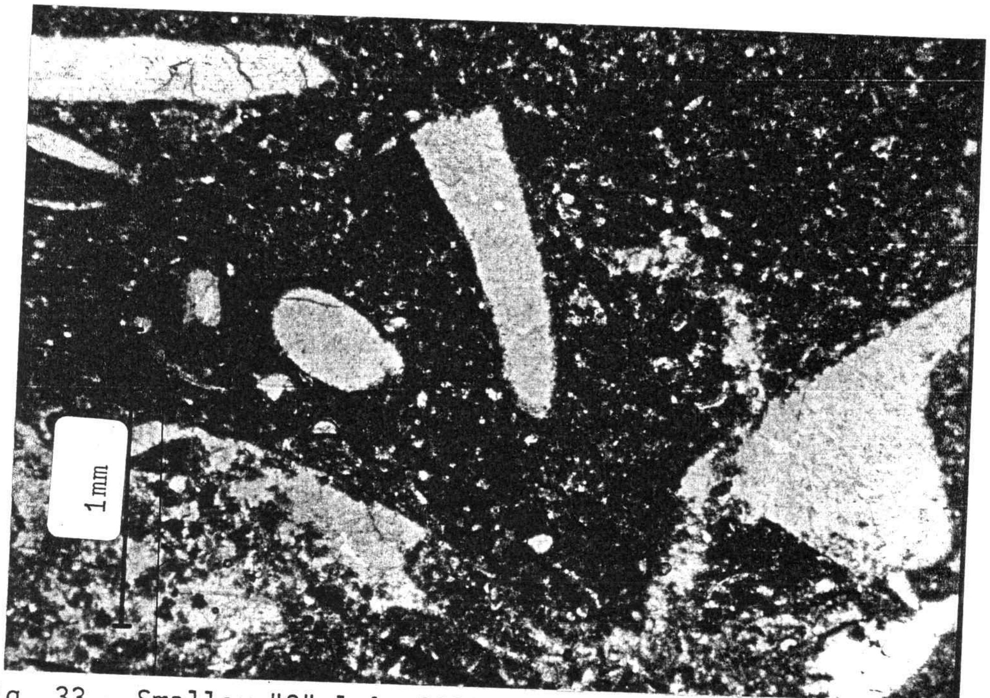

Fig. 33.--Smalley "C" 1-A, 2680 ft. Aragonitic pelecypod shells were dissolved out by fresh groundwater to form biomolds, which were later filled by sparry calcite cement.

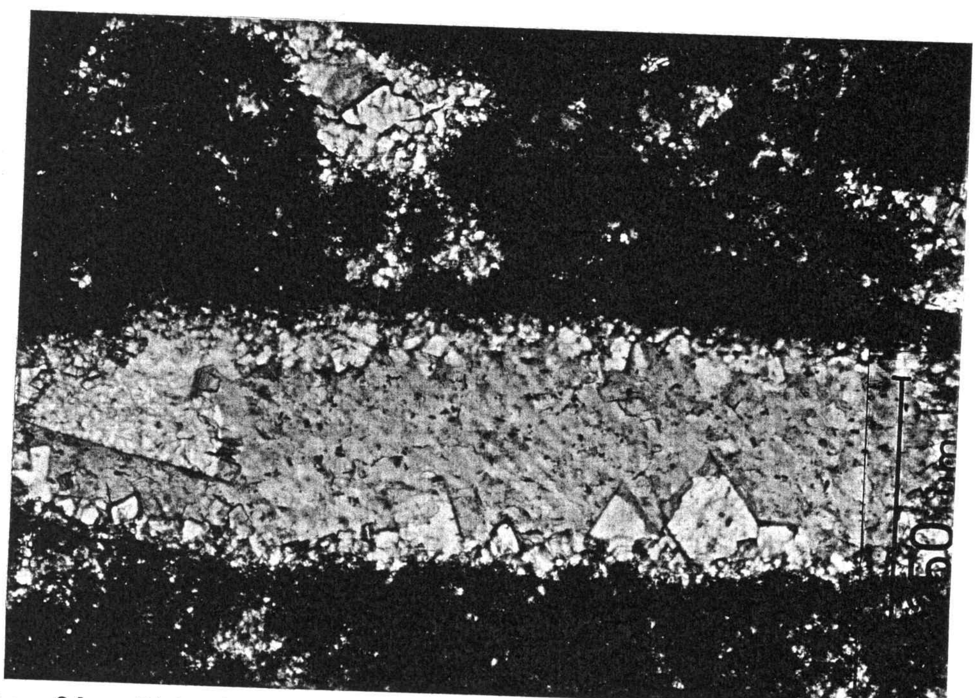

Fig. 34.--Rhinehart Estate, 2883.5 ft., d=11u. Slightly ferroan dolomite cement lines a biomold, which was later filled with ferroan calcite. Some dolomite was partially dedolomitized.

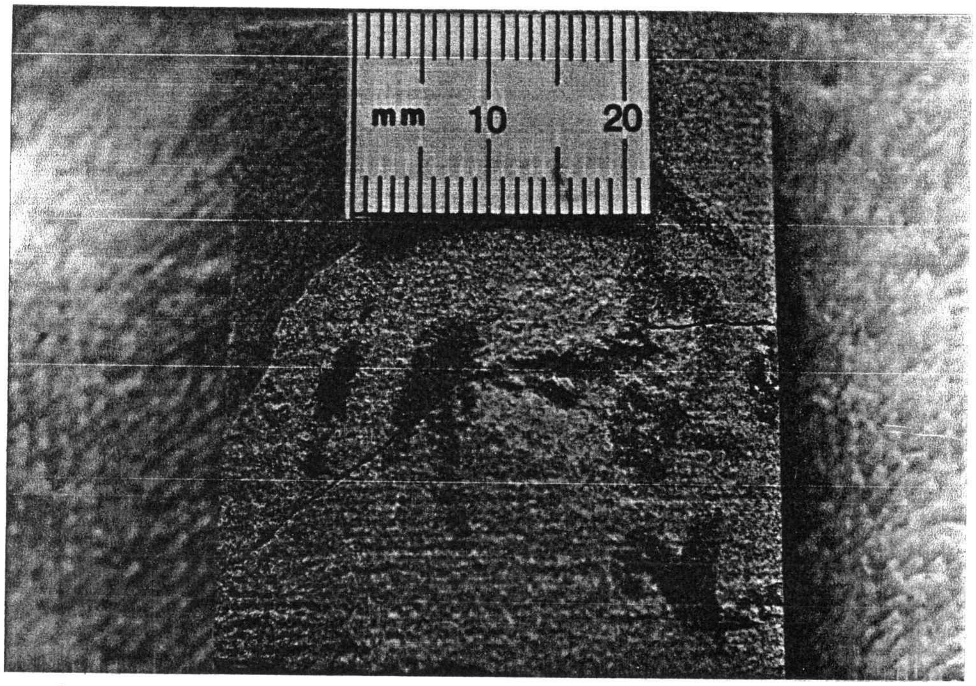

Fig. 35.--Core chip of a small nontectonic crumbly fracture in a limestone from the Wagner and Brown Rose #1 (2931 ft.).

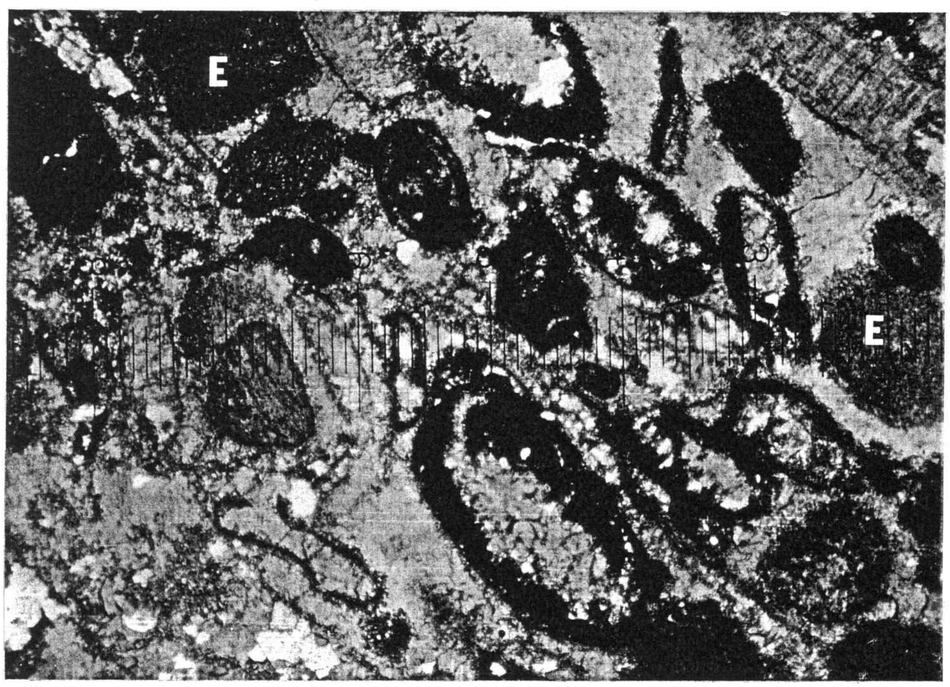

Fig. 36.--Rose #1, 2933 ft., d=42u. Biopelgrainstone. Primary interparticle voids and secondary hollow micrite envelopes are filled by sparry calcite cement. Epitaxial calcite cement occurs on monocrystalline echinoderm components (E).

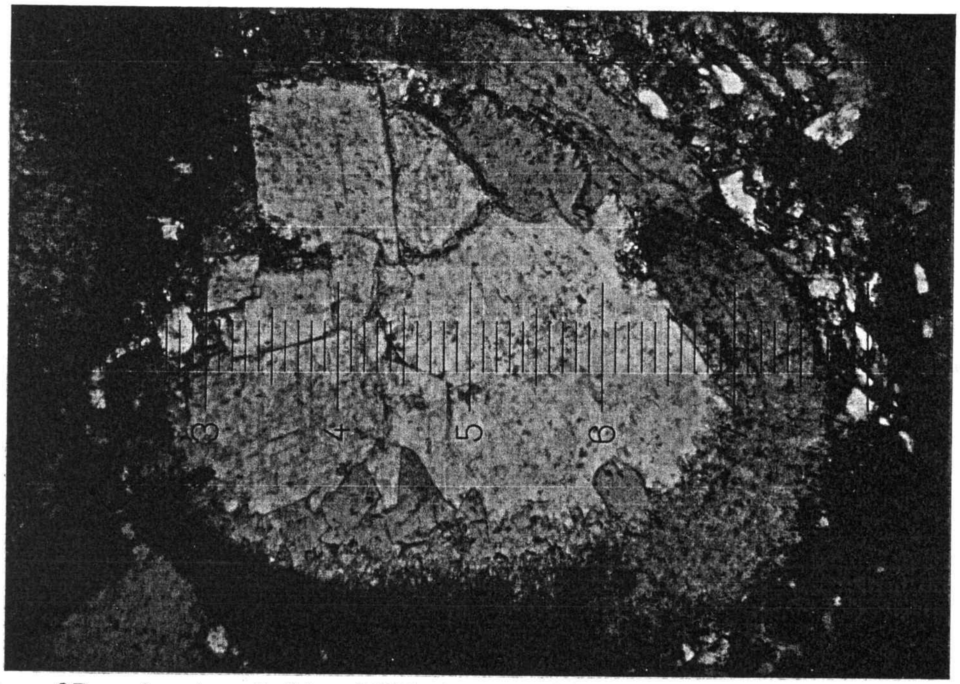

Fig. 37.--Garden C-10, 2772 ft., d=11u. Epitaxial calcite cement crystals line the intrabiotic pore of an ostracod. Calcite crystals are overlain and partially replaced by rhombic dolomite cement.

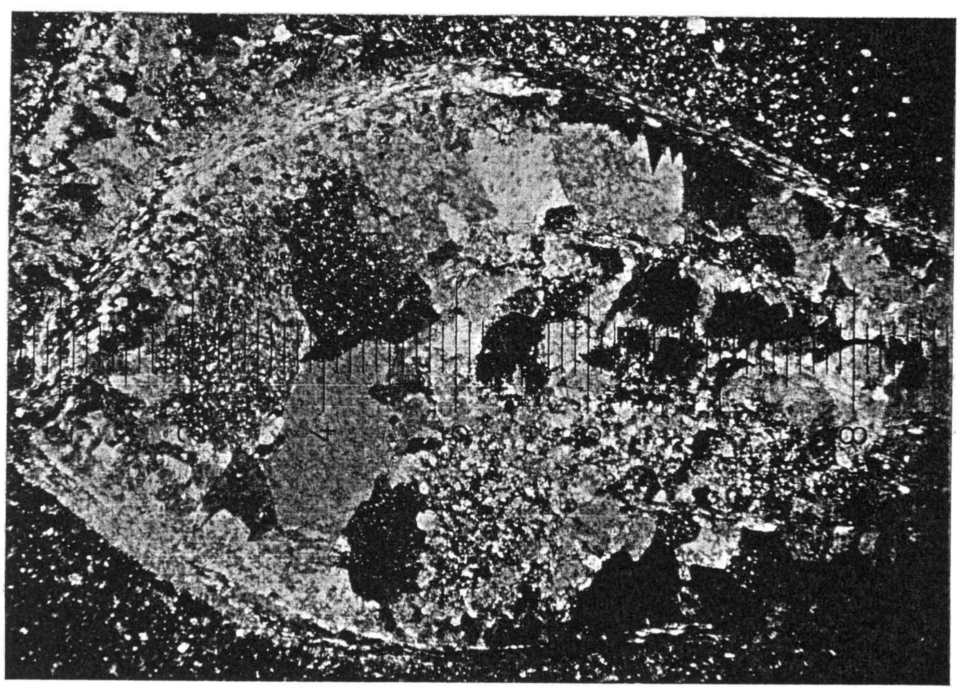

Fig. 38.--Rhinehart Estate "C" #1, 2902.5 ft., d=42u, (X). Epitaxial calcite cement crystals line the intrabiotic cavity of a brachiopod. The remainder of the void is filled with drusy calcite cement. Portions of the shell are silicified.

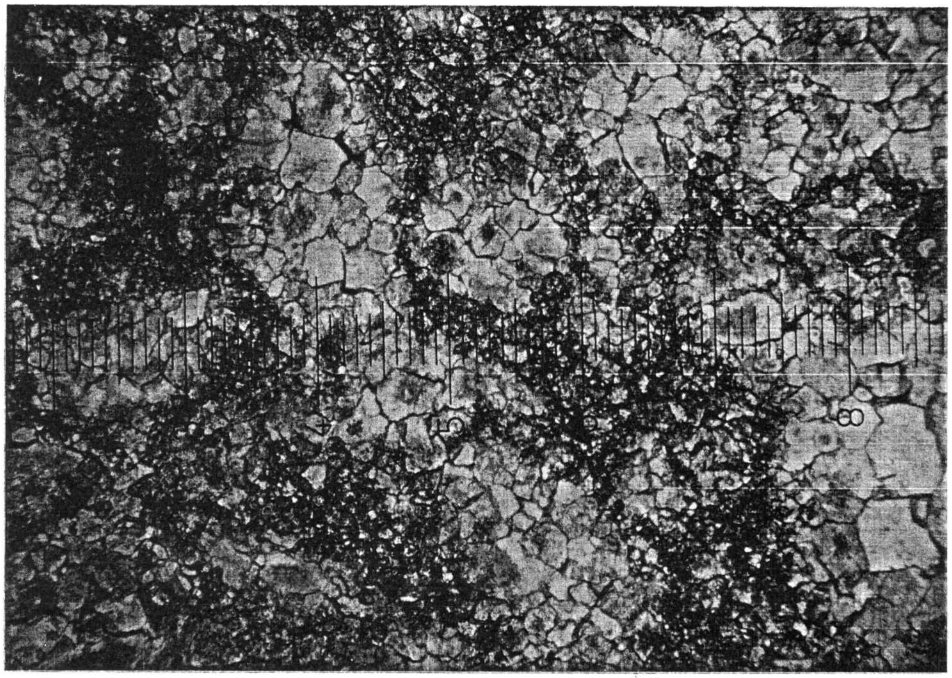

Fig. 39.--Dreese #1, 2996 ft., d=42u. Neomorphic dolomitization of a biopackstone. Aragonitic shells were partially dissolved and partially replaced by coarse, inclusion-rich dolomite. Interiors of biomolds were filled with clear rhombic dolomite cement.

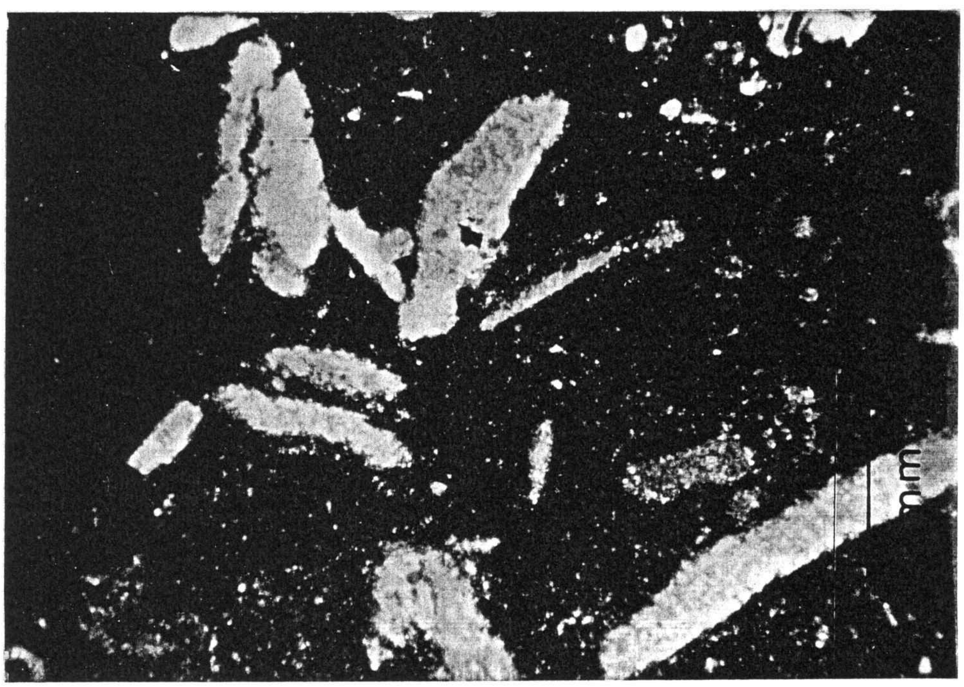

Fig. 40.--Rhinehart Estate "C" #1, 2885 ft., (X). Biowackestone. Lime and matrix was neomorphically dolomitized. Aragonitic shells dissolved to form biomolds which were filled with sparry anhydrite.

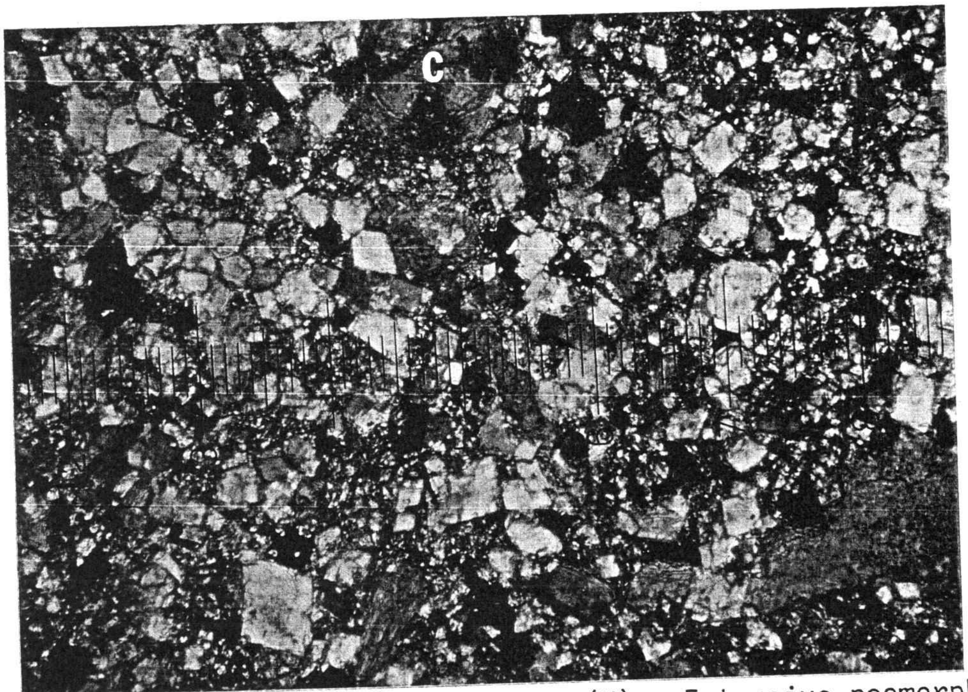

Fig. 41.--Rose #1, 2935 ft., d=11u, (X). Extensive neomorphic dolomitization of a biowackestone. Lime mud matrix was replaced by rhombic dolomite; calcitic shells (C) were largely unaffected by dolomitization.

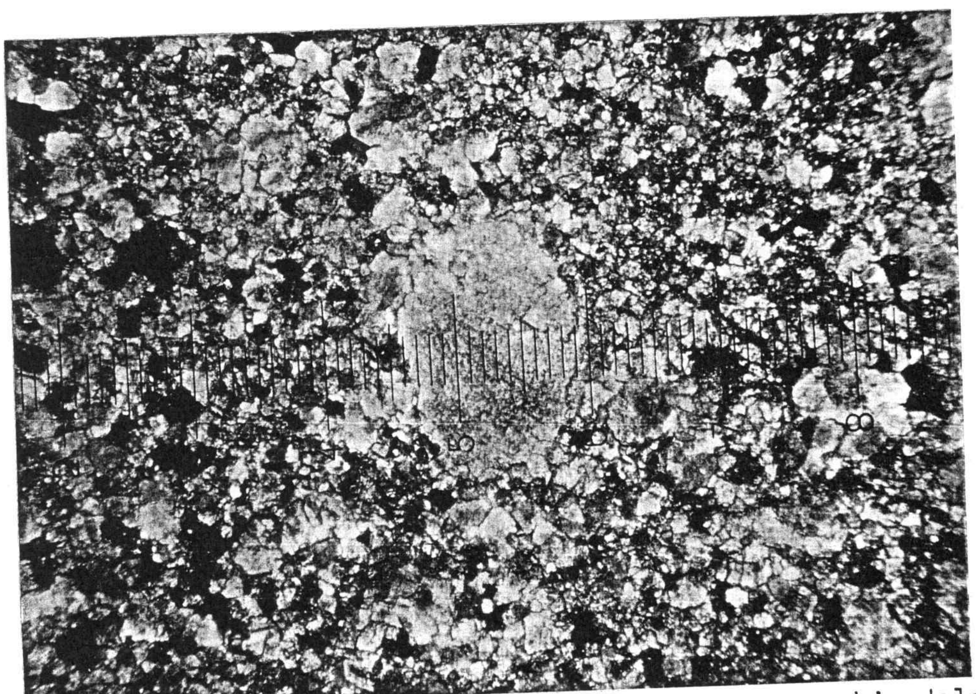

Fig. 42.--Dreese #1, 2996 ft., d=42u, (X). Paramorphic dolomitization of an echinoderm component in a neomorphic dolostone.

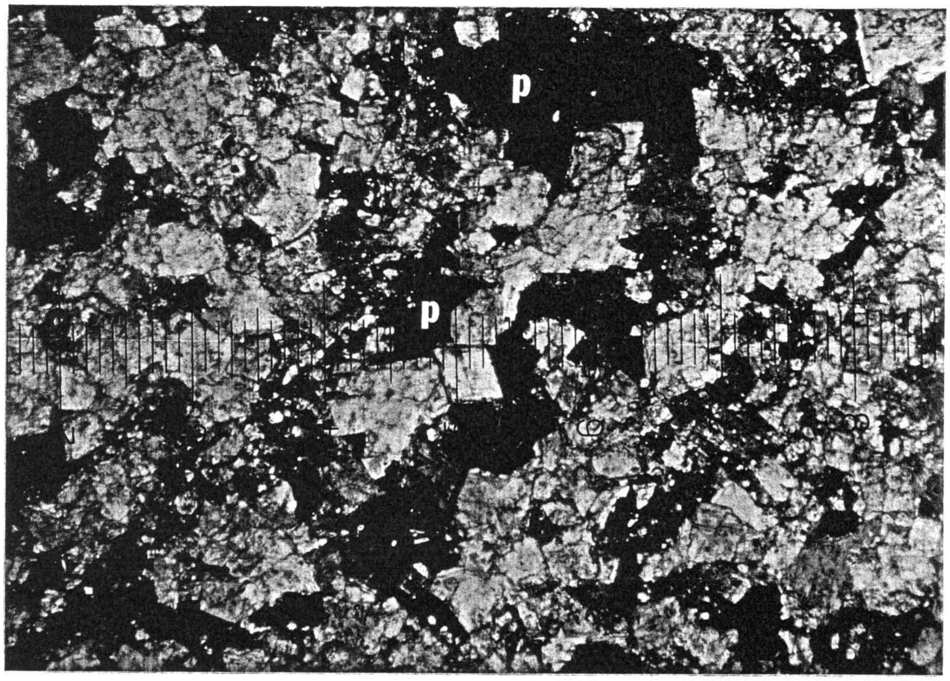

Fig. 43.--Bowlus #1, 2834-54 ft., d=11u, (X). Idiotopic fabric of a neomorphic dolostone with preserved secondary intercrystalline porosity (p).

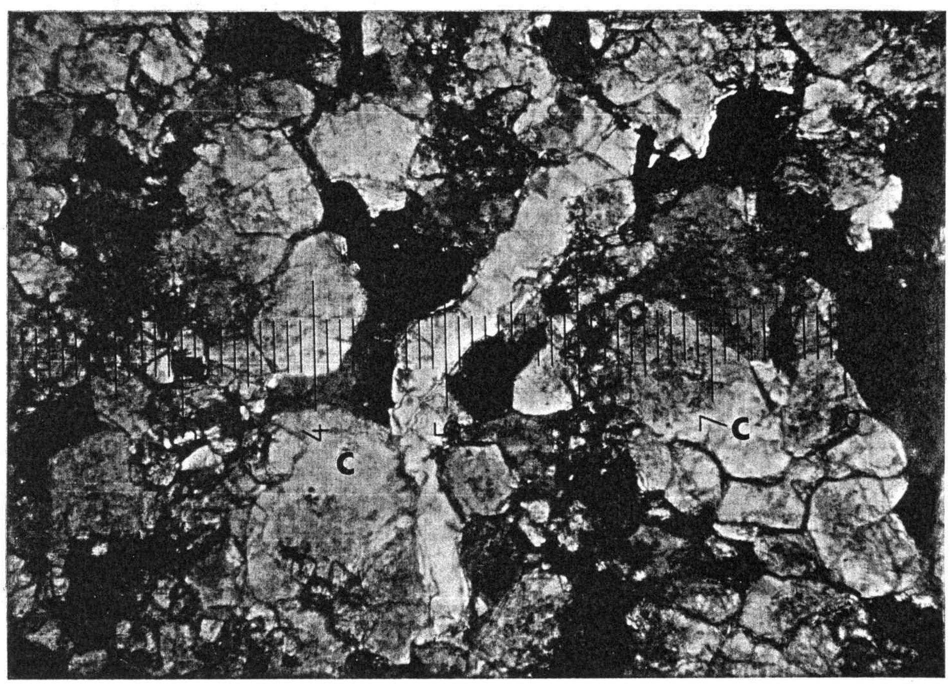

Fig. 44.--Dreese #1, 2996 ft., d=11u, (X). Sparry anhydrite cement partially fills a fracture in a neomorphic dolostone. Intercrystalline porosity is largely occluded by epitaxial cementation (c) on replacement rhombs.

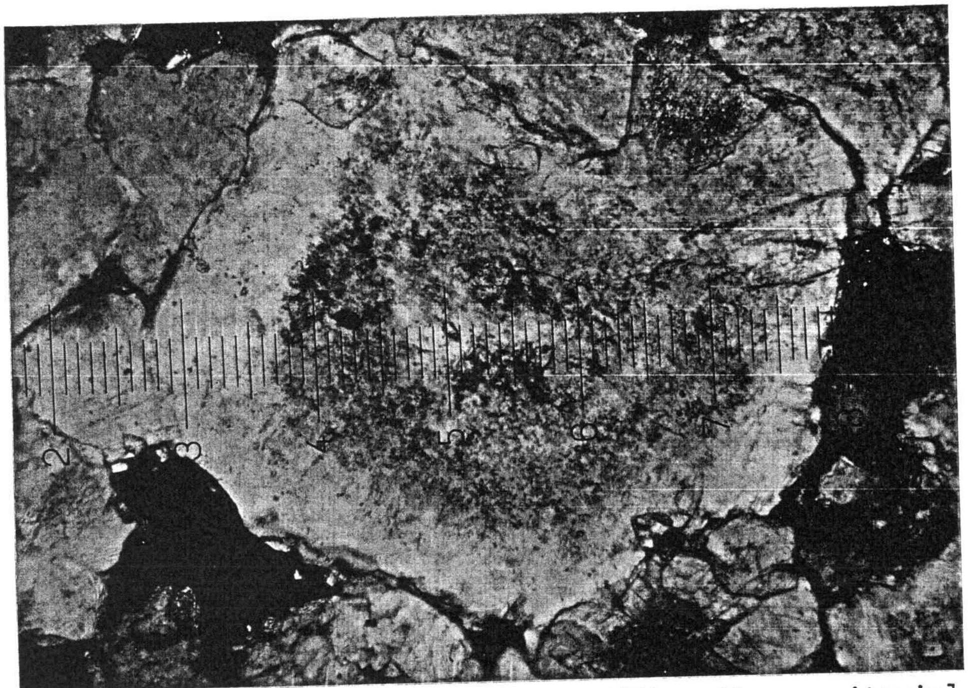

Fig. 45.--Dreese #1, 2996 ft., d=11u, (X). Clear epitaxial dolomite cement surrounds a cloudy, inclusion-rich replacement rhomb.

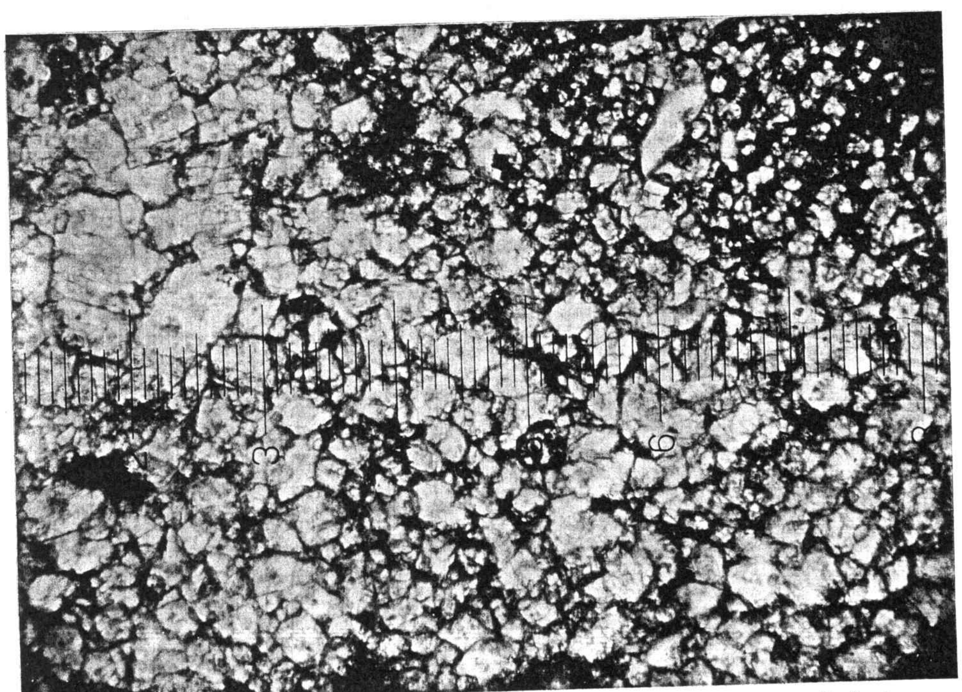

Fig. 46.--Dreese #1, 2989 ft., d=11u. Occlusion of intercrystalline porosity in a neomorphic dolostone by clays and iron oxides.

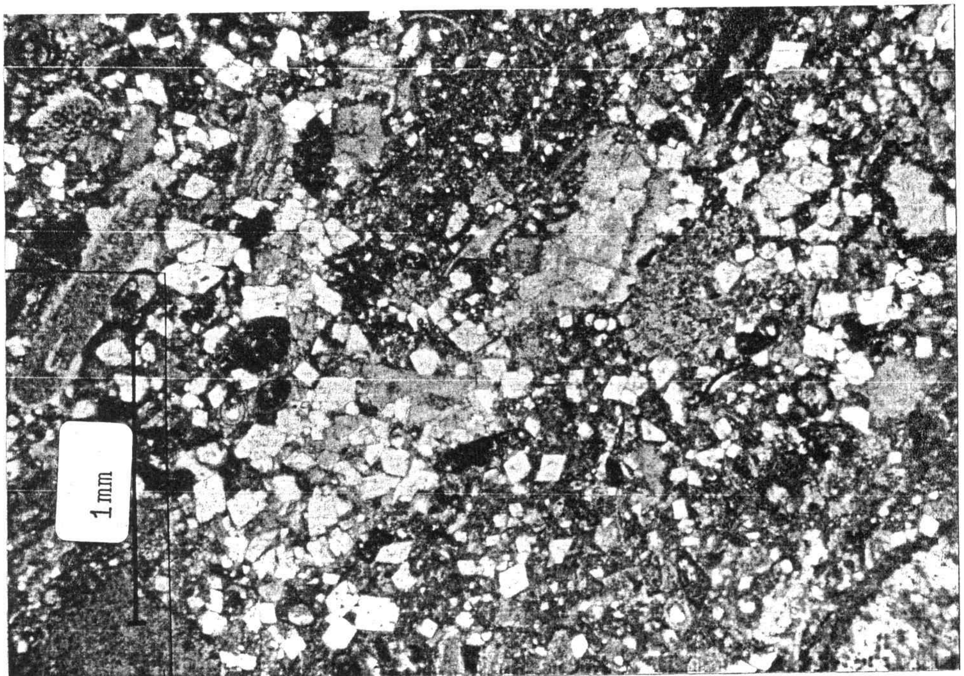

Fig. 47.--Garden C-10, 2765 ft. Rhombic dolomite replacement porphyroblasts are scattered throughout matrix and grains of a biopelpackstone.

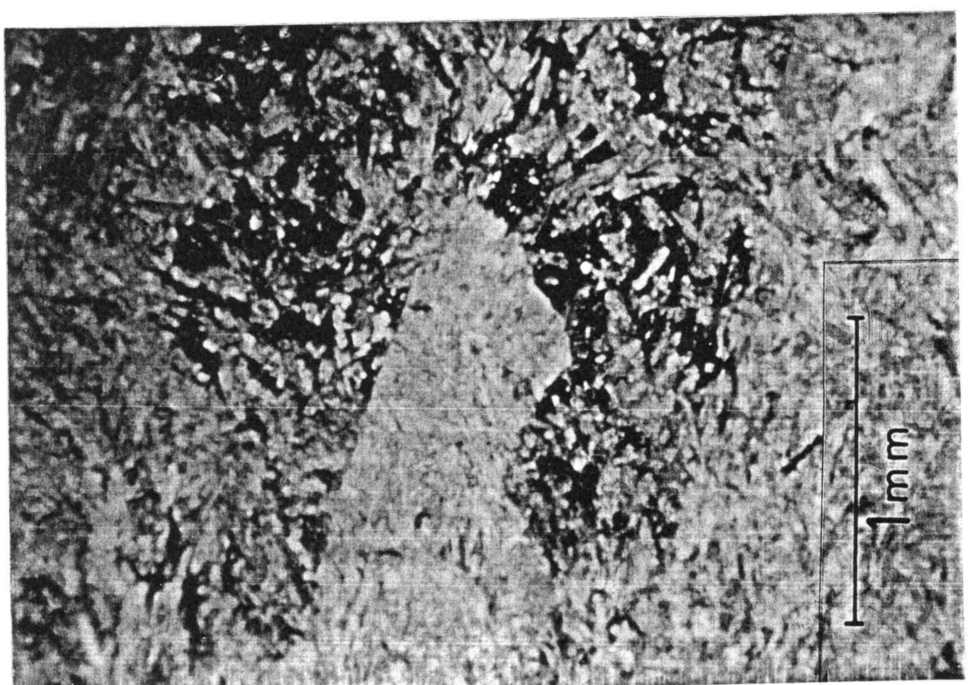

Fig. 48.--Tate-Hutton #2, (X). Recrystallization of nodular anhydrite to large blocky crystals of anhydrite spar.

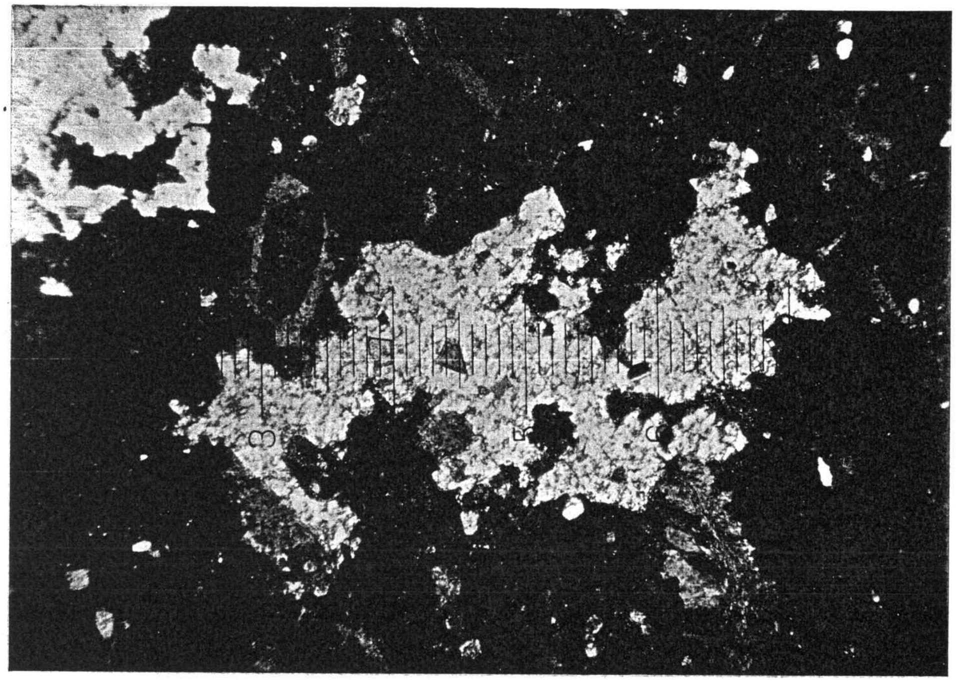

Fig. 49.--Rose #1, 2927 ft., d=42u, (X). Sparry anhydrite replacement porphyroblast. Note distinctive rectangular stairstep morphology.

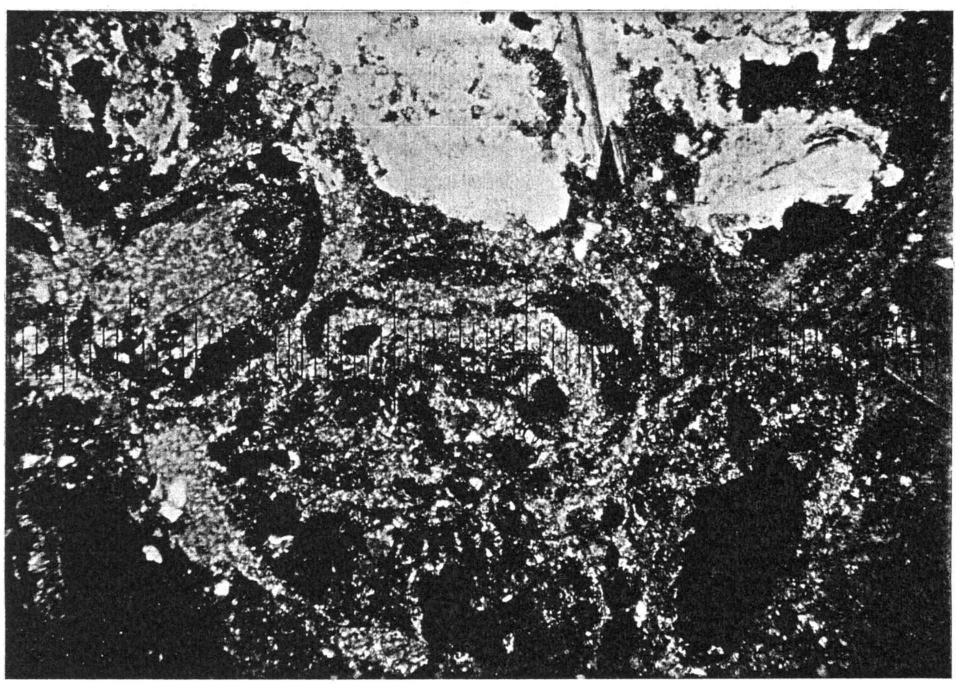

Fig. 50.--Eveleigh "A" #2, 2741 ft., d=42u, (X). Replacement of algal coated grains by sparry anhydrite.

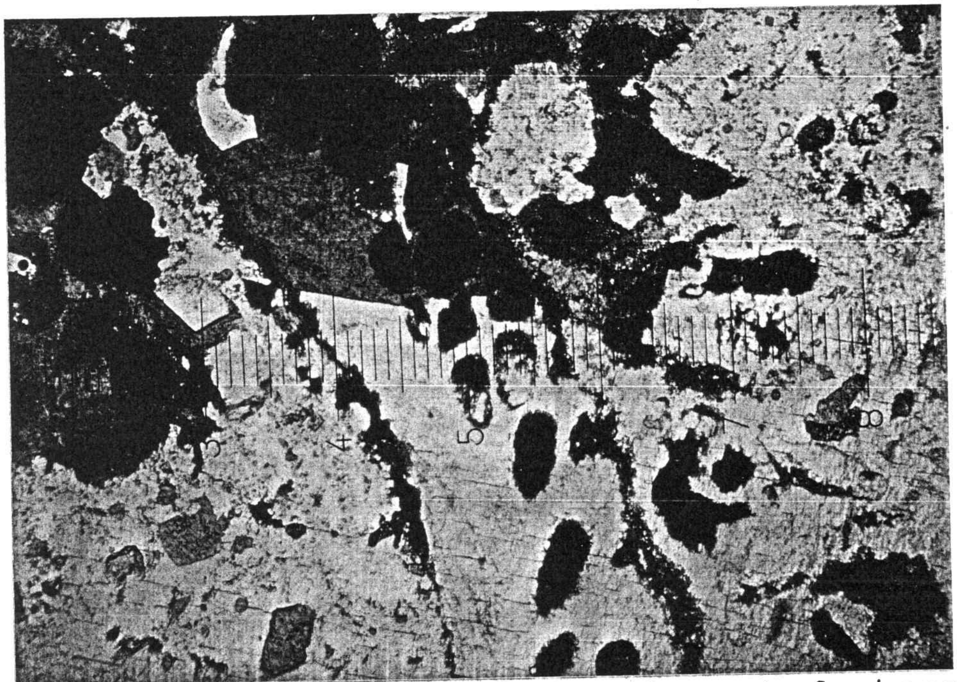

Fig. 51.--Rose #1, 2933 ft., d=42u. Replacement of a bryozoan fragment by anhydrite. Micritic calcite in body cavities (zoecia) resisted replacement.

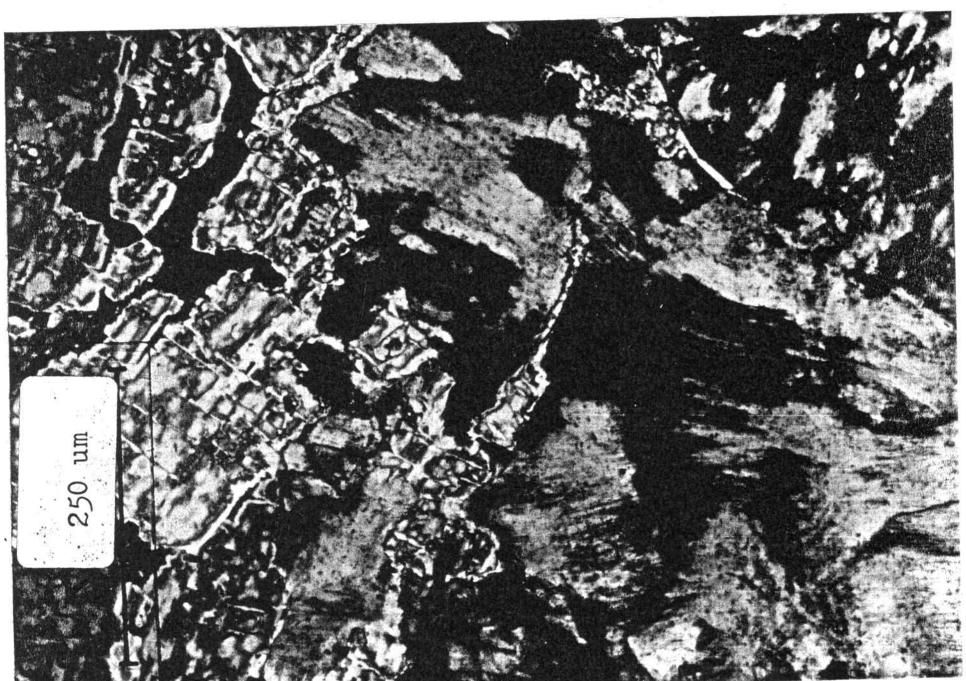

Fig. 52.--Miles "B" #2, 2903 ft., (X). Replacement of sparry anhydrite by fibrous length-slow chalcedony.

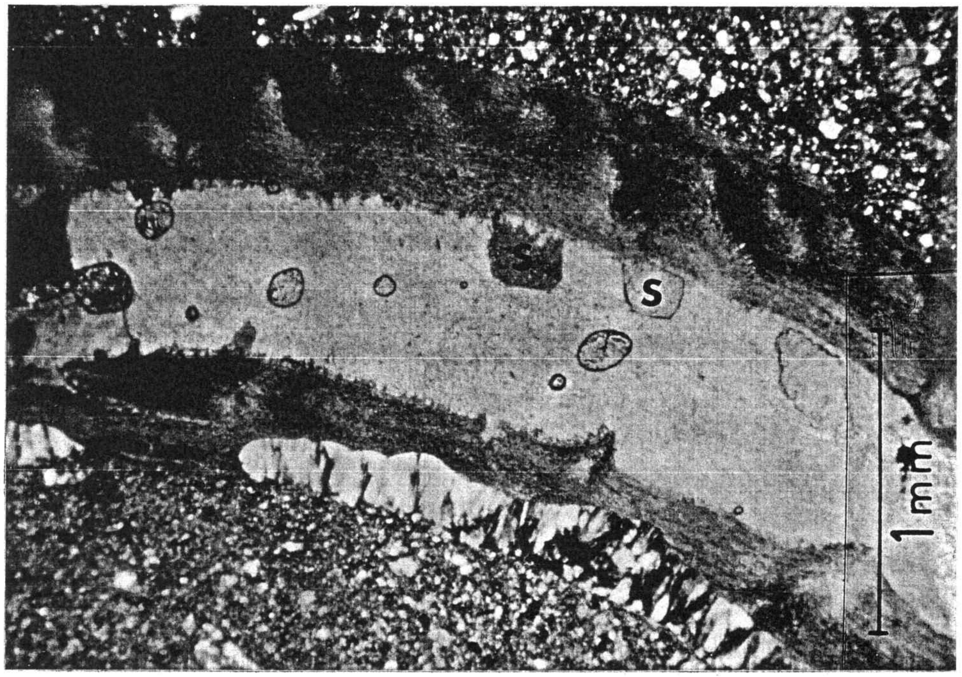

Fig. 53.--Light "D" #1, 2873 ft., (X). Scalenohedral calcite (S) lines the intrabiotic void of a partially silicified brachiopod. Sparry calcite cement fills the remainder of the void.

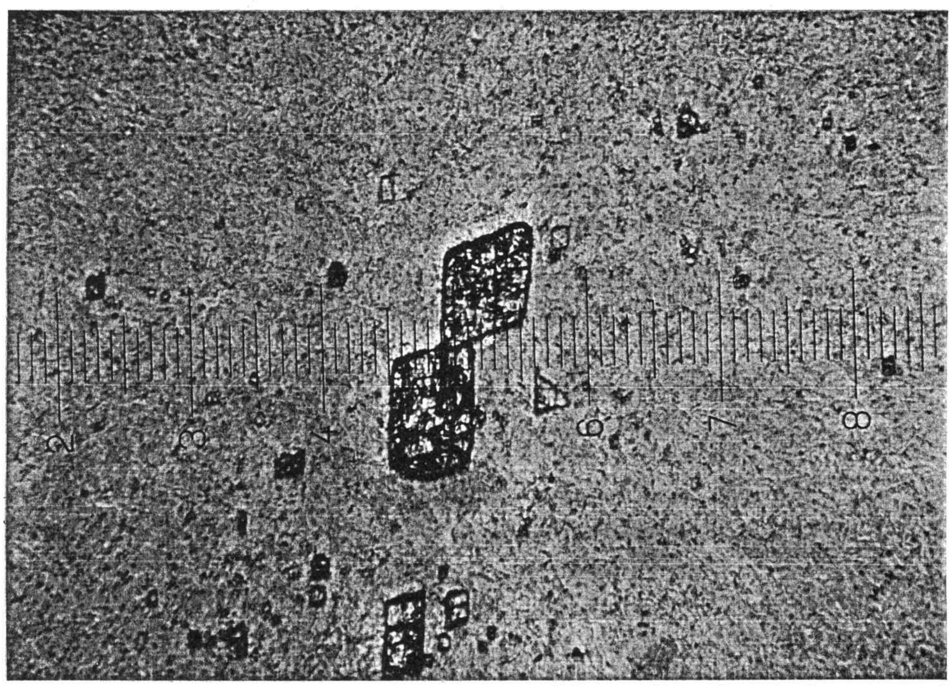

Fig. 54.--Neer "A" #1, 2830 ft., d=11u. Exsolved ferroan dolomite rhombs in a silicified portion of an echinoderm fragment.

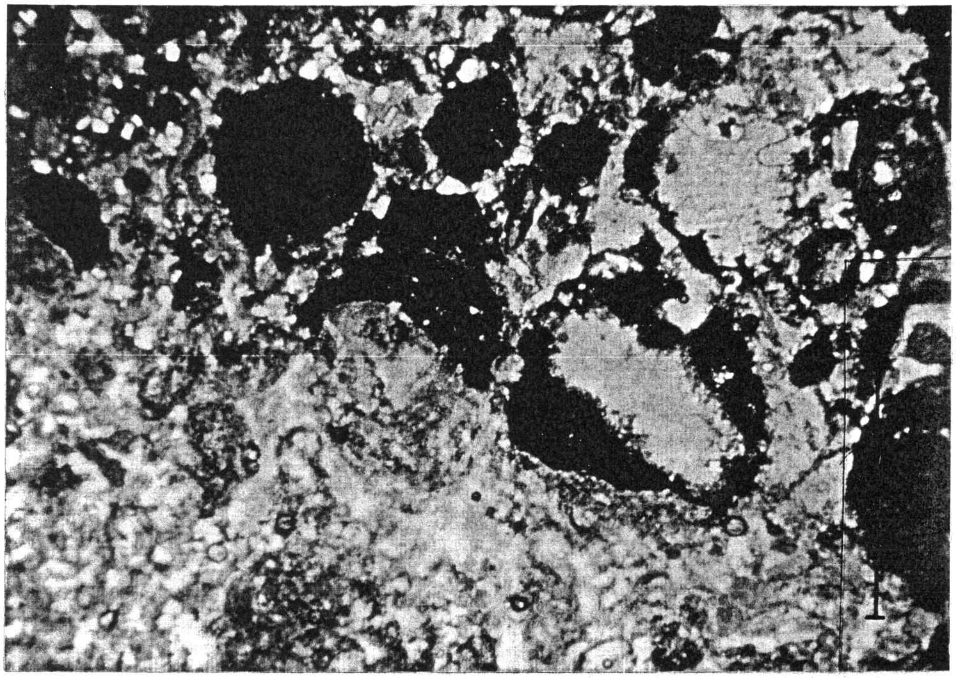

Fig. 55.--Smalley "C" 1-A, 2674 ft., d=42u. Silicification of a biopelgrainstone along a replacement front.

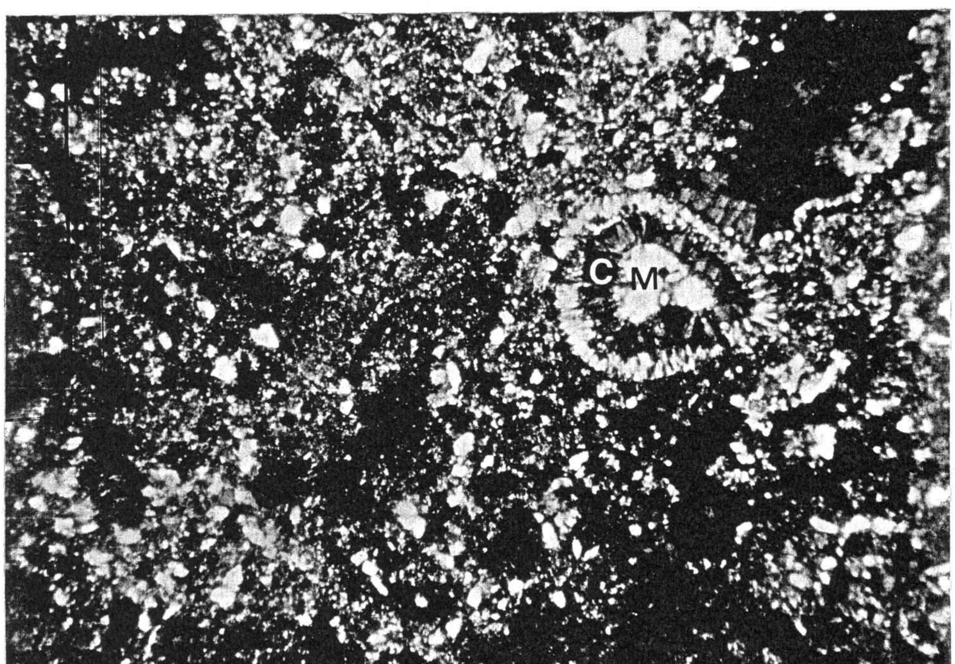

Fig. 56.--Smalley "C" 1-A, 2674 ft., (X). Massive silicification of a limestone. Micritic material was replaced by microquartz. Ostracod to left of center was replaced by L-S chalcedony, and the intrabiotic void was filled with L-F chalcedony (c) and megaquartz (m).

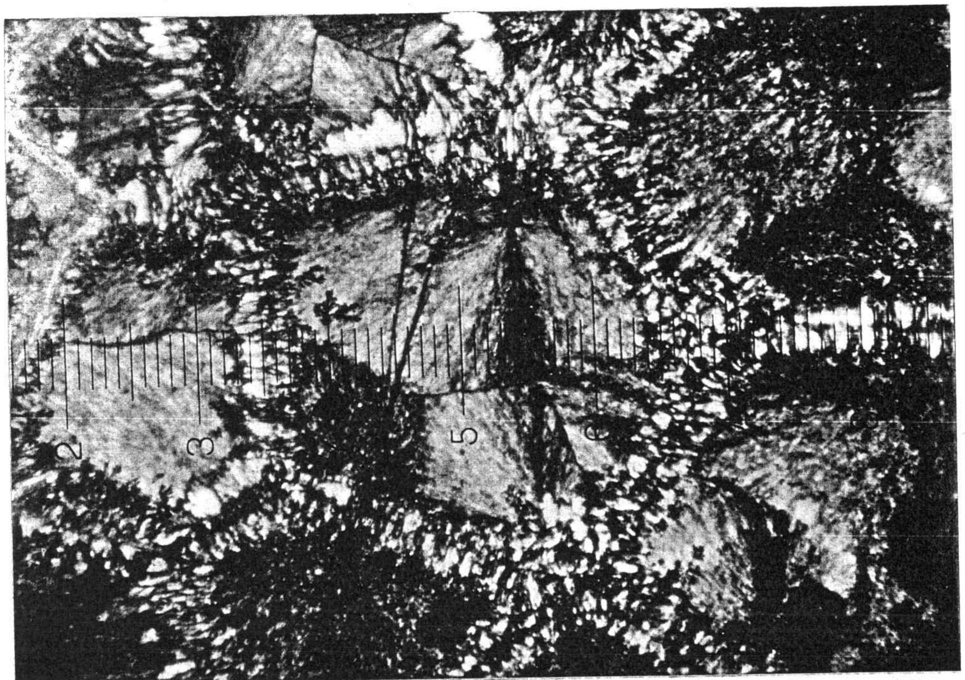

Fig. 57.--Garden C-10, 2770 ft., d=11u, (X). Body cavities (zoecia) of a bryozoan were cemented by length-fast chalcedony. Shell walls were replaced by lengh-slow chalcedony.

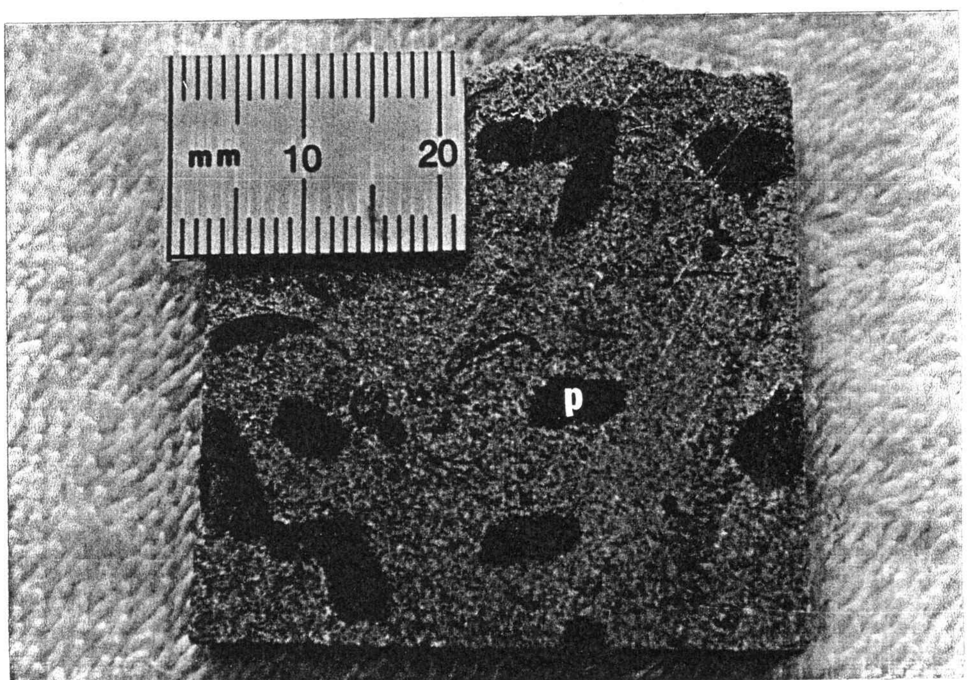

Fig. 58.--Core chip of anhydrite porphyroblasts in a limestone from the Rose #1 (2933 ft.).

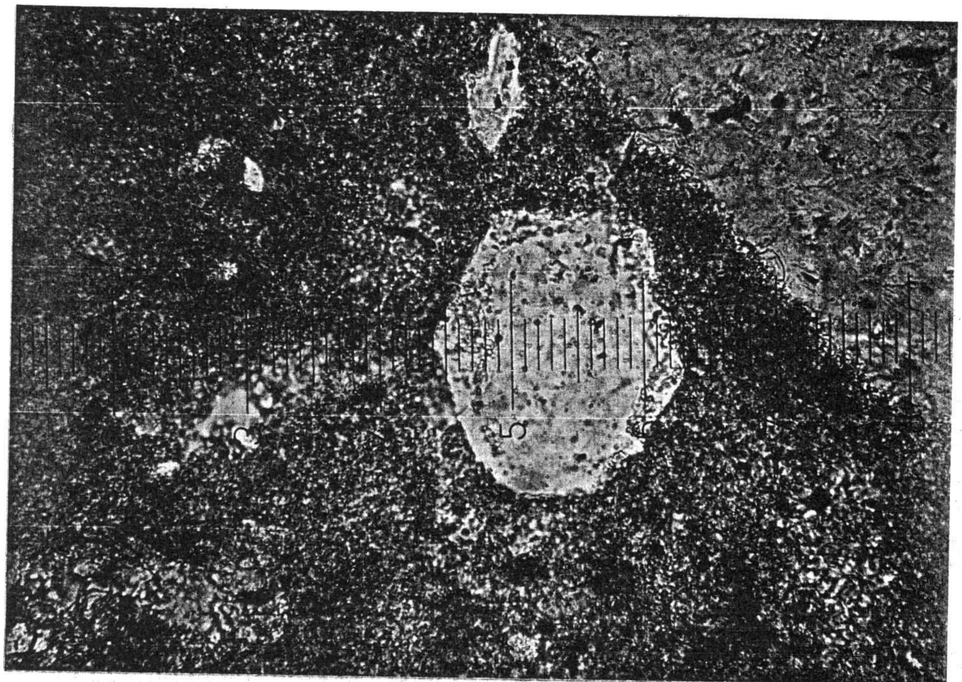

Fig. 59.--Neer "A" #1, 2814 ft., d=4.3u. An authigenic quartz overgrowth surrounds a detrital quartz grain. Micritic inclusions outline the original boundaries of the grain.

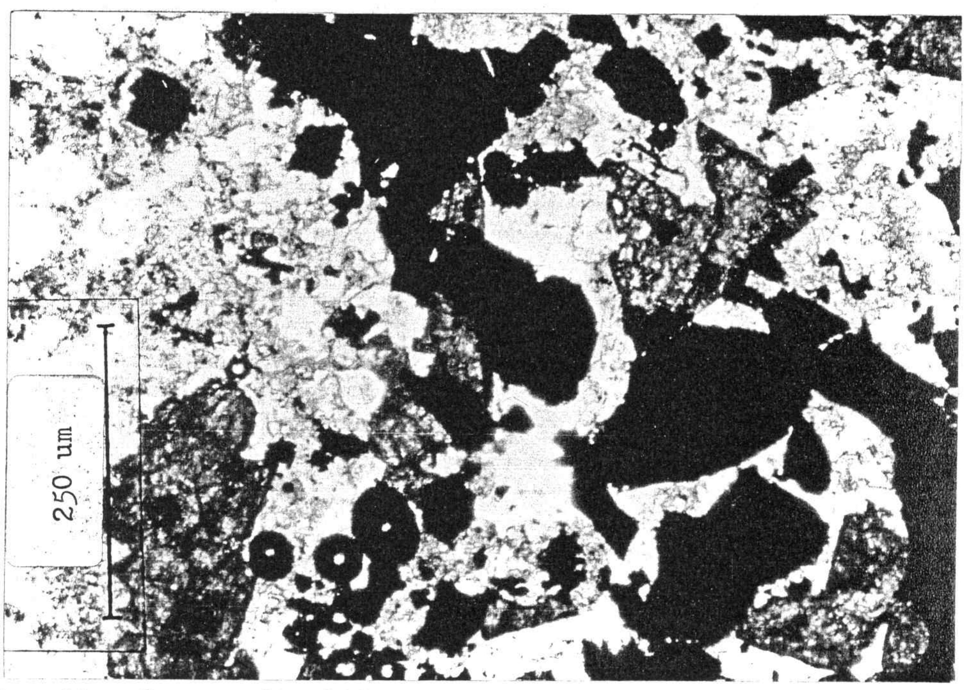

Fig. 60.--Dotson #3, 2827 ft. Pyritization of small shell fragments.

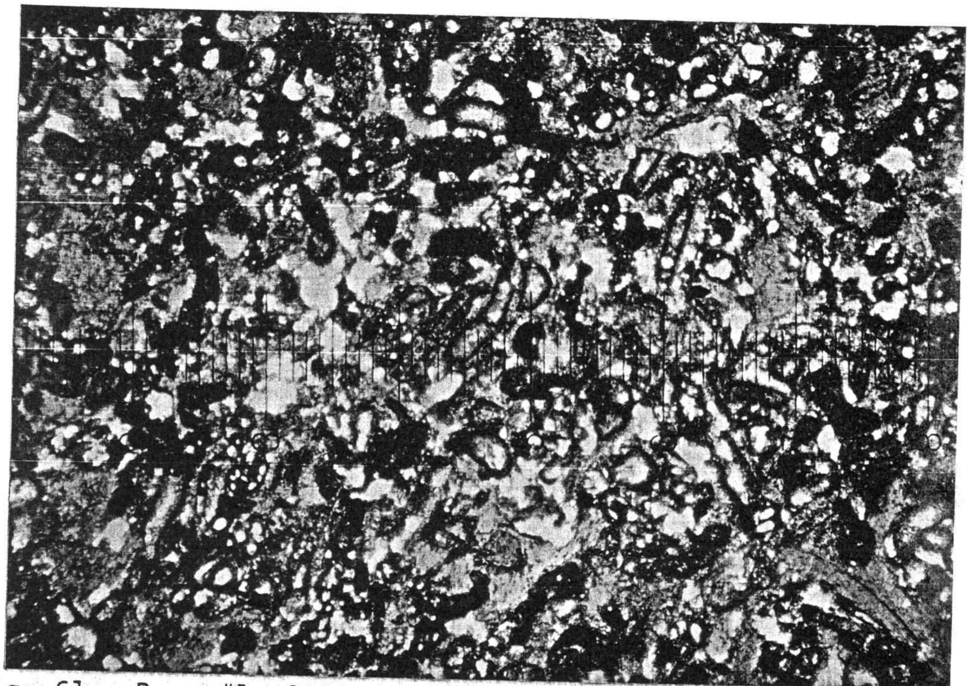

Fig. 61.--Rose #1, 2923 ft., d=42u. Biopelgrainstone. Preserved porosity consists of primary intrabiotic pores, secondary hollow micrite envelopes and tertiary anhydrite molds.

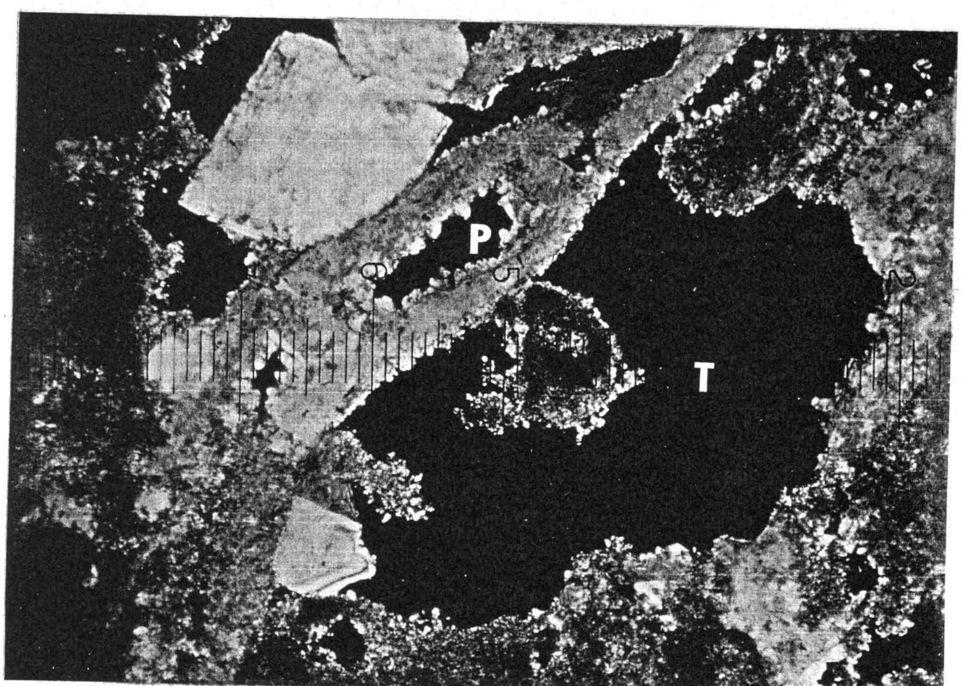

Fig. 62.--Rose #1, 2927 ft., d=11u, (X). Primary intrabiotic porosity (P) in a collapsed ostracod is enhanced by tertiary anhydrite moldic porosity (T). Anhydrite mold is partially cemented by slightly ferroan dolomite.

Fig. 63.--Rose #1, 2927 ft., d=11u, (X). Partial cementation of a first generation anhydrite mold by second generation sparry anhydrite.

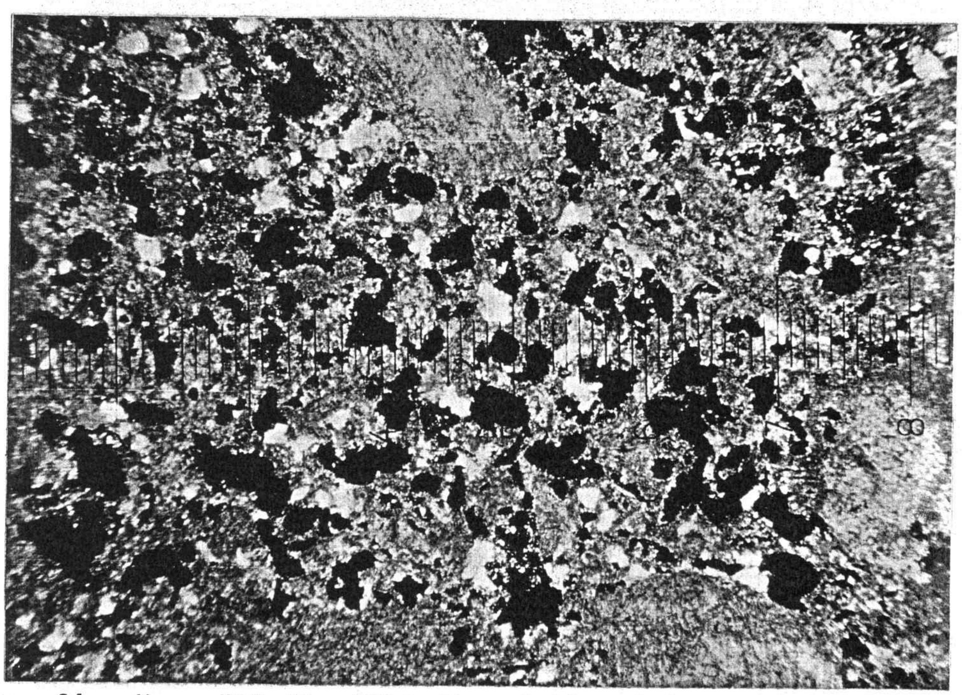

Fig. 64.--Neer "A" #1, 2816 ft., d=42u, (X). Dissolution of first generation anhydrite has produced numerous tertiary anhydrite molds.

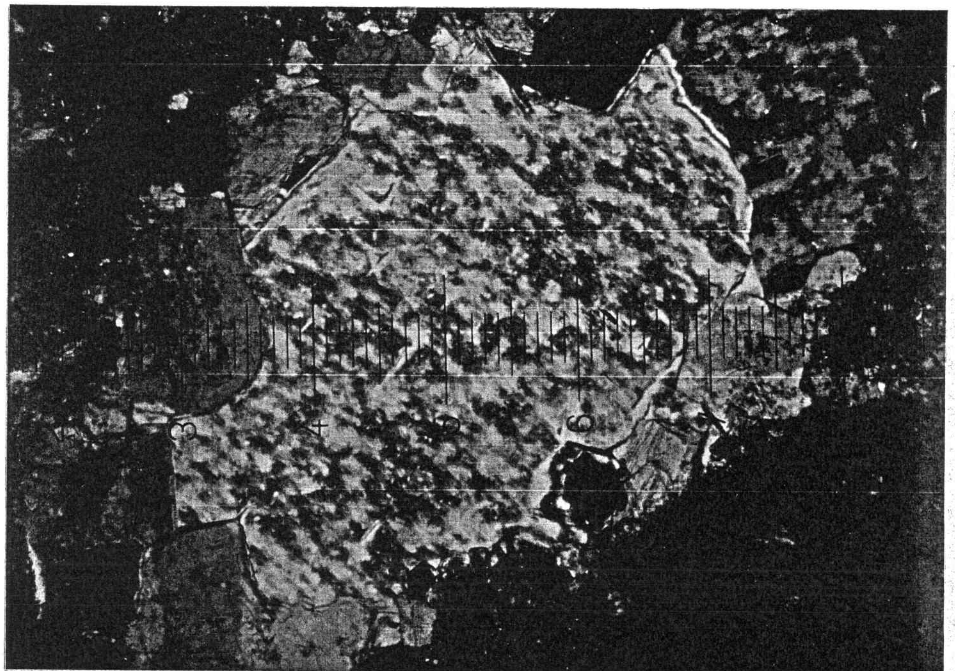

Fig. 65.--Dreese #1, 2998 ft., d=11u, (X). A first generation anhydrite mold is cemented by second generation dolomite which rims the mold, and by second generation anhydrite which fills the remainder of the mold, and partially replaces earlier dolomite.

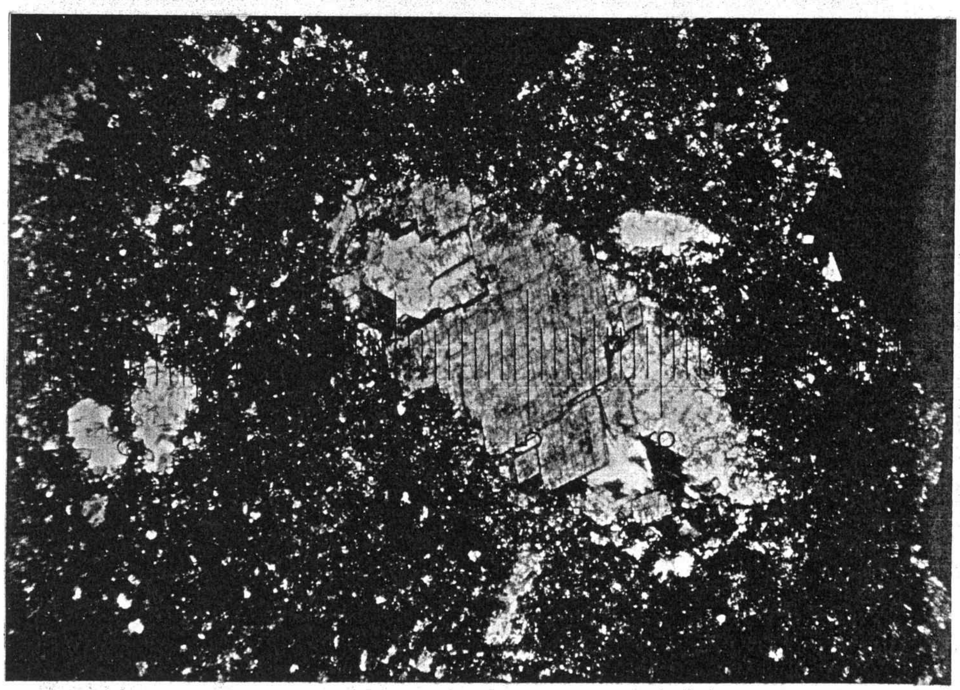

Fig. 66.--Miller #3, 2870-91 ft., d=42u, (X). A first generation anhydrite mold was cemented by coarse second generation dolomite, and later by second generation anhydrite, which partially replaced earlier dolomite cement.

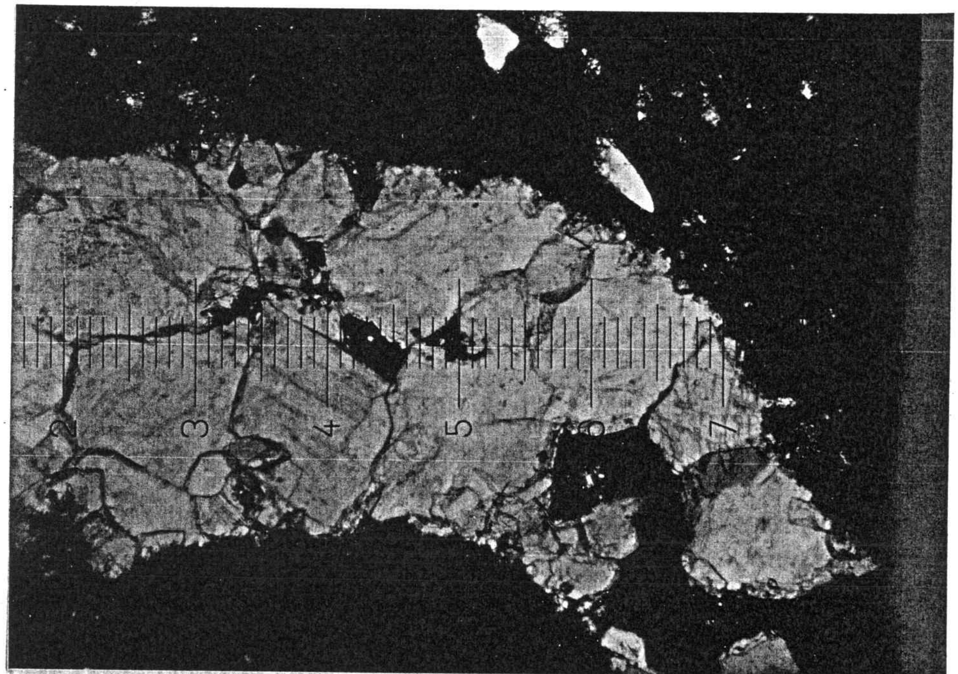

Fig. 67.--Dreese #1, 2989 ft., d=11u, (X). Coarse rhombic dolomite cement partially fills a fracture in a dolostone.

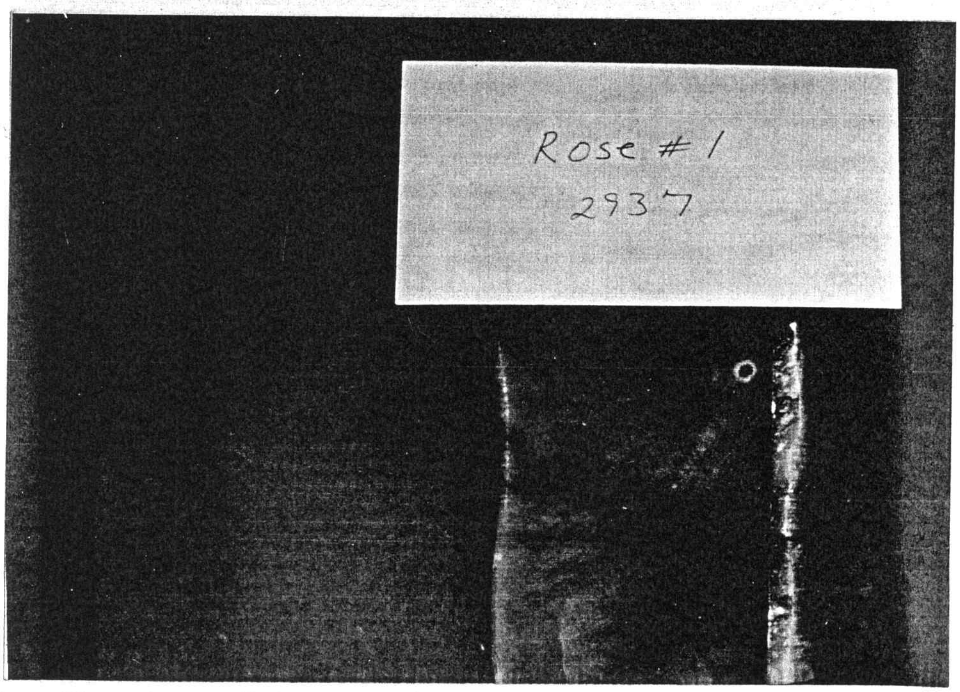

Fig. 68.--Core slab from the Wagner and Brown Rose #1, showing massive replacement of a limestone by nodular anhydrite (card is 6 inches long).

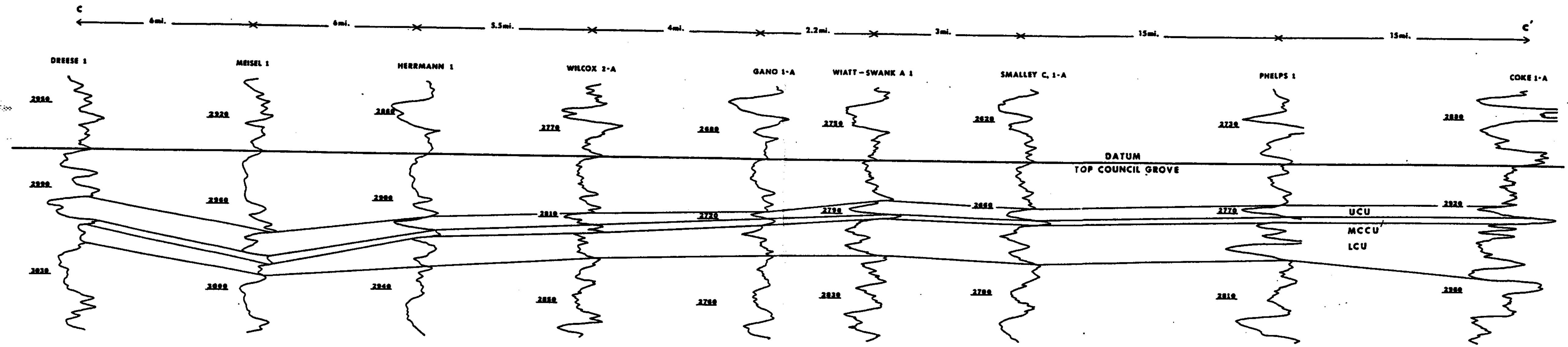

FIGURE 9 - STRATIGRAPHIC CROSS SECTION C-C'

ALL LOGS GAMMA RAY

20 ft.
0
not to scale

KEY TO FACIES

UCU-UPPER CARBONATE UNIT

MCCU-MIDDLE CLASTIC/CARBONATE UNIT

LCU-LOWER CARBONATE UNIT

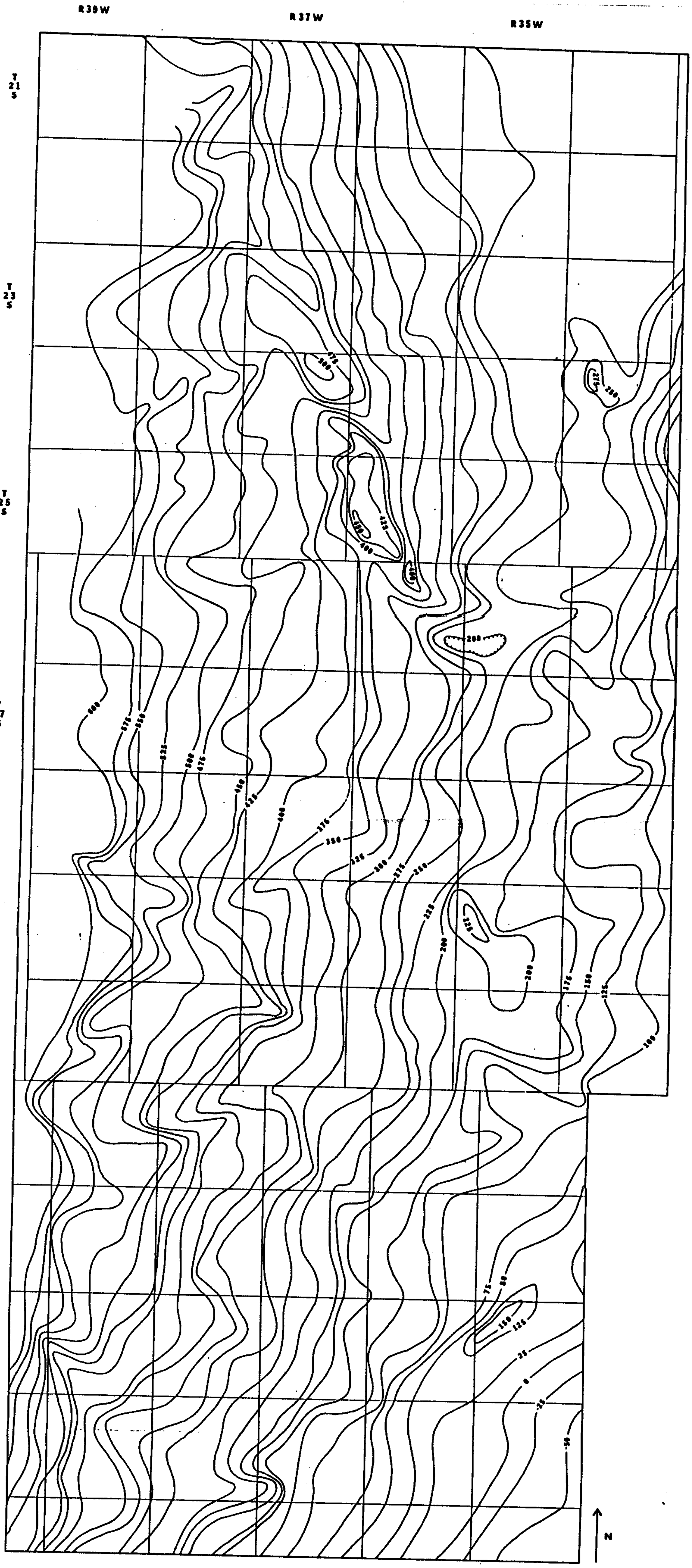

FIGURE 4

STRUCTURE CONTOUR MAP

TOP COUNCIL GROVE

CI = 25 ft.

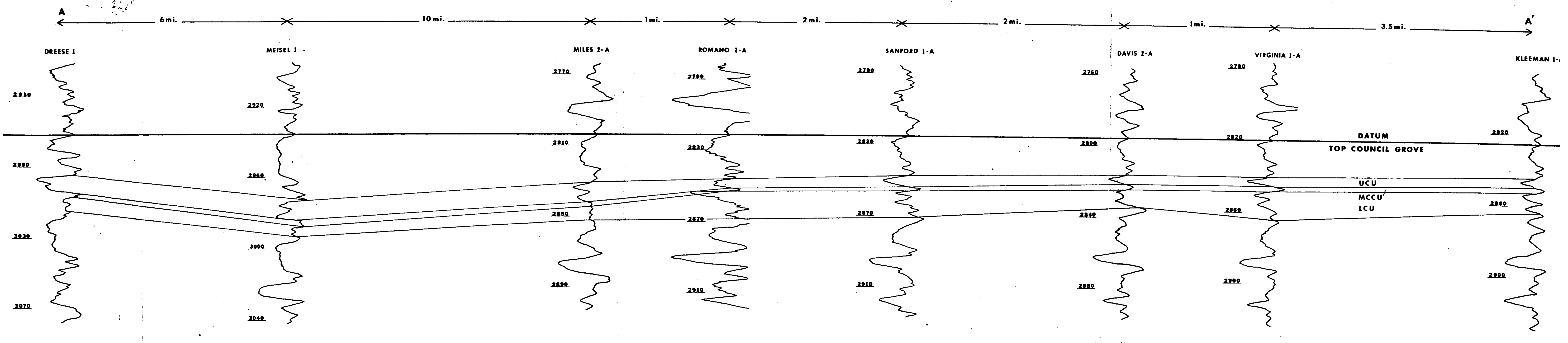

FIGURE 5 - STRATIGRAPHIC CROSS SECTION A-A'

ALL LOGS GAMMA RAY

20 ft. — 0 (not to scale)

KEY TO FACIES

UCU-UPPER CARBONATE UNIT

MCCU-MIDDLE CLASTIC/CARBONATE UNIT

LCU-LOWER CARBONATE UNIT

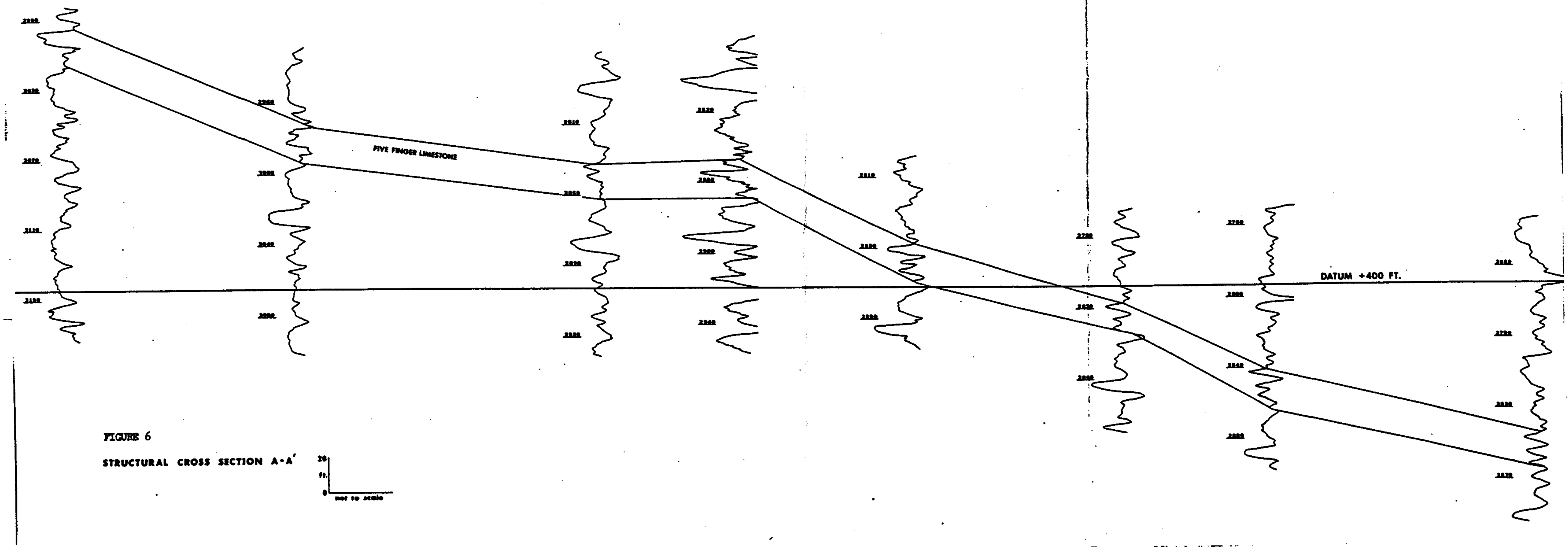

FIGURE 6

STRUCTURAL CROSS SECTION A-A'

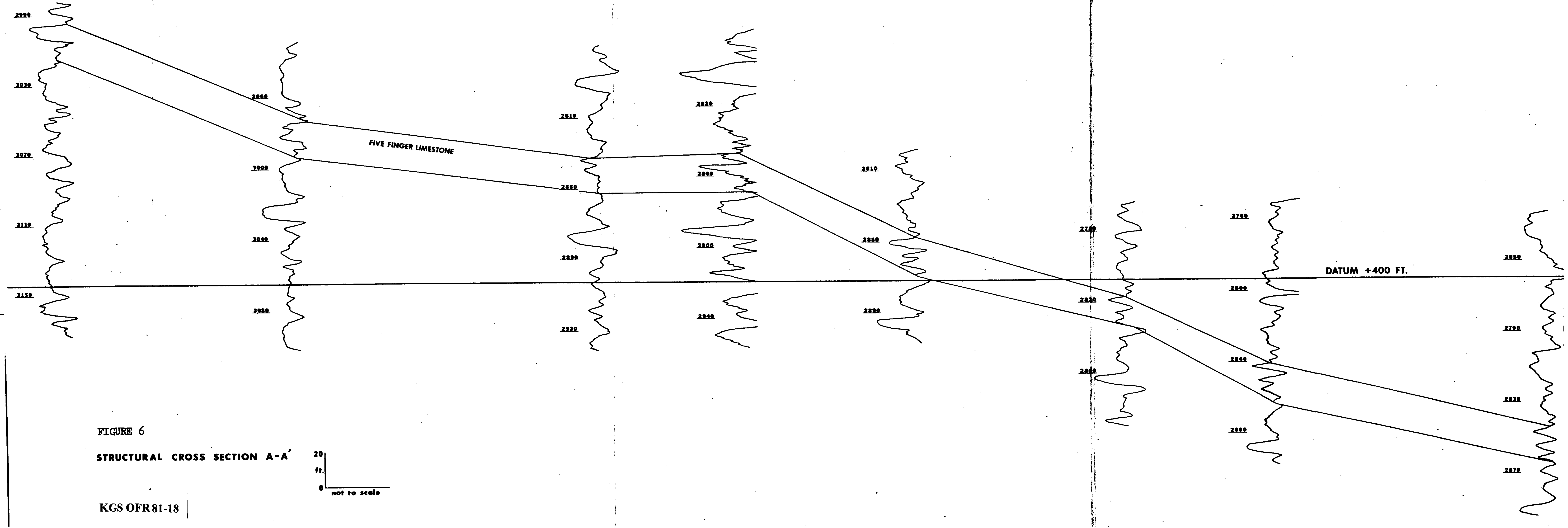

FIGURE 6

STRUCTURAL CROSS SECTION A-A′

KGS OFR 81-18

FIGURE 7 - STRATIGRAPHIC CROSS SECTION B - B'
ALL LOGS GAMMA RAY

KGS OFR 81-18

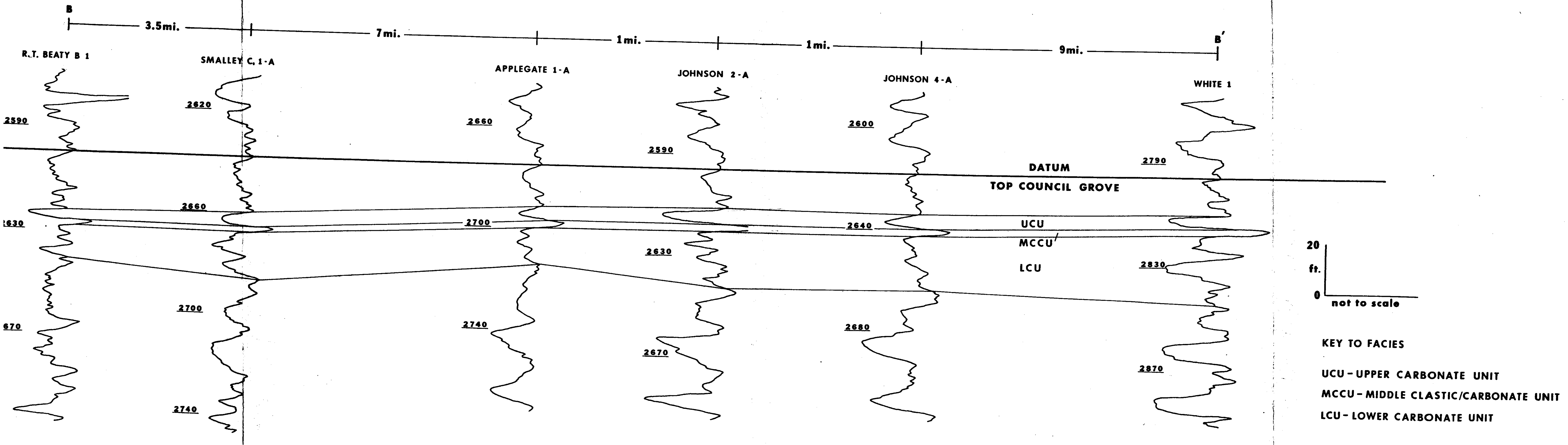

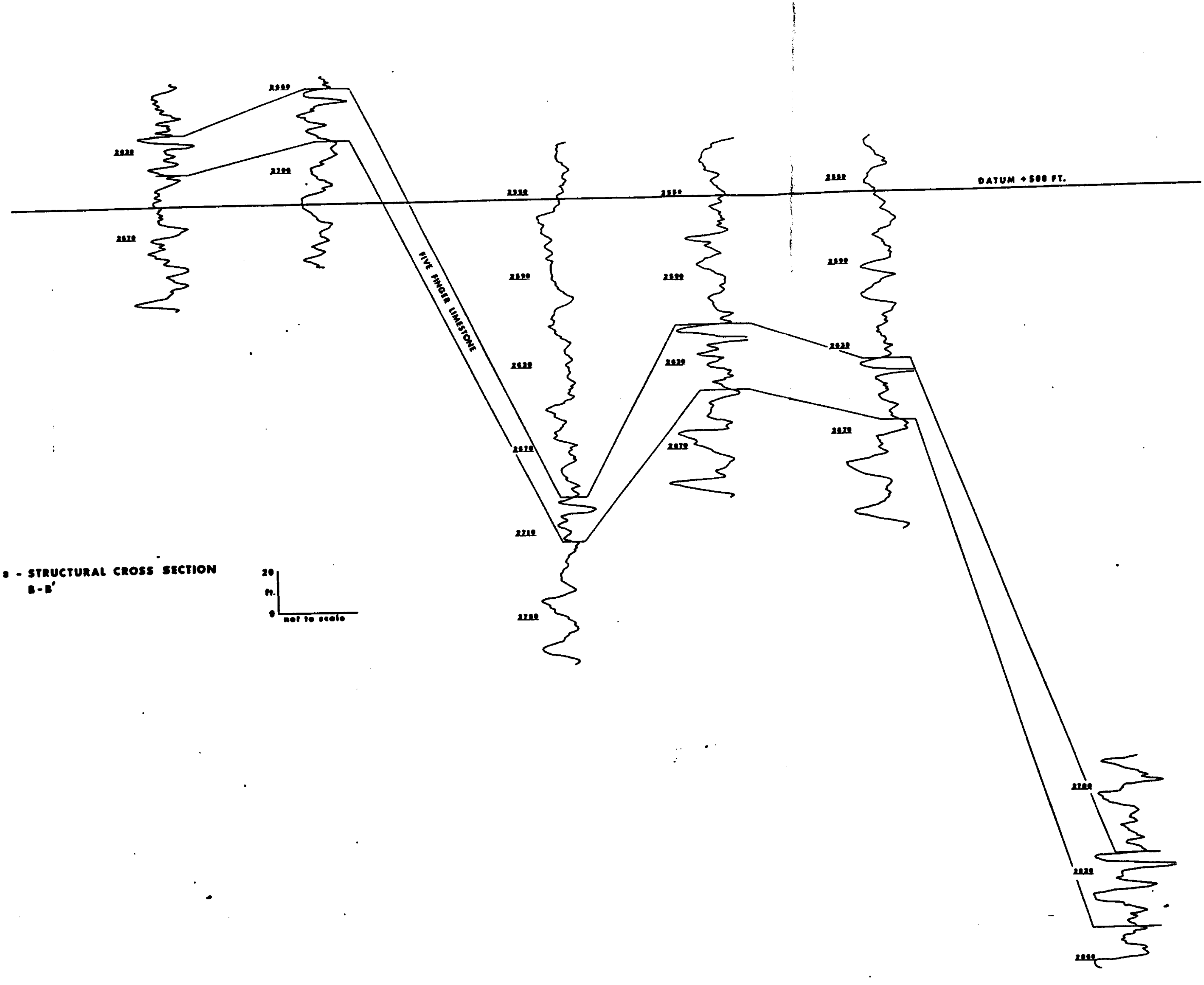

FIGURE 8 - STRUCTURAL CROSS SECTION
B-B'

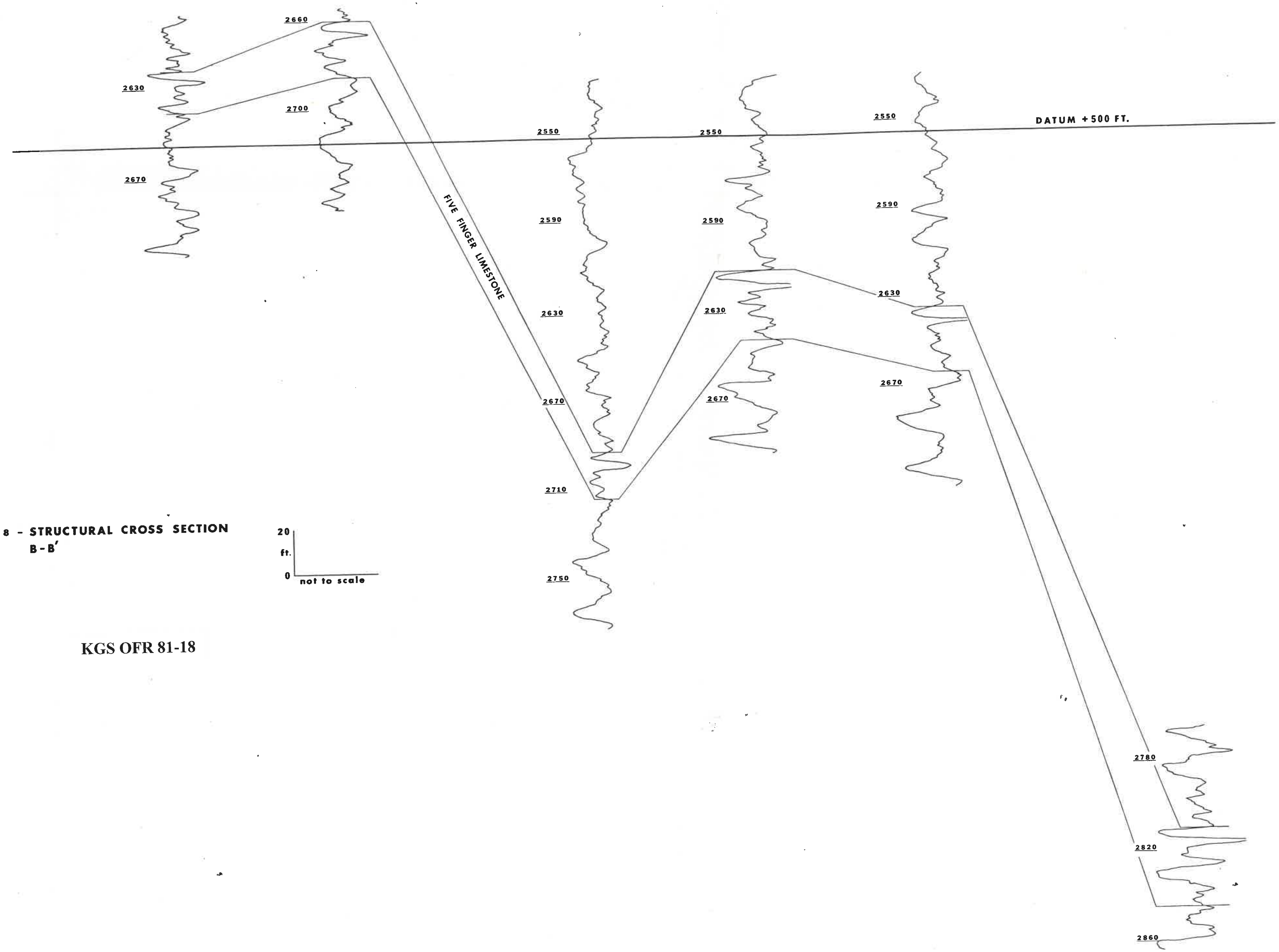

FIGURE 8 - STRUCTURAL CROSS SECTION B-B′

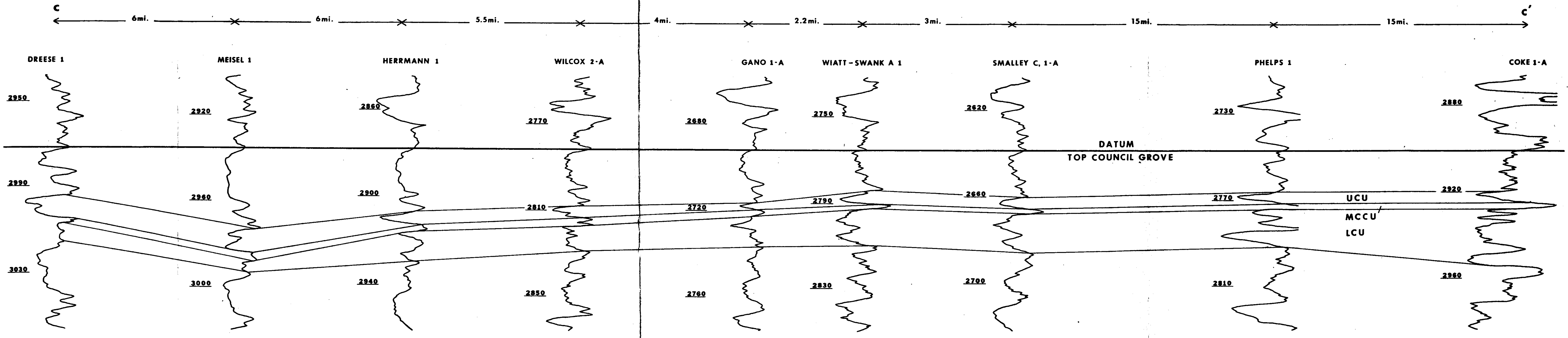

IGURE 9 - STRATIGRAPHIC CROSS SECTION C-C′

LL LOGS GAMMA RAY

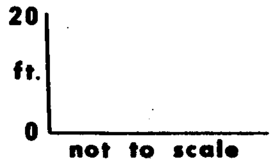

KEY TO FACIES

UCU-UPPER CARBONATE UNIT

MCCU-MIDDLE CLASTIC/CARBONATE UNIT

LCU-LOWER CARBONATE UNIT

KGS OFR 81-18

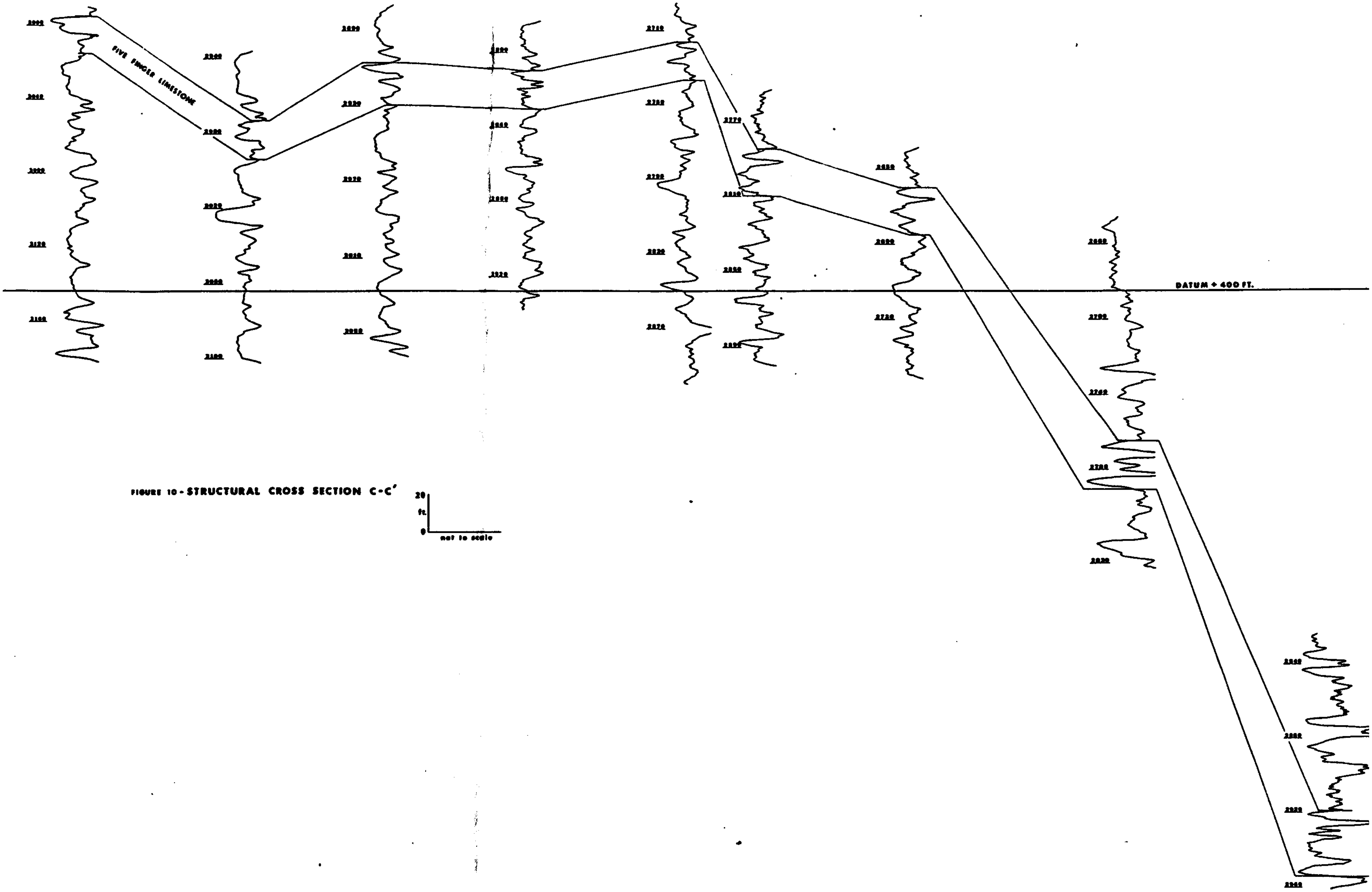

FIGURE 10 - STRUCTURAL CROSS SECTION C-C'

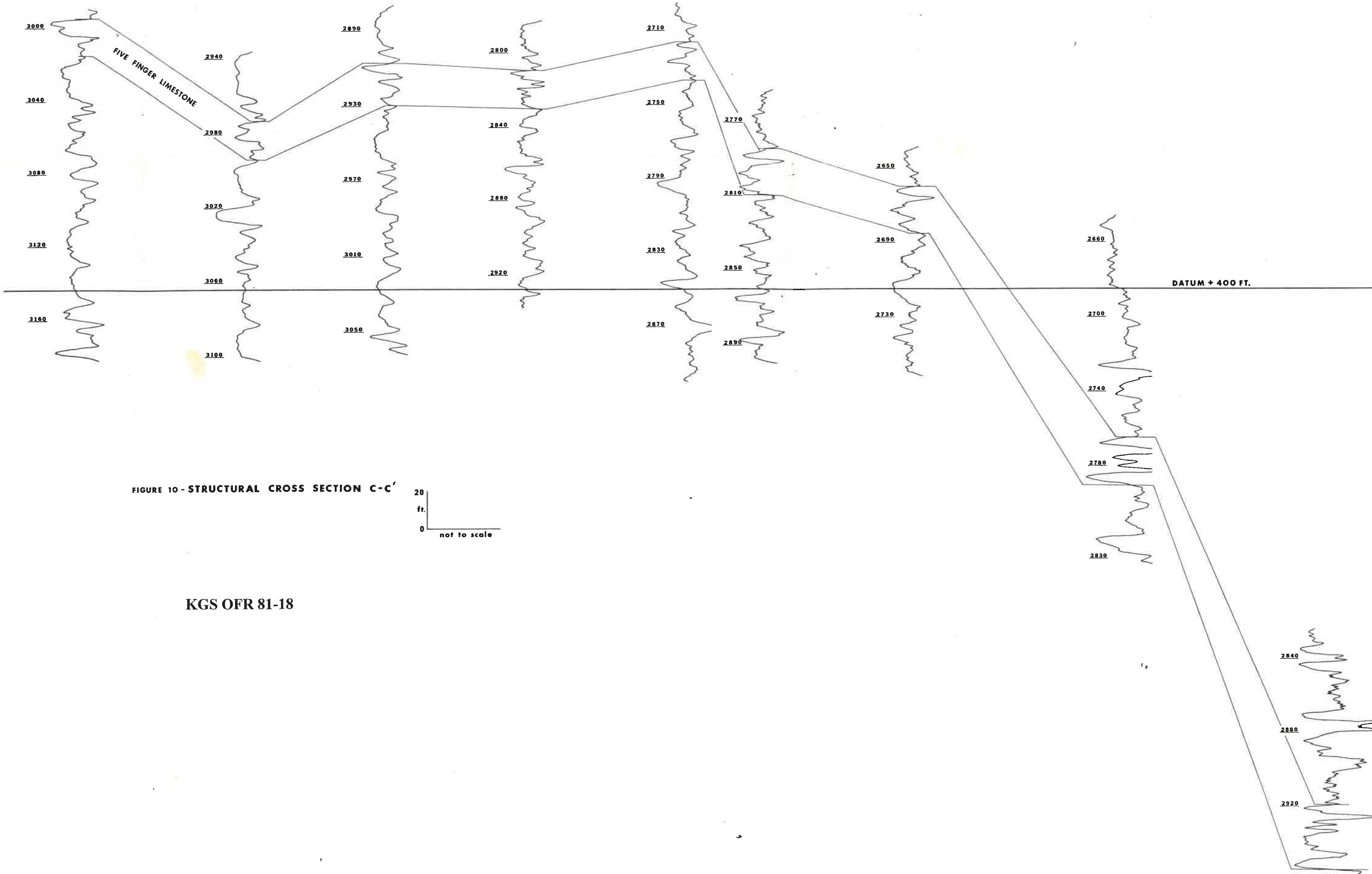

FIGURE 10 - STRUCTURAL CROSS SECTION C-C'

KGS OFR 81-18

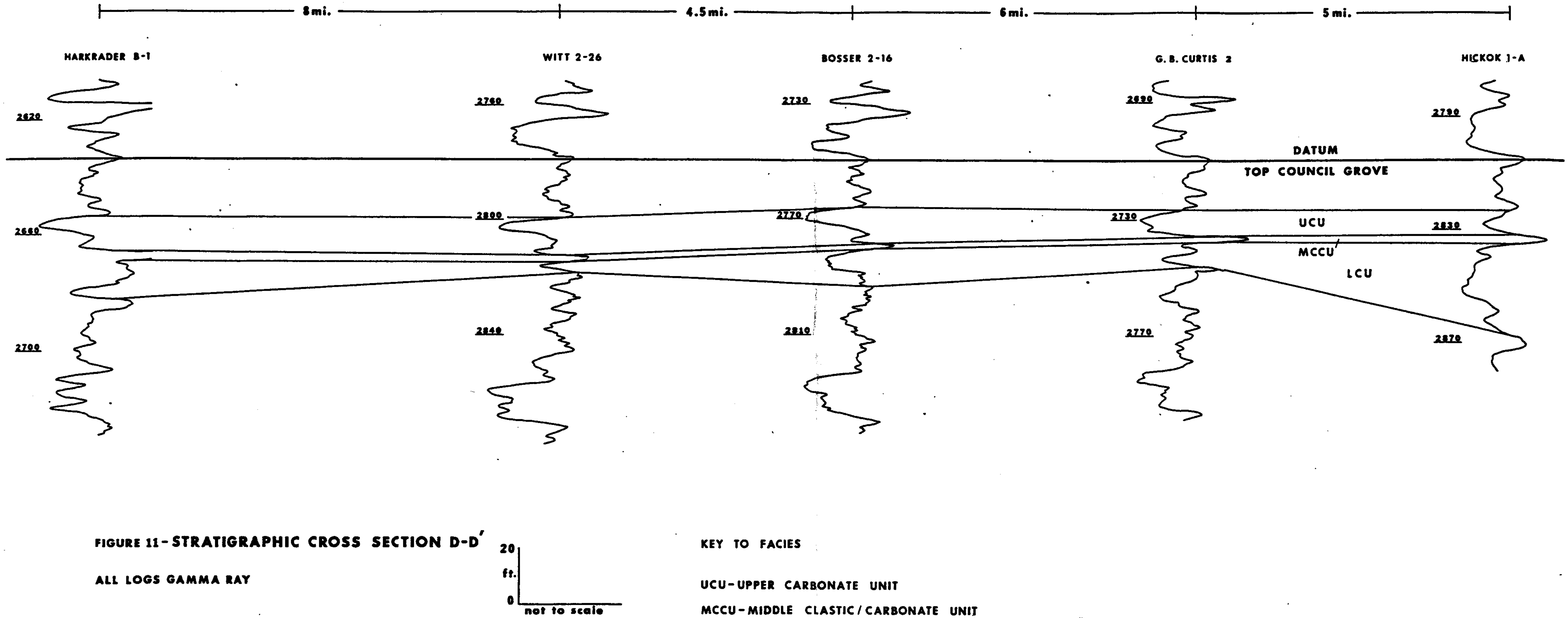

FIGURE 11 - STRATIGRAPHIC CROSS SECTION D-D′

ALL LOGS GAMMA RAY

KEY TO FACIES

UCU - UPPER CARBONATE UNIT

MCCU - MIDDLE CLASTIC / CARBONATE UNIT

LCU - LOWER CARBONATE UNIT

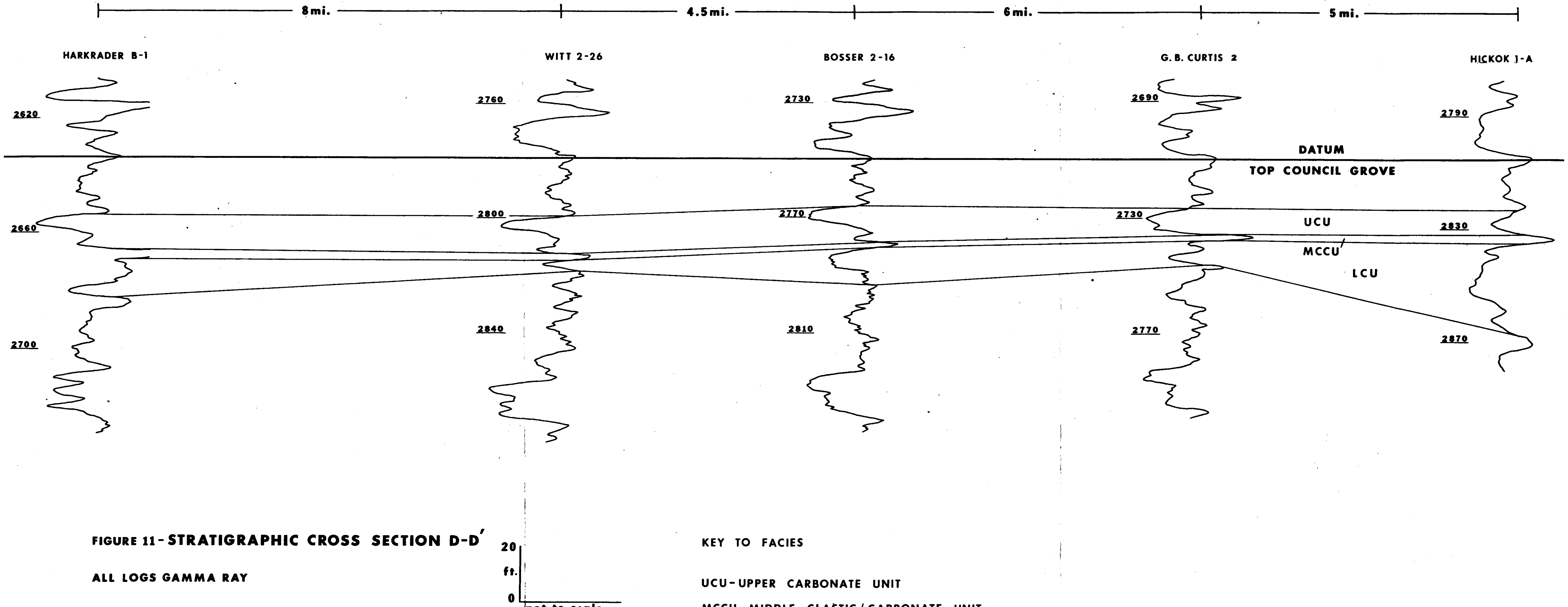

FIGURE 11 - STRATIGRAPHIC CROSS SECTION D-D′

ALL LOGS GAMMA RAY

KEY TO FACIES

UCU - UPPER CARBONATE UNIT

MCCU - MIDDLE CLASTIC / CARBONATE UNIT

LCU - LOWER CARBONATE UNIT

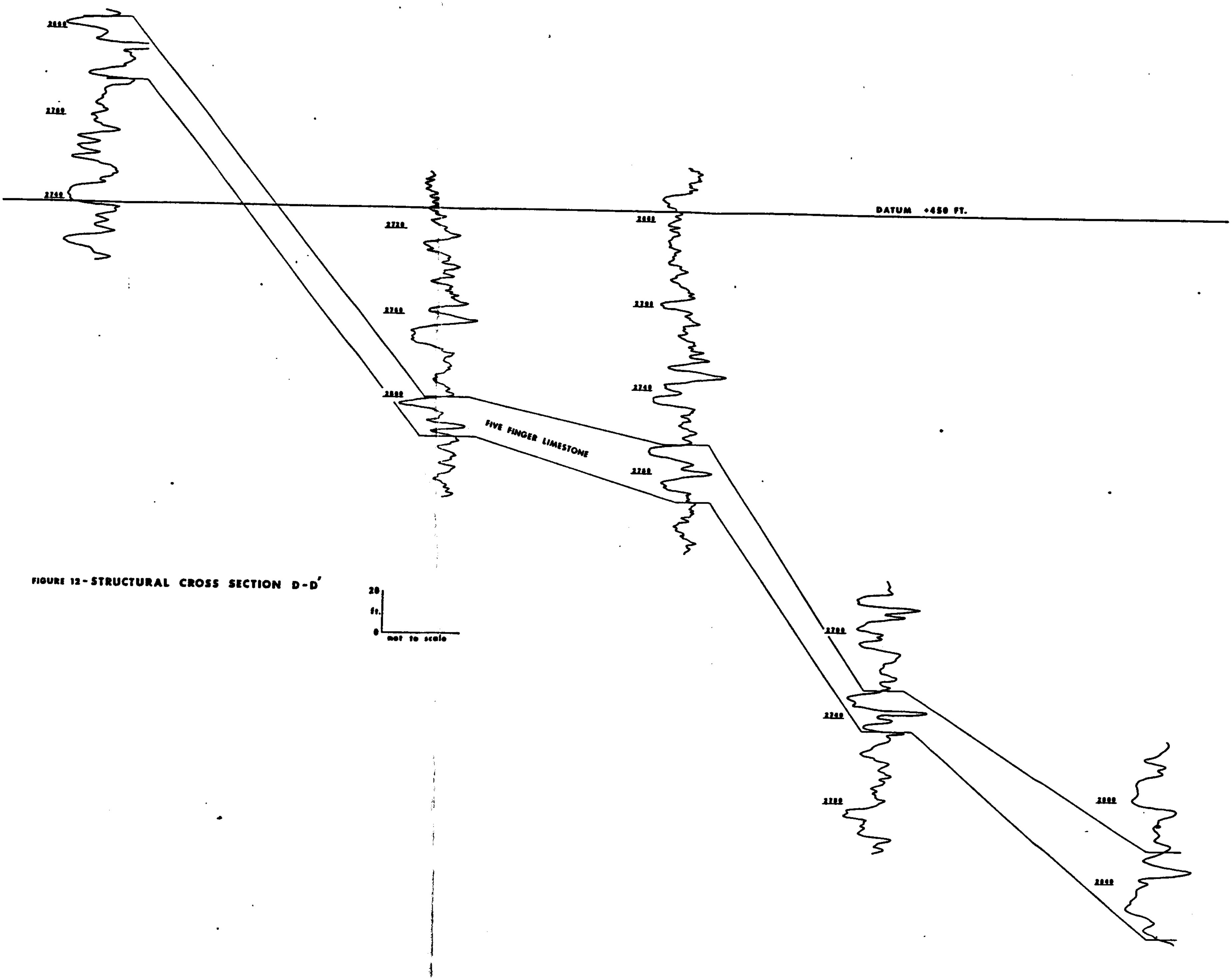

FIGURE 12 - STRUCTURAL CROSS SECTION D-D'

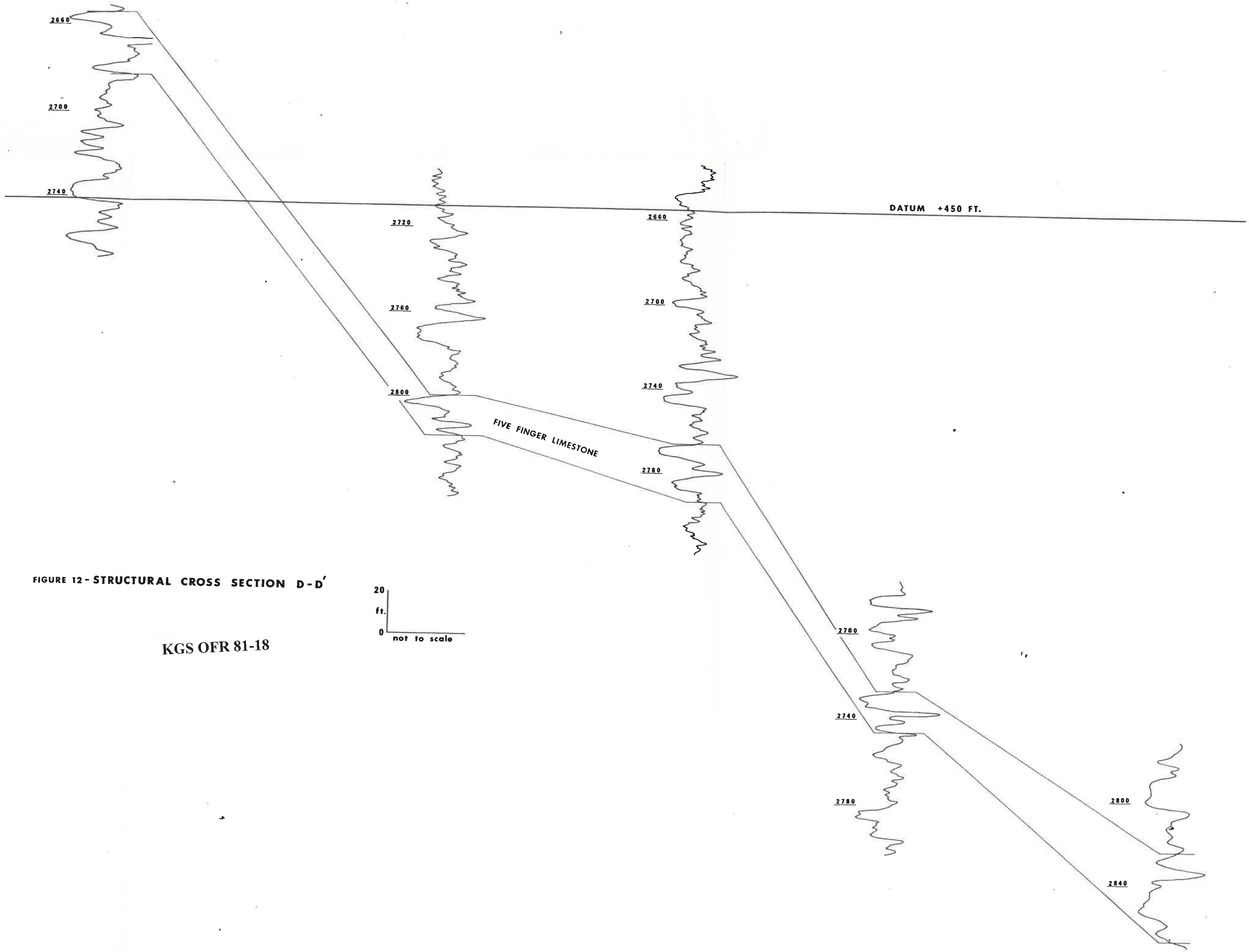

FIGURE 12 - STRUCTURAL CROSS SECTION D-D'

KGS OFR 81-18

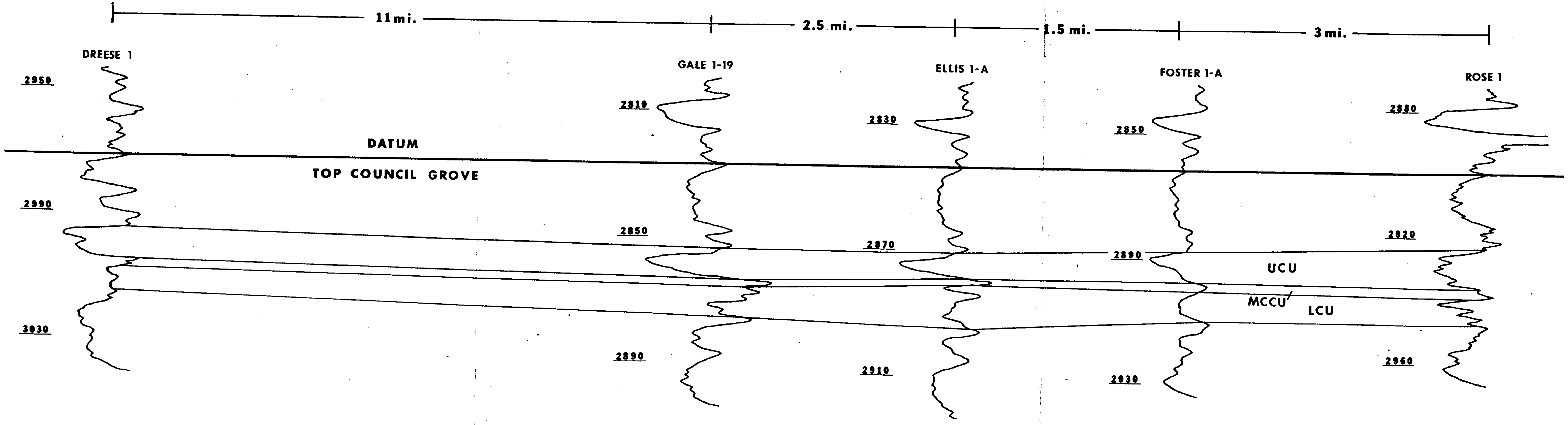

FIGURE 13 - STRATIGRAPHIC CROSS SECTION E-E′

ALL LOGS GAMMA RAY

KGS OFR 81-18

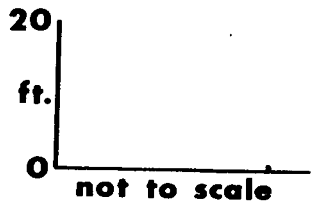

KEY TO FACIES

UCU – UPPER CARBONATE UNIT

MCCU – MIDDLE CLASTIC/CARBONATE UNIT

LCU – LOWER CARBONATE UNIT

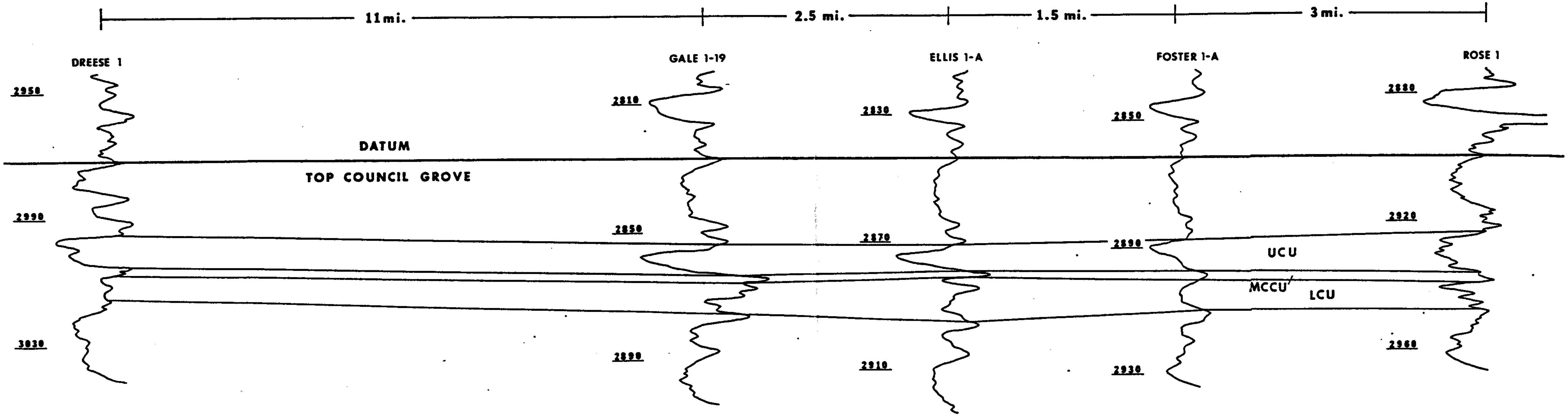

FIGURE 13 - **STRATIGRAPHIC CROSS SECTION E-E′**

ALL LOGS GAMMA RAY

20 ft.
0
not to scale

KEY TO FACIES

UCU - UPPER CARBONATE UNIT

MCCU - MIDDLE CLASTIC/CARBONATE UNIT

LCU - LOWER CARBONATE UNIT

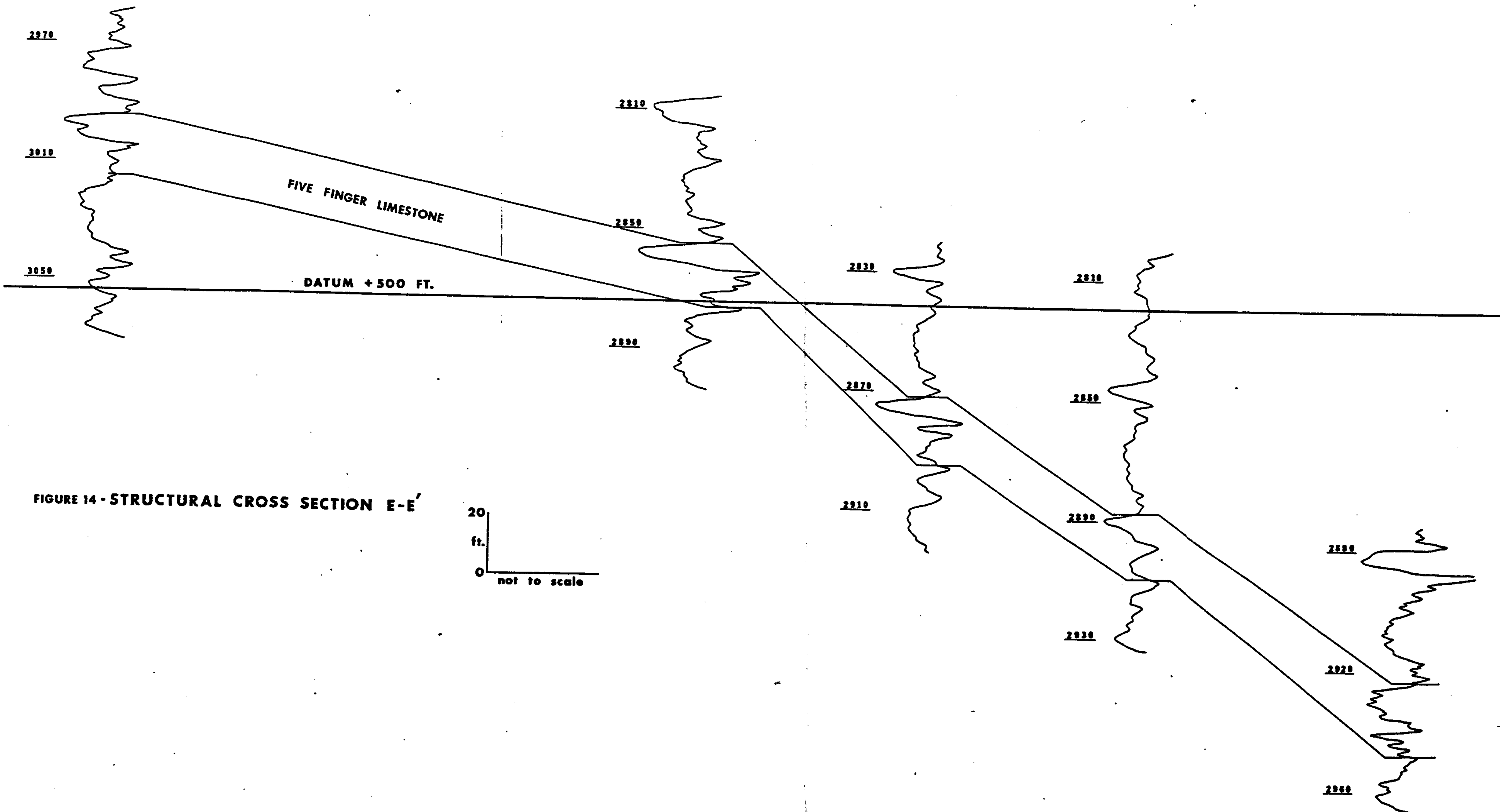

FIGURE 14 - STRUCTURAL CROSS SECTION E-E'